

Accepted 12 May 2003 for publication in the *Astronomical Journal*, scheduled for August 2003 issue.

## The *IRAS* Revised Bright Galaxy Sample (RBGS)

D. B. Sanders,<sup>1,2</sup> J. M. Mazzarella,<sup>3</sup> D.-C. Kim,<sup>3,4</sup> J. A. Surace,<sup>5</sup> B. T. Soifer<sup>5,6</sup>

### ABSTRACT

*IRAS* flux densities, redshifts, and infrared luminosities are reported for all sources identified in the *IRAS* Revised Bright Galaxy Sample (RBGS), a complete flux-limited survey of all extragalactic objects with total  $60\ \mu\text{m}$  flux density greater than  $5.24\ \text{Jy}$ , covering the entire sky surveyed by *IRAS* at Galactic latitude  $|b| > 5^\circ$ . The RBGS includes 629 objects, with a median (mean) sample redshift of 0.0082 (0.0126) and a maximum redshift of 0.0876. The RBGS supersedes the previous two-part *IRAS* Bright Galaxy Samples (hereafter BGS<sub>1</sub>+BGS<sub>2</sub>), which were compiled before the final (“Pass 3”) calibration of the *IRAS* Level 1 Archive in May 1990. The RBGS also makes use of more accurate and consistent automated methods to measure the flux of objects with extended emission. The RBGS contains 39 objects which were not present in the BGS<sub>1</sub>+BGS<sub>2</sub>, and 28 objects from the BGS<sub>1</sub>+BGS<sub>2</sub> have been dropped from RBGS because their revised  $60\ \mu\text{m}$  flux densities are not greater than  $5.24\ \text{Jy}$ . Comparison of revised flux measurements for sources in both surveys shows that most flux differences are in the range  $\sim 5 - 25\%$ , although some faint sources at  $12\ \mu\text{m}$  and  $25\ \mu\text{m}$  differ by as much as a factor of 2. Basic properties of the RBGS sources are summarized, including estimated total infrared luminosities, as well as updates to cross-identifications with sources from optical galaxy catalogs established using the NASA/IPAC Extragalactic Database (NED). In addition, an atlas of images from the Digitized Sky Survey with overlays of the *IRAS* position uncertainty ellipse and annotated scale bars is provided for ease in visualizing the optical morphology in context with the angular and metric size of each object. The revised bolometric infrared luminosity function,  $\phi(L_{\text{ir}})$ , for infrared bright galaxies in the local Universe remains best fit by a double power law,  $\phi(L) \propto L^\alpha$ , with  $\alpha = -0.6 (\pm 0.1)$ , and  $\alpha = -2.2 (\pm 0.1)$  below and above the “characteristic” infrared luminosity  $L_{\text{ir}}^* \sim 10^{10.5} L_\odot$ , respectively. A companion paper provides *IRAS* High Resolution (HIRES) processing of over 100 RBGS sources where improved spatial resolution often provides better *IRAS* source positions or allows for deconvolution of close galaxy pairs.

*Subject headings:* galaxies: general — infrared: general — infrared: sources

### 1. Introduction

This paper presents the complete list of objects contained in the *IRAS* Revised Bright Galaxy Sample (RBGS), a flux-limited sample of all extragalactic objects brighter than  $5.24\ \text{Jy}$  at  $60\ \mu\text{m}$ , covering the entire sky surveyed by the *Infrared Astronomical Satellite* (*IRAS*; Neugebauer et al. 1984) at Galactic latitude  $|b| > 5^\circ$ . The RBGS replaces the earlier *IRAS* Bright Galaxy Samples (BGS<sub>1</sub>+BGS<sub>2</sub>), which were compiled using the *IRAS Point Source Catalog* (PSC: 1988) along with other intermediate releases of the *IRAS* data

<sup>1</sup>Institute for Astronomy, University of Hawaii, 2680 Woodlawn Drive, Honolulu, HI 96822; E-mail: sanders@ifa.hawaii.edu

<sup>2</sup>Max-Planck Institut für Extraterrestrische Physik, D-85740, Garching, Germany

<sup>3</sup>IPAC, MS 100-22, California Institute of Technology, Jet Propulsion Laboratory, Pasadena, CA 91125; Email: mazz@ipac.caltech.edu

<sup>4</sup>Current Address: School of Earth and Environmental Sciences (BK21), Seoul National University, Seoul, Korea; Email: dckim@astro.snu.ac.kr

<sup>5</sup>SIRTF Science Center, MS 314-6, California Institute of Technology, Pasadena, CA 91125; Email: jason@ipac.caltech.edu, bts@ipac.caltech.edu

<sup>6</sup>Division of Physics, Math and Astronomy, Downes Lab, MS 320-47, California Institute of Technology,

Pasadena, CA 91125; Email: bts@mop.caltech.edu

products and are therefore now out of date with the more accurate “Pass 3” calibration <sup>7</sup> adopted for the final release of the *IRAS* Level 1 Archive.

The RBGS objects are the brightest  $60\ \mu\text{m}$  sources in the extragalactic infrared sky, and as such they remain the best sources for studying the infrared emission processes in galaxies and for comparison with extragalactic observations at other wavelengths. In this regard the RBGS can be considered the infrared equivalent of the 3CR survey of extragalactic radio sources. Most sources in the RBGS have extended *IRAS* flux densities that are underestimated by measurements in the *IRAS* PSC and in the *Faint Source Catalog* (FSC: Moshir et al. 1992), because the *IRAS* catalogs are the result of point-source filtering. Therefore, the RBGS should be the reference of choice for accurate *IRAS* fluxes and infrared luminosities of galaxies in the local Universe.

In this paper we report revised  $12\ \mu\text{m}$ ,  $25\ \mu\text{m}$ ,  $60\ \mu\text{m}$  and  $100\ \mu\text{m}$  total flux densities for all 629 infrared sources in the RBGS. Section 2 describes the methods used to select the objects. Details of the *IRAS* data processing are deferred to the Appendix. Section 3 presents the summary data for the RBGS objects, including the revised *IRAS* flux measurements, source size information, and derived infrared luminosities. Also included is an atlas of images from the Digitized Sky Survey with overlays of the *IRAS* position uncertainty ellipse and annotated scale bars; this is intended as a reference to visualize the optical morphology of the infrared source in context with the angular and metric size of each object, and more importantly, in the case of confused or double sources, to quickly see how large the *IRAS* position offset may be from the optical sources. Section 4 is a discussion of the general properties of the RBGS which includes a comparison of the revised measurements with those published previously, and a summary of the sky coverage, number counts, infrared colors, and infrared luminosity function. A companion paper (Surace, Sanders & Mazzarella

<sup>7</sup>“Pass 3” refers to the final calibration adopted for the archived *IRAS* data by the Infrared Processing and Analysis Center (IPAC) in 1990. Details of the calibration methods for each of the *IRAS* infrared bands, and the various *IRAS* catalogs and atlases can be found in the Explanatory Supplement to the *IRAS Faint Source Survey* (Moshir et al. 1992).

2003) provides High Resolution (HIRES) processing of  $\sim 20\%$  of the RBGS sources where it was thought that enhanced resolution might provide better source positions, or in the case of close galaxy pairs, allow deconvolution of the individual components.

## 2. Sample Selection and Data Processing

In constructing the RBGS, the basic methods used to extract candidate bright galaxies from the *IRAS* catalogs and to compute total fluxes in each of the four *IRAS* bands using ADDSCAN/SCANPI (hereafter referred to as SCANPI; Helou et al. 1988) were similar to procedures used in earlier compilations of the *IRAS* BGS (here referred to as BGS<sub>1</sub>: Soifer et al 1989, 1987, 1986) and the *IRAS* BGS–Part II (here referred to as BGS<sub>2</sub>: Sanders et al 1995); the reader is referred to these papers for historical perspective as well as for a more thorough description of original sample membership criteria. In this paper we outline the major steps that were followed to construct the new sample, and where appropriate, emphasize the differences between the earlier BGS<sub>1</sub>+BGS<sub>2</sub> procedures and the more refined RBGS processing.

The *IRAS* FSC and *IRAS* PSC were used as starting points for the initial search of the *IRAS* data archive. It was necessary to use the PSC because the FSC does not include objects in confused regions of the infrared sky with Galactic latitude  $|b| < 10^\circ$ . The FSC Rejects (FSCR) <sup>8</sup> were also examined for bright objects at  $60\ \mu\text{m}$ . In the end, the only source accepted from the FSCR is NGC 4151 (*IRAS* Z12080+3940). The reasons for its inclusion in RBGS are: a) the SCANPI signals in all 4 *IRAS* bands are very strong (see Table 1); b) the FIR signal is positionally coincident with the optical galaxy, and the coadded scan profile from ADDSCAN/SCANPI is consistent with the opti-

<sup>8</sup>The FSCR, along with all other *IRAS* catalogs, is available for queries through the GATOR service of the Infrared Science Archive (IRSA) at IPAC; <http://irsa.ipac.caltech.edu/>. The FSCR contains objects that have only one *IRAS* hours-confirmed (HCON) observation; however, *IRAS* measurements in the FSCR are much more reliable when a high signal-to-noise detection is combined with confirmation via positional cross-identification with a known source detected at another wavelength.

cal size of the galaxy; c) the *IRAS* SCANPI flux density values at  $12\ \mu\text{m}$  and  $25\ \mu\text{m}$  are comparable (slightly higher, as expected given some extended flux) to independent ground-based measurements at  $10.6\ \mu\text{m}$  and  $21\ \mu\text{m}$  in apertures centered on the nucleus (Lebofsky & Rieke 1979).

A second step involved another search of the *IRAS* PSC and FSC, this time with a lower  $60\ \mu\text{m}$  point source threshold of  $4.5\ \text{Jy}$ , which was designed primarily for the purpose of capturing sources that might have a reasonable chance of having extended flux sufficient to bring their total  $60\ \mu\text{m}$  flux densities above the RBGS threshold. To investigate how many objects with total  $60\ \mu\text{m}$  flux density greater than  $5.24\ \text{Jy}$  may be “hiding” among objects with even fainter point-source components, a few dozen galaxies randomly selected from the FSC with  $4.0\ \text{Jy} < S_\nu(60\ \mu\text{m}) < 4.5\ \text{Jy}$  were also coadded with SCANPI. These objects were not found to contain sufficient extended emission to bring their total fluxes above the RBGS flux limit. Searches of NED for optical galaxies larger than 4 arcminutes, without regard for their (likely underestimated) flux measurements from the *IRAS* catalogs, were also performed to obtain additional candidates. However, objects with total  $S_\nu(60\ \mu\text{m}) > 5.42\ \text{Jy}$  among these large optical galaxies objects were also recovered in the *IRAS* catalog searches noted above. This provides confidence that our procedures resulted in a sample with a very high level of completeness at  $60\ \mu\text{m}$ .

All candidate *IRAS* sources were compared with the latest catalog cross-correlations available in the NASA/IPAC Extragalactic Database (NED)<sup>9</sup>, which were then inspected using overlays on the DSS1 images. The data were then reprocessed (co-addition of all acceptable *IRAS* scans) using SCANPI, and the resulting 1-D coadded scan profiles were visually inspected to determine the amount of extended emission, and in the case of blended or confused sources, to determine the best method for computing the total flux density. A computer program was written to determine objectively and consistently whether the total flux density of each source is better represented by the baseline zero-crossing method  $f_\nu(z)$ , the value integrated within the nominal *IRAS* detector size  $f_\nu(t)$ , the point source template fit

amplitude (“template”), or the peak flux in the profile (“peak”). This was accomplished by checking whether the  $f_\nu(t)$  value is significantly larger than the template fit and peak values (considering also the RMS noise in the coadded scan outside the detected signal range), and if so whether the  $f_\nu(z)$  value is significantly larger than the  $f_\nu(t)$  value. This procedure, combined with comparisons of the coadded scan profile widths at 25% (“W25”) and 50% (“W50”) of the peak flux with the nominal beam size (point-spread function), was also used to determine whether each *IRAS* source is resolved, marginally extended or unresolved. All measurements were performed using SCANPI’s median (1002) method of coadding the individual *IRAS* scans, and all sources with  $60\ \mu\text{m}$  point source flux greater than  $5.24\ \text{Jy}$  (the completeness limit of the original BGS) were included in the final sample.

Appendix A gives more details regarding the various methods used for setting thresholds to select between the flux density estimators and for estimating the total flux densities of the extended sources, and provides a tabular listing of all key SCANPI measurements in each *IRAS* band, as well as the ratio of the new RBGS total flux density measurements compared with the old values reported in the  $\text{BGS}_1 + \text{BGS}_2$  (where available). Example coadded scan profiles are also plotted to illustrate the extent of *IRAS* emission compared to the point spread function and to show how different flux measurement methods were objectively selected in the automated SCANPI reprocessing of the data for all potential RBGS sources.

Finally, *IRAS* flux measurements from the “Catalog of *IRAS* Observations of Large Optical Galaxies” (Rice et al. 1988) and “An Atlas of High-Resolution *IRAS* Maps of Nearby Galaxies” (Rice 1993) were examined. Careful comparison of flux densities integrated within the signal range between SCANPI’s baseline fit zero-crossing points,  $f_\nu(z)$ , to those measured by Rice et al. from *IRAS* 2-D image products showed generally good agreement for galaxies with optical diameters smaller than about 25 arcminutes. For objects with optical diameters larger than  $\sim 25$  arcminutes it is clear that even SCANPI’s  $f_\nu(z)$  method systematically underestimates the total flux density compared to the 2-D method used by Rice. Therefore, to maintain consistency with other objects

<sup>9</sup>NED is available at <http://ned.ipac.caltech.edu/>.

in the RBGS to the highest degree possible, in the final compilation we adopted Rice et al. measurements over those from SCANPI’s  $f_\nu(z)$  estimator only for objects larger than 25 arcminutes; such objects are flagged in Table 1.

### 3. The *IRAS* RBGS Data

Table 1 presents the summary data for all of the sources in the *IRAS* RBGS. The complete sample contains 629 galaxies that met our threshold criteria of  $S_{60} > 5.24$  Jy. The column entries are as follows:

(1) *Common Name* – Common name taken in decreasing priority order from the NGC, UGC, ESO, IC, A, MCG, CGCG, Zwicky compact galaxies, Markarian, and *IRAS* catalogs. “N” follows the common name for “new” RBGS objects which were not included in the compilation of the BGS<sub>1</sub> (Soifer et al. 1989) or BGS<sub>2</sub> (Sanders et al. 1995); “1” flags objects from the BGS<sub>1</sub>, and “2” flags objects from the BGS<sub>2</sub>.

(2) *IRAS Name* – Names from the *IRAS* Faint Source Catalog (FSC) are given using the standard “F” prefix; if the source is not in the FSC, the name from the Point Source Catalog (PSC) is given, which has no letter prefix. *IRAS* source names are based on equinox B1950.0 coordinates. Names from the *IRAS Faint Source Catalog Rejects* (FSCR) are given using the standard “Z” prefix. (NGC 4151 is the only FSCR object in the RBGS; see Section 2.) *IRAS* catalog names are not listed for a few very large galaxies (indicated by “—”) because entries in the *IRAS* catalogs do not represent the total flux and generally correspond only to the nucleus or other bright component. Flags following the *IRAS* name are as follows: “R” indicates large galaxies with for which total flux densities derived from *IRAS* images were published by Rice et al. (1988) or Rice (1993); the Rice et al. values are adopted here only in cases listing an “R” value for the Method code in columns (8) – (11); see text for details. “\*” identifies objects located in regions of the Milky Way, LMC, or SMC with high source confusion. [Note: The objects are listed in order of increasing B1950 right ascension (R.A.), as reflected in the source names from the *IRAS* catalogs; this places some objects out of order in terms of their J2000 coordinates.]

(3–4) *R.A., Dec* – Equinox J2000.0 R.A. and declination (Dec), transformed from equinox B1950.0 coordinates published in the *IRAS* FSC (Version 2.0) or PSC (Version 2), as indicated in Col. (2). These coordinates correspond to the centroid of the *IRAS* positional uncertainty ellipse as superimposed on the Digitized Sky Survey fields shown in Figure 1. Exceptions are for the large galaxies NGC 55, SMC, NGC 300, LMC, NGC 6744, and NGC 6822 whose positions are taken from Rice et al. (1988).

(5–6) *ℓ, b* – Galactic latitude and longitude in decimal degrees.

(7) *HIRES code* – *IRAS* HIRES code from Surace, Sanders & Mazzarella (2003). A listing here indicates that the infrared source contains two or more objects that were confused in one or more of the *IRAS* detectors. The high-resolution image restoration algorithm HIRES (Aumann, Fowler, & Melnyk 1990) was applied to these sources in an attempt to resolve flux from individual galaxies. “R” means the source was resolved into two or more components, resulting in new *IRAS* positions and fluxes; “\*” means the source was resolved, but the *IRAS* position lies between the two galaxies as seen on the DSS; “S” means the source was partially resolved into two or more components, and fluxes were estimated for each object, but no new reliable positions were derived; “U” means HIRES was unsuccessful at resolving separate components. See Surace et al. (2003) for detailed HIRES results for these objects. For consistency, the fluxes listed in Table 1 were derived using SCANPI in the same manner as the single objects in the table. There are known calibration problems with the HIRES data product (Surace et al. 1993), and while the flux ratio between individual galaxies within a system can be more accurately measured using HIRES, the absolute calibration of the galaxy system flux is better determined by SCANPI. Since in many cases a single galaxy dominates the far-infrared flux of a multiple galaxy system, there are only a handful of systems that would have not been selected in the RBGS but which are included by virtue of having an integrated flux above the selection limit.

(8–11) *Flux Densities* – Total *IRAS* flux densities (Jy) in the 12  $\mu\text{m}$ , 25  $\mu\text{m}$ , 60  $\mu\text{m}$ , and 100  $\mu\text{m}$  bands, respectively. Following each flux density value are the uncertainty ( $1\sigma$  in mJy) followed

by three code letters (**SMF**) indicating the infrared **S**ize (U = “unresolved”, M = “marginally extended”, R = “resolved”); the **M**ethod chosen as the best flux estimate from SCANPI (Z = “zero crossing”, I = “in-band total”, T = “template fit”, P = “peak value”, S = “deconvolution with SCLEAN” (see Appendix), R = from Rice et al. (1988); and a **F**lag indicating the type of confusion (c = “cirrus”, g = “nearby galaxy”, n = “excessive noise”, b = “blended objects”) causing large uncertainty as indicated by a colon (“:”) prefix on the flux density. Note that some large galaxies flagged with “R” in Col. (2) have new SCANPI zero-crossing estimates, indicated here using “Z” for the second flag, which are judged to have more accurate calibration than previously adopted values from Rice et al. (1988).

(12) *cz* – The Heliocentric radial velocity ( $\text{km s}^{-1}$ ) of the *IRAS* source computed as  $c$  times the redshift  $z$ . The source for the redshift is given in Col. (2) of Table 2 as a 19 digit reference code from NED. In cases where either a millimeter (e.g. CO) or HI 21-cm line measurement has been reported we have chosen to adopt these redshifts given that they better reflect the systemic velocity of the galaxy, as opposed to optical measurements which are often biased (typically blue-shifted) due to optical depth effects.

(13) *Distance* – The estimated source distance in Mpc; metric (“proper”) distance is listed, not luminosity distance. For most objects this was calculated from  $cz$  using the cosmic attractor model outlined in Appendix A of Mould et al. (2000), using  $H_0 = 75 \text{ km s}^{-1} \text{ Mpc}^{-1}$  and adopting a flat cosmology in which  $\Omega_M = 0.3$  and  $\Omega_\Lambda = 0.7$  (which corresponds to  $q_0 = -0.55$ ). Superscripts are defined as follows: “P” indicates the distance is not computed by correcting the heliocentric redshift using the cosmic attractor model, but comes from a direct *primary* distance measurement; “S” flags a direct *secondary* distance measurement; “V” indicates that the cosmic attractor flow model places the object within the *Virgo* cluster at a distance of 15.3 Mpc; “G” indicates that the cosmic attractor flow model places the object within the *Great Attractor*. References for the adopted primary and secondary distance indicators are Freedman et al. (2001), Madore & Freedman (1998), Ferrarese et al. (2000), Mould et al. (1991), Tully & Shaya (1984), Aaronson &

Mould (1983), Aaronson et al. 1982, and Aaronson, Mould & Huchra (1980).

(14–15) *Luminosities* – The base<sub>10</sub> logarithm of the far-infrared luminosity,  $L_{\text{fir}} = L(40 - 400\mu\text{m})$ , determined using the prescription described in Appendix B of Cataloged Galaxies and Quasars Observed in the *IRAS* Survey (1989), and the infrared luminosity,  $L_{\text{ir}} = L(8 - 1000\mu\text{m})$ , determined using the fluxes in all four *IRAS* bands (Perault 1987; see also Table 1 in Sanders & Mirabel 1996), in units of solar bolometric luminosity,  $L_\odot = 3.83 \times 10^{33} \text{ erg s}^{-1}$ .

(16) *Rank* – The object’s sequential rank in the distribution of  $L_{\text{ir}}$  values, where 1 is the most luminous source.

(17) *Other Names* – Other names from catalogs of interacting galaxies (IG) or active galactic nuclei (AGN). Spaces between catalog name prefix and number (as standard in NED) are omitted here to save space.









TABLE 1—*Continued*

Name		R.A. (J2000) DEC		$l$	$b$	HR	12 $\mu$ m		25 $\mu$ m		60 $\mu$ m		100 $\mu$ m		$cz$	$D$	$\log(L_{\text{fir}}, L_{\text{ir}})$			IG/AGN Names
Common	IRAS	hh:mm:ss.s	° : ' : "	°	°	(7)	Jy	mJy SMF	Jy	mJy SMF	Jy	mJy SMF	Jy	mJy SMF	km/s	Mpc	$L_{\odot}$	$L_{\odot}$	Rank	(17)
(1)	(2)	(3)	(4)	(5)	(6)	(7)	(8)	(8)	(9)	(9)	(10)	(10)	(11)	(11)	(12)	(13)	(14)	(15)	(16)	(17)
IRAS 05223+1908	2 05223+1908	05:25:16.3	+19:10:46	185.78	-9.14		0.97	37 UT	2.06	83 UT	5.37:	194 UPc	10.69:	1384 UPc	8867	116.77	11.30:	11.59:	56	
	LMC 2	---	R 05:23:34.5	-69:45:22	280.47	-32.89	2781.9	- RR	7824.2	- RR	82917.0	- RR	184686.	- RR	278	0.05 <sup>P</sup>	8.76	8.83	620	
	NGC 1964	2 F05312-2158	05:33:21.8	-21:56:44	225.27	-26.50	0.69	22 RI	1.02	26 RI	9.17	43 RI	23.48	110 MI	1663	18.65 <sup>S</sup>	9.99	10.09	506	
	NGC 1961	2 F05365+6921	05:42:03.9	+69:22:33	143.82	+19.47	0.90	27 RI	0.99	16 RI	7.17	41 RI	23.37	209 MI	3975	55.27	10.93	11.02	196	ARP184
	MCG+08-11-002	2 05368+4940	05:40:43.3	+49:41:41	161.67	+9.96	0.52	29 RI	1.08	48 MI	14.03	36 UT	24.82	183 UT	5743	77.22	11.32	11.41	89	
IRAS F05405+0035	N F05405+0035	* 05:43:05.5	+00:37:10	204.39	-14.87		0.33:	53 UPn	1.04:	37 UPn	7.03:	78 UPn	15.96:	2467 UPn	4290	57.68	10.83:	10.93:	222	
	UGC 03351	2 F05414+5840	05:45:48.6	+58:42:02	153.99	+15.01	0.55	26 RZ	0.86	36 UT	14.26	47 UT	29.46	120 UT	4445	60.87	11.15	11.22	134	
IRAS 05442+1732	2 05442+1732	05:47:10.7	+17:33:44	189.93	-5.58		0.50	34 RZ	1.70	43 UT	10.02	41 UT	12.73	249 UT	5613	74.95	11.08	11.25	127	
	NGC 2076	2 F05445-1648	05:46:47.9	-16:46:58	221.31	-21.64	0.71	26 RI	0.76	32 RI	7.03	36 RI	20.46	79 UT	2156	29.48	10.33	10.41	389	
	UGCA 116	N F05530+0323	* 05:55:42.0	+03:23:30	203.42	-10.78	0.45	26 UT	1.91	32 UT	6.57	166 UT	5.27	840 UT	789	11.64	9.28	9.47	595	IIZw040
	NGC 2139	2 F05590-2340	06:01:07.2	-23:40:25	229.53	-21.14	0.28	22 UT	0.86	18 RI	7.05	35 RI	14.05	121 UT	1843	25.11	10.06	10.16	479	AM0559-234
	UGC 03410	2 F06052+8027	06:14:27.0	+80:27:00	133.36	+25.21	S 0.71:	25 RIb	0.92:	19 RIb	9.87:	33 RIb	22.98:	161 MIb	3887	54.78	10.94:	11.04:	188	KPG108B
	ESO 121-G006	2 F06070-6147	06:07:29.5	-61:48:28	270.97	-28.82	0.58	13 RI	0.68	11 RI	6.11	18 RI	15.20	70 UT	1211	14.52	9.59	9.70	582	
IRAS F06076-2139	N F06076-2139	* 06:09:45.1	-21:40:22	228.35	-18.54		0.06	23 UT	0.63	16 UT	6.43	54 UT	8.47	180 UT	11226	148.80	11.51	11.59	58	
	NGC 2146	2 F06107+7822	06:18:39.8	+78:21:25	135.65	+24.90	* 6.83:	22 MI	18.81:	30 MI	146.69:	63 MI	194.05:	240 UT	885	16.47	10.93:	11.07:	171	KPG110A
	IC 2163	N F06142-2121	* 06:16:22.9	-21:22:20	228.69	-17.00	* 1.37:	23 RI	2.45:	24 RI	17.55:	26 RI	40.85:	140 MI	2688	36.93	10.84:	10.96:	212	
IRAS 06164+0311	2 06164+0311	06:19:02.7	+03:09:53	206.40	-5.74		1.14	26 RZ	0.85	30 UT	8.34	50 UT	24.88	460 UT	2902	40.17	10.68	10.79	264	
	UGCA 127	N F06185-0828	* 06:20:56.9	-08:29:42	217.11	-10.61	1.41	19 RI	1.62	24 RI	17.61	71 RI	39.38	532 MI	734	10.19	9.71	9.82	562	
	UGCA 128	N F06189-2001	* 06:21:05.4	-20:02:53	227.88	-15.47	0.54	19 RI	0.93	22 RI	5.38	39 RI	11.90	123 UT	1981	27.28	10.05	10.21	461	
	NGC 2221	N F06194-5733	06:20:16.0	-57:34:43	266.44	-26.72	S 0.30:	20 RIg	0.56:	17 UTg	6.41:	63 RZg	13.94:	125 RZb	2532	33.83	10.31:	10.39:	391	AM0619-573NED01
	ESO 5-G004	2 F06218-8636	06:05:36.5	-86:37:53	299.20	-27.75	0.61	11 UT	0.81	15 MI	7.48	25 UT	19.25	93 UT	1809	22.36	10.07	10.16	480	
	ESO 255-IG007	2 F06259-4708	06:27:21.1	-47:10:38	255.47	-23.45	U 0.32	13 UT	1.42	13 UT	9.05	24 UT	11.85	79 UT	11630	155.32	11.69	11.84	31	AM0626-470
	ESO 557-G002	N F06298-1735	* 06:31:46.3	-17:37:15	226.67	-12.16	U 0.17	18 RI	0.86	31 RI	7.42	28 RI	10.50	189 MI	6339	85.61	11.09	11.19	140	
	NGC 2280	2 F06428-2735	06:44:50.0	-27:38:23	237.31	-13.55	0.68	33 RI	0.85	17 RI	7.11	42 RI	18.78	140 MI	1906	21.54 <sup>S</sup>	10.02	10.13	492	AM0642-273
	NGC 2273	2 F06456+6054	06:50:07.8	+60:50:45	154.97	+23.31	0.44	31 UT	1.36	22 UT	6.41	46 UT	9.55	136 UT	1832	28.16	10.05	10.25	446	MRK0620
IRAS 06478-1111	2 06478-1111	06:50:11.2	-11:15:14	222.84	-5.38		0.41	49 UT	0.66	23 UT	5.96	82 UT	8.34:	1534 UPn	2602	36.36	10.24:	10.39:	390	
	UGC 3608	2 F06538+4628	06:57:34.0	+46:24:10	170.23	+20.28	0.41	27 RI	1.20	30 UT	8.05	37 UT	11.33	115 UT	6538	88.51	11.15	11.30	113	
IRAS F06592-6313	2 F06592-6313	06:59:40.3	-63:17:53	273.70	-23.14		0.14	16 UT	0.78	15 UT	5.74	23 UT	7.52	101 UT	6882	94.76	11.05	11.17	144	
	NGC 2268	2 F07007+8427	07:14:12.5	+84:22:58	129.24	+27.54	0.69	27 RI	0.72	20 RI	5.64	34 MI	14.48	110 UT	2222	30.24 <sup>S</sup>	10.21	10.34	412	
	AM 0702-601	N F07027-6011	07:03:27.5	-60:16:05	270.66	-21.89	R 0.43	13 RI	1.37	23 RI	6.70	23 RI	9.26	125 MI	9390	127.33	11.39	11.58	63	
	NGC 2339	2 F07054+1851	07:08:20.8	+18:46:46	197.84	+12.06	0.59	40 UT	2.40	38 MI	17.60	48 UT	31.82	146 UT	2206	32.10	10.65	10.76	274	
	NGC 2342	2 07063+2043	07:09:19.6	+20:38:12	196.20	+13.04	S 0.46:	25 UTg	1.64:	44 RZg	7.73:	37 UPg	24.10:	78 RIb	5276	72.21	11.18:	11.25:	126	
ESO 491-G020/021	2 07077-2729	07:09:47.0	-27:34:10	239.62	-8.51	R 0.91	0.91	36 RI	2.70	18 MI	15.23	52 UT	22.85	169 UT	2961	41.10	10.76	10.93	220	AM0707-273
	ESO 492-G002	2 07096-2637	07:11:40.7	-26:42:19	239.03	-7.75	0.41:	21 RIg	0.79:	21 UTg	7.94:	36 UPg	14.88:	397 UPg	2611	36.22	10.42:	10.53:	350	AM0709-263
	NGC 2276	2 F07104+8550	07:27:17.8	+85:45:16	127.67	+27.71	S 1.07:	23 RI	1.63:	26 RI	14.29:	58 RI	28.97:	133 UT	2380	35.83	10.68:	10.81:	257	ARP025-VIIZw134,KPG127A
	NGC 2350	2 F07104+1221	07:13:11.9	+12:15:58	204.35	+10.33	0.25	32 UT	0.96	41 UT	6.31	82 UT	8.45	451 UT	1910	28.04	10.03	10.17	476	
	NGC 2369	2 F07160-6215	07:16:37.7	-62:20:35	273.31	-21.01	0.74	27 UT	2.20	18 UT	20.35	32 UT	38.31	146 UT	3237	44.02	11.00	11.10	162	AM071 6-621
ESO 428-G023	2 07202-2908	07:22:10.7	-29:14:13	242.36	-6.83		0.45	21 RI	1.36	21 MI	9.94	62 UT	17.69	873 UT	3026	42.07	10.63	10.76	275	
	UGC 03829	2 F07204+3332	07:23:43.1	+33:26:32	185.05	+20.83	0.42	26 RI	1.73	52 RI	6.95	43 UT	8.91	165 UT	4031	56.37	10.67	10.88	239	MRK1199
	NGC 2397	2 F07214-6854	07:21:19.5	-69:00:02	280.30	-22.60	0.73	11 RI	1.08	13 RI	8.48	33 MI	19.18	206 UT	1355	16.08	9.79	9.92	544	AM0721-685
	ESO 428-G028	2 07216-2957	07:23:38.3	-30:03:08	243.24	-6.92	0.45	22 RI	0.78	18 RI	6.10	26 MI	14.82	262 UT	2258	31.08	10.24	10.35	408	
IRAS 07251-0248	2 07251-0248	07:27:37.5	-02:54:55	219.69	+6.69		<0.07	-	0.66	33 UT	6.49	32 UT	6.35	330 UT	26257	343.74	12.27	12.32:	4	
	NGC 2388	2 F07256+3355	07:28:54.2	+33:49:07	185.05	+21.97	S 0.69:	38 RZg	1.98:	57 UTg	16.74:	42 UPg	24.58:	152 UPg	4134	57.80	11.10:	11.23:	133	
	NGC 2403	2 F07320+6543	07:36:51.3	+65:36:30	150.56	+29.19	2.82	24 RZ	3.57	55 RZ	41.47	81 RZ	99.13	212 RI	161	3.22 <sup>P</sup>	9.10	9.19	608	
	MCG+02-20-003	2 F07329+1149	07:35:42.5	+11:42:36	207.29	+15.06	R 0.26:	26 UTg	0.81:	40 UTg	9.38:	39 UTg	13.33:	110 UPg	4881	67.63	10.98:	11.08:	166	
	NGC 2415	2 F07336+3521	07:36:56.0	+35:14:31	184.14	+23.98	0.61	31 RI	1.19	34 RI	8.75	33 UT	13.58	70 UT	3784	53.41	10.76	10.92	224	
	NGC 2442	2 F07365-6924	07:36:25.9	-69:31:17	281.29	-21.50	1.62	16 RZ	1.83	11 RZ	14.85	30 RI	46.61	163 RI	1449	17.33	10.22	10.30	428	AM0736-692
ESO 163-G011/010	2 F07369-5504	07:38:04.3	-55:11:27	267.42	-15.77	S 0.40	0.40	17 UT	0.75	18 RI	6.18	34 RI	13.27	124 UT	2828	38.07	10.39	10.50	358	AM0737-550
	ESO 209-G009	2 F07568-4942	07:58:14.9	-49:51:09	264.01	-10.58	0.87	16 RI	1.29	21 RI	12.09	53 RI	31.84	792 RI	1119	11.81 <sup>S</sup>	9.73	9.81	564	AM0756-494
	NGC 2525	2 F08032-1117	08:05:37.9	-11:25:40	231.85	+10.79	0.68	38 RI	0.89											

TABLE 1—Continued

Name		R.A. (J2000) DEC		$l$	$b$	HR	$12\mu\text{m}$		$25\mu\text{m}$		$60\mu\text{m}$		$100\mu\text{m}$		$c_z$	$D$	$\log(L_{\text{fir}}, L_{\text{ir}})$			IG/AGN Names				
Common	IRAS	hh:mm:ss.s	° : ' "	°	°	(7)	Jy	mJy	SMF	Jy	mJy	SMF	Jy	mJy	SMF	Jy	mJy	SMF	km/s	Mpc	$L_{\odot}$	$L_{\odot}$	Rank	(17)
(1)	(2)	(3)	(4)	(5)	(6)	(7)	(8)	(8)	(9)	(9)	(10)	(10)	(11)	(11)	(12)	(12)	(13)	(13)	(14)	(15)	(16)			
	NGC 2566	2 08166-2520	08:18:45.6	-25:29:59	245.55	+5.88	1.26	27	RI	4.03	25	MI	24.33	50	RI	37.23	174	UT	1637	22.43	10.44	10.60	330	AM0816-252
	NGC 2613	2 F08311-2248	08:33:23.2	-22:58:28	245.36	+10.06	1.05	29	MI	1.32	16	RZ	7.48	39	RI	25.86	152	UT	1678	20.18 <sup>S</sup>	10.09	10.18	470	AM0831-224
	IRAS F08339+6517	1 F08339+6517	08:38:22.7	+65:07:14	150.45	+35.60	0.25	25	UT	1.13	21	UT	5.81	35	UT	6.48	88	UT	5730	79.33	10.89	11.05	181	
	NGC 2623	1 F08354+2555	08:38:23.8	+25:45:17	198.84	+33.97	0.21	23	UT	1.81	41	UT	23.74	28	UT	25.88	111	UT	5538	77.43	11.48	11.54	72	ARP243,VV079
	IRAS 08355-4944	2 08355-4944	08:37:02.3	-49:54:32	267.52	-5.39	0.64	25	RZ	2.27	25	UT	9.44	47	UT	8.02	809	UT	7764	107.50	11.38	11.56	67	
	ESO 432-IG006	2 08424-3130	08:44:27.6	-31:41:41	253.92	+6.83	U 0.58	23	MI	0.84	27	UT	6.48	42	MI	9.31	319	UT	4846	68.55	10.83	11.02	195	
	NGC 2633	1 F08425+7416	08:48:05.0	+74:05:55	139.68	+33.87	0.92	20	RZ	2.47	26	MI	15.98	32	UT	25.43	113	UT	2187	33.65	10.62	10.77	268	ARP080,VV519,KPG169
	NGC 2665	2 F08437-1907	08:46:00.3	-19:18:08	244.07	+14.59	0.29	34	UT	1.09	25	UT	6.43	42	UT	9.62	195	UT	1734	24.35	9.93	10.08	507	
	ESO 563-G028	2 F08485-2146	08:50:45.1	-21:57:45	246.96	+13.89	0.36	24	UT	0.81	21	MI	8.21	27	UT	15.84	152	UT	2574	36.31	10.44	10.54	345	
	NGC 2683	1 F08495+3336	08:52:40.1	+33:25:23	190.45	+38.76	1.05	30	RI	1.15	38	RZ	9.70	39	RI	30.68	185	RI	425	7.34 <sup>S</sup>	9.28	9.36	601	
	NGC 2681	1 F08499+5130	08:53:33.6	+51:18:46	167.33	+39.68	0.43	24	RI	0.58	26	UT	7.14	41	UT	11.22	74	UT	642	12.47	9.40	9.53	590	
	ESO 60-IG016	2 F08520-6850	08:52:31.1	-69:01:59	284.24	-15.38	0.15:	16	UPn	0.73	15	MI	5.71	28	UT	6.12	139	UT	13888	186.88	11.65	11.76:	38	AM0852-685
	NGC 2706	2 F08536-0222	08:56:12.2	-02:33:47	230.81	+26.11	0.56	25	RI	0.59	32	RZ	6.64	28	MI	14.01	80	UT	1631	24.36	10.02	10.15	485	
	IRAS F08572+3915	1 F08572+3915	09:00:25.0	+39:03:56	183.40	+41.00	0.33	31	UT	1.76	33	UT	7.30	28	UT	4.77	152	UT	17455	232.19	12.01	12.10	15	
	ESO 564-G011	2 F09004-2031	09:02:45.9	-20:43:28	247.73	+16.85	0.52	28	RI	1.32	26	UT	8.95	29	UT	11.41	132	UT	2596	36.73	10.41	10.57	336	
	IRAS 09022-3615	2 09022-3615	09:04:12.8	-36:27:02	260.24	+6.95	0.20	32	UT	1.19	20	UT	11.64	57	UT	11.08	356	UT	17880	238.84	12.19	12.26	8	
	NGC 2748	1 F09080+7640	09:13:44.5	+76:28:31	136.25	+34.36	0.60	31	RI	0.87	28	RI	8.02	36	RI	17.88	393	UT	1477	24.68	10.13	10.25	445	
	UGCA 150 N	F09083-0841	09:10:49.5	-08:53:36	238.91	+25.59	0.64	32	RI	0.73	27	RI	6.03	29	RI	20.65	126	RI	1838	26.85	10.24	10.30	426	
	NGC 2782	1 F09109+4019	09:14:05.7	+40:06:47	182.15	+43.68	0.64	38	RI	1.51	36	UT	9.17	52	UT	13.76	139	UT	2600	39.51	10.51	10.68	302	ARP215
	IRAS F09111-1007	2 F09111-1007	09:13:37.6	-10:19:28	240.64	+25.30	U 0.11	24	MI	0.74	40	RI	6.75	37	UT	10.68	246	UT	16273	218.20	11.91	12.00	21	
	NGC 2785	1 F09120+4107	09:15:16.7	+40:54:57	181.04	+43.91	0.49	30	UT	1.09	32	UT	8.40	23	UT	15.79	116	UT	2734	41.27	10.56	10.69	300	
	ESO 126-G002	2 09122-6034	09:13:30.2	-60:47:24	279.26	-8.38	0.54	25	UT	2.04	17	UT	11.61	77	UT	15.39	179	UT	2858	37.25	10.54	10.70	296	
	UGC 04881	1 F09126+4432	09:15:54.8	+44:19:58	176.30	+43.94	0.14	37	UT	0.61	34	UT	6.07	48	UT	10.33	109	UT	11957	161.16	11.60	11.69	43	ARP055,VV155,Grasshopper
	NGC 2798	1 F09141+4212	09:17:24.5	+41:59:52	179.53	+44.30	S 0.76	22	UT	3.21	31	UT	20.60	48	UT	29.69	156	UT	1706	27.84	10.55	10.69	301	ARP283NED01,VV050a,KPG195A
	NGC 2856	1 F09209+4927	09:24:17.2	+49:14:53	169.24	+44.81	S 0.35	31	UTg	0.94:	26	UTg	5.73:	39	UPg	10.15:	140	UPg	2638	40.08	10.35:	10.50:	359	ARP285NED02
	NGC 2903	1 F09293+2143	R 09:32:10.5	+21:30:05	208.71	+44.54	5.29	35	RZ	8.64	69	RZ	60.54	52	RI	130.43	208	RI	566	8.26 <sup>S</sup>	10.05	10.19	469	
	UGC 05101	1 F09320+6134	09:35:48.8	+61:21:22	152.48	+42.89	0.25:	27	UPn	1.02	27	UT	11.68	34	UT	19.91	137	UT	11785	158.61	11.87	11.95:	22	
	MCG+08-18-013	1 F09333+4841	09:36:39.3	+48:28:19	169.79	+46.96	S 0.10	19	UT	0.75	28	UT	5.68	28	UT	8.42	143	UT	7777	107.06	11.18	11.28	118	
	ESO 091-G016	2 09369-6315	09:38:13.6	-63:29:12	283.25	-8.26	0.31	16	UT	0.79	19	UT	6.63	24	UT	10.11	97	UT	2162	26.56	10.02	10.15	484	
	NGC 2967	1 F09395+0033	09:42:04.2	+00:20:09	235.38	+37.28	0.64	33	RI	1.09	40	RZ	5.69	27	RI	14.48	738	UT	1892	28.65	10.16	10.31	424	
	NGC 2966	1 F09395+0454	09:42:11.2	+04:40:22	230.76	+39.68	0.46	34	RI	0.80	40	UT	5.36	48	UT	8.24	234	UT	2044	31.16	10.07	10.25	441	MRK0708
	NGC 2964	1 F09399+3204	09:42:55.3	+31:50:44	194.62	+49.02	0.82	29	MI	1.92	43	RI	12.07	31	UT	25.42	110	UT	1332	22.82	10.23	10.36	402	MRK0404,KPG210A
	NGC 2976	1 F09431+6809	09:47:14.5	+67:55:10	143.91	+40.90	0.92	20	RI	1.71	20	RI	13.09	29	RI	33.43	344	UT	11	2.68	8.46	8.55	623	
	NGC 2992	N 09432-1405	09:45:42.0	-14:19:35	249.71	+28.78	S 0.63	25	RI	1.38:	34	UPn	7.51:	46	UPn	17.22:	146	RIb	2314	33.15	10.37:	10.52:	353	ARP245NED01
	NGC 2993	2 F09433-1408	09:45:47.3	-14:21:58	249.76	+28.77	S 0.63	22	RZ	1.61:	42	UPn	10.58:	53	UPn	23.07:	237	RIb	2420	34.69	10.55:	10.67:	307	ARP245NED02
	IC 0563/4	1 F09437+0317	09:46:20.3	+03:03:22	233.26	+39.69	S 0.46	21	RI	0.54	39	RI	5.26:	26	RIb	12.18:	58	RIb	6136	87.01	11.07:	11.19:	142	ARP303
	NGC 2985	1 F09458+7230	09:50:20.7	+72:16:47	139.01	+38.68	0.90	20	RI	0.86	17	RI	6.31	38	RI	21.28	118	MI	1322	22.92	10.12	10.21	457	
	NGC 3059	2 F09496-7341	09:50:08.1	-73:55:24	291.15	-15.36	1.06	20	RI	1.62	18	RI	13.52	32	RI	30.51	94	MI	1260	14.24	9.88	10.00	526	
	NGC 3044	1 F09510+0149	09:53:40.0	+01:34:53	236.19	+40.37	0.60	22	MI	1.11	86	UT	9.64	30	UT	19.38	89	UT	1292	19.98	10.00	10.12	494	
	NGC 3031	1 F09514+6918	R 09:55:33.6	+69:03:56	142.09	+40.90	5.86	-	RR	5.42	-	RR	44.73	-	RR	174.02	-	RR	-34	3.63 <sup>P</sup>	9.42	9.47	594	KPG218A
	NGC 3034	1 F09517+6954	R 09:55:53.1	+69:40:41	141.41	+40.57	79.43	34	RZ	332.63	46	RZ	1480.42	74	MI	1373.69	694	RI	187	3.63 <sup>P</sup>	10.61	10.77	270	ARP337,KPG218B
	IC 2522	N F09529-3253	09:55:07.3	-33:08:04	265.49	+16.63	S 0.43:	37	RIg	0.64:	26	RIg	6.47:	44	RZg	18.06:	219	RZg	3012	41.16	10.57:	10.63:	317	AM0952-325NED02
	NGC 3067	1 F09554+3236	09:58:20.3	+32:22:19	194.22	+52.32	0.60	21	UT	1.17	38	MI	8.91	30	UT	18.11	104	UT	1476	25.09	10.17	10.30	427	
	UGC 5376	1 F09578+0336	10:00:26.5	+03:22:29	235.52	+42.79	0.29	23	UT	0.62	48	UT	5.36	50	UT	10.41	267	UT	2050	31.28	10.13	10.24	448	
	NGC 3095	2 F09578-3118	10:00:06.2	-31:33:15	265.27	+18.51	0.40	33	MI	1.00	28	MI	8.33	42	UT	16.22	185	UT	2723	36.86	10.46	10.57	335	AM0957-311
	NGC 3079	1 F09585+5555	10:01:57.9	+55:40:51	157.81	+48.36	2.54	30	RI	3.61	27	RI	50.67	64	RI	104.69	141	MI	1142	18.19 <sup>S</sup>	10.65	10.73	282	
	NGC 3094	1 F09587+1600	10:01:25.5	+15:46:15	220.09	+49.06	0.82	32	UT	2.89	62	UT	10.88	44	UT	13.89	71	UT	2404	37.04	10.50	10.73	285	
	NGC 3077	1 F09593+6858	10:03:19.5	+68:43:59	141.90	+41.66	0.76	23	RI	1.88	25	UT	15.90	39	MI	26.53	132	MI	-5	2.46	8.35	8.47	624	
	NGC 3110	1 F10015-0614	10:04:02.7	-06:28:35	246.38	+37.39	0.59:	35	UPg	1.13:	48	UPg	11.28:	33	UPg	22.27:	85	UPg	5091	73.48	11.21:	11.31:	111	
	IC 2545	2 F10038-3338	10:06:04.2	-33:53:04	267.84	+17.49	* 0.28	28	UT	1.21	29	UT	9.79	66	UT	9.02	263	UT	10267	141.58	11.64	11.73	41	AM1003-333

TABLE 1—*Continued*

Name		R. A. (J2000) DEC		$\ell$	$b$	HR	12 $\mu$ m		25 $\mu$ m		60 $\mu$ m		100 $\mu$ m		$cz$	$D$	$\log(L_{\text{fir}}, L_{\text{IR}})$			IG/AGN Names				
Common	IRAS	hh:mm:ss.s	° : ' : "	°	°	(7)	Jy	mJy	SMF	Jy	mJy	SMF	Jy	mJy	SMF	Jy	mJy	SMF	km/s	Mpc	$L_{(4)}$	$L_{(15)}$	Rank	(17)
(1)	(2)	(3)	(4)	(5)	(6)		(8)	(9)		(10)	(11)		(12)	(13)	(14)	(15)	(16)							
NGC 3125	N F10042-2941	10:06:32.3	-29:56:06	265.33	+20.65		0.31	25	RI	0.74	36	UT	5.33	31	MI	6.67:	396	UTc	865	9.39	8.99:	9.15:	611	AM1004-294
IC 2554	2 10075-6647	10:08:50.4	-67:01:53	288.02	-8.99		1.10	21	MI	2.71	20	UT	16.96	34	UT	34.84	264	MI	1378	15.72	10.04	10.18	474	AM1007-664
NGC 3166	1 F10111+0340	10:13:44.4	+03:25:38	238.14	+45.52	S	0.29	28	UT	0.32	57	UT	5.78	44	UT	13.25	136	UT	1345	21.27	9.87	9.94	540	KPG228A
NGC 3169	1 F10116+0342	10:14:15.2	+03:27:57	238.20	+45.65	S	1.15	31	RI	0.94	28	RI	7.88	38	RI	22.06	83	MI	1305	20.61	10.05	10.18	472	KPG228B
NGC 3175	2 F10124-2837	10:14:42.9	-28:52:25	266.12	+22.58		1.06	23	RI	1.67	22	RI	13.70	37	RI	31.49	70	UT	1101	13.45	9.85	9.96	532	VV796;AM1012-283
NGC 3147	1 F10126+7338	10:16:55.4	+73:23:54	136.29	+39.47		1.95	21	RZ	1.03	16	RI	8.17	38	RI	29.61	222	MI	2756	41.41	10.78	10.91	229	
NGC 3177	1 F10138+2122	10:16:33.5	+21:07:27	214.02	+54.30		0.66	30	RI	1.30	39	RI	9.20	30	UT	16.78	105	UT	1302	22.34	10.05	10.20	465	MRK9018
NGC 3184	1 10152+4140	10:18:12.1	+41:25:53	178.33	+55.62		0.93	32	RI	1.32	25	RI	8.72	29	RI	28.58	118	RI	593	12.58 <sup>S</sup>	9.72	9.80	567	
NGC 3198	1 F10168+4547	10:19:55.6	+45:32:54	171.22	+54.83		0.71	21	RI	1.08	29	RI	7.15	41	RI	18.44	103	RI	663	13.79 <sup>P</sup>	9.62	9.75	576	
IRAS F10173+0828	1 F10173+0828	10:20:00.1	+08:13:31	233.59	+49.52		0.19	29	RI	0.55	49	MI	5.61	25	UT	5.86	100	UT	14669	198.65	11.70	11.80	34	
NGC 3221	1 F10196+2149	10:22:20.5	+21:34:10	213.98	+55.71		0.52	29	RI	0.93	46	RI	7.72	55	MI	18.76	70	UT	3971	58.68	10.90	11.00	200	
NGC 3227	1 F10207+2007	10:23:31.4	+19:51:50	217.00	+55.45	S	0.94	21	RI	1.83	45	UT	8.42	35	RI	17.30	131	UT	1157	19.81	9.94	10.13	487	ARP094NED02;VV209a;KPG234B
ESO 500-G034	2 F10221-2318	10:24:32.4	-23:33:17	264.50	+28.14		0.38	30	RI	1.43	32	MI	10.46	22	UT	16.01	131	UT	3662	52.10	10.81	10.94	218	
ESO 317-G023	2 F10225-3903	10:24:43.4	-39:18:29	274.31	+15.27		0.34	33	UT	0.89	19	UT	13.83	49	UT	23.08	172	UT	2892	37.69	10.67	10.74	278	
NGC 3256	2 F10257-4339	10:27:52.4	-43:54:25	277.38	+11.73		3.57	31	MI	15.69	45	UT	102.63	52	MI	114.31	296	UT	2781	35.35	11.43	11.56	66	VV065;AM1025-433
NGC 3263	2 F10270-4351	10:29:12.3	-44:07:13	277.70	+11.67	S	0.53	22	UT	0.91	29	UT	8.59	54	UT	19.00	112	UT	3015	38.79	10.56	10.66	308	AM1027-435
NGC 3278	2 F10293-3941	10:31:35.7	-39:57:25	275.82	+15.44		0.59	16	RI	0.91	25	RZ	7.10	21	MI	14.66	75	UT	2961	38.41	10.45	10.59	332	
NGC 3281	2 F10295-3435	10:31:52.1	-34:51:14	273.01	+19.78		0.91	33	UT	2.63	31	UT	6.73	27	UT	7.89	152	UT	3200	42.91	10.42	10.73	283	AM1029-343
NGC 3294	1 F10333+3735	10:36:15.3	+37:19:29	184.62	+59.84		0.86	29	RI	0.69	27	UT	5.98	32	UT	16.58	109	UT	1586	23.69 <sup>S</sup>	10.05	10.18	473	
NGC 3310	1 F10356+5345	10:38:46.2	+53:30:08	156.60	+54.06		1.54	32	RI	5.32	28	MI	34.56	54	MI	44.19	172	UT	1060	19.81	10.45	10.61	326	ARP217;VV356;VV406
NGC 3344	1 F10407+2511	10:43:31.5	+24:55:18	210.04	+61.26		1.01	25	RI	1.35	50	RZ	9.71	74	RI	28.92	268	RI	556	6.70	9.18	9.28	605	
ESO 264-G036	2 F10409-4556	10:43:07.0	-46:12:43	280.94	+11.11		0.36	30	UT	0.67	41	UT	6.07	61	UT	13.37	564	UT	7000	100.50	11.25	11.35	100	
NGC 3351	1 F10413+1157	10:43:58.1	+11:42:10	233.95	+56.37		1.04	34	RI	2.79	53	RI	19.66	62	MI	41.10	102	MI	769	9.99 <sup>P</sup>	9.72	9.83	559	
NGC 3359	1 F10433+6329	10:46:36.6	+63:13:25	143.60	+48.59		0.44	16	RI	0.54	21	RI	6.49	42	RI	17.16	145	RI	971	16.81 <sup>S</sup>	9.76	9.83	558	
NGC 3367	1 F10439+1400	10:46:35.2	+13:45:02	231.31	+57.97		0.51	49	UT	1.98	51	RZ	6.44	37	RI	13.48	86	UT	3039	46.13	10.57	10.76	273	
NGC 3368	1 F10441+1205	10:46:45.6	+11:49:13	234.43	+57.01		0.98	36	RI	0.51	50	MI	10.51	64	RI	31.63	148	MI	916	10.51 <sup>P</sup>	9.61	9.67	584	
NGC 3395/6	1 F10470+3315	10:49:52.2	+32:59:18	192.91	+63.15	S	0.47	27	RI	1.47	44	RI	10.92	33	RI	17.83	97	MI	1623	27.85	10.29	10.42	387	ARP270;VV246
NGC 3424	1 F10489+3310	10:51:46.0	+32:54:03	193.03	+63.55	S	0.52	29	UT	0.92	40	UT	8.44	57	UT	17.05	163	UT	1494	26.17	10.18	10.30	430	
NGC 3432	1 F10497+3653	10:52:32.7	+36:37:30	184.76	+63.17		0.25	27	RI	0.43	29	RI	8.42	42	RI	16.01	139	RI	616	9.48 <sup>S</sup>	9.28	9.34	603	ARP206NED02;VV011a
NGC 3437	1 F10498+2311	10:52:36.8	+22:55:58	215.19	+62.82		0.68	32	RI	1.35	36	MI	10.91	43	UT	20.29	176	UT	1239	22.23	10.13	10.26	439	
NGC 3448	1 F10516+5434	10:54:38.7	+54:18:25	153.05	+55.45	S	0.22	20	RZ	0.64	30	UT	6.64	27	MI	11.17	80	UT	1350	24.06	9.96	10.06	513	ARP205
NGC 3471	1 F10560+6147	10:59:08.7	+61:31:53	143.73	+50.82		0.33	15	UT	1.26	17	MI	8.31	32	UT	12.21	141	UT	2129	34.07	10.33	10.47	368	MRK0158
IRAS F10565+2448	1 F10565+2448	10:59:17.4	+24:32:38	212.45	+64.69		0.20	30	UT	1.27	31	MI	12.10	25	UT	15.01	122	UT	12927	176.26	11.93	12.02	17	
ESO 264-G057	2 F10567-4310	10:59:02.4	-43:26:33	282.21	+14.86	S	0.34	23	UT	0.81	29	UT	5.69	37	UT	12.16:	746	UPc	5156	75.74	10.96:	11.08:	168	AM1056-430NED01;AM1056-431
ESO 093-G003	2 10574-6603	10:59:22.8	-66:19:23	292.00	-5.86		0.67	20	RI	1.00	26	MI	10.05	62	MI	17.89	532	UT	1890	22.07	10.07	10.21	460	
NGC 3486	1 F10576+2914	11:00:23.6	+28:58:38	202.07	+65.49		0.62	28	RI	0.24	46	RI	6.26	34	RI	16.42	88	MI	682	9.23	9.22	9.31	604	
NGC 3504	1 F11004+2814	11:03:11.1	+27:58:22	204.60	+66.04		1.11	30	UT	4.03	45	MI	21.43	52	UT	34.05	86	UT	1550	27.07	10.56	10.72	289	
NGC 3508	1 F11005-1601	11:03:00.1	-16:17:23	268.55	+39.24		0.52	34	RI	0.91	48	UT	6.82	52	UT	13.90	207	UT	3889	56.26	10.76	10.90	232	
NGC 3511	1 F11009-2249	11:03:24.2	-23:05:15	272.90	+33.41	U	1.03	47	RI	0.83	27	RI	8.98	67	RI	21.87	197	MI	1106	13.60	9.69	9.82	561	AM1100-224
MCG+07-23-019	1 F11011+4107	11:03:54.2	+40:50:58	174.19	+63.99	U	0.20	19	RI	0.71	22	RI	6.38	34	UT	10.30	106	UT	10438	143.21	11.51	11.61	52	AR P148;VV032;Mayall's Object
NGC 3521	1 F11032+0014	11:05:49.2	-00:02:15	255.54	+52.83		5.04	70	RI	5.46	82	RI	49.19	100	RI	121.76	405	RI	736	6.84	9.84	9.96	534	
ESO 265-G007	2 F11055-4615	11:07:48.8	-46:31:38	284.99	+12.70		0.54	28	RI	0.84	28	RI	6.45	36	RI	17.78	204	UT	1067	11.66	9.46	9.55	589	AM1105-461
ESO 215-G031	2 F11082-4849	11:10:34.7	-49:06:05	286.45	+10.52		0.33	21	UT	0.72	13	UT	5.38	88	UT	10.12	306	UT	2722	32.40	10.15	10.29	432	
NGC 3568	2 F11084-3710	11:10:50.4	-37:27:05	281.71	+21.24		0.93	59	RI	1.05	22	RI	8.03	40	RI	15.95	267	UT	2445	30.06	10.27	10.45	374	
NGC 3556	1 F11085+5556	11:11:31.5	+55:40:23	148.31	+56.25		2.29	27	RI	4.19	27	RI	32.55	68	RI	76.90	231	RI	698	13.85	10.26	10.37	400	
NGC 3583	1 F11113+4835	11:14:09.7	+48:19:12	158.12	+61.63		0.60	26	MI	0.77	23	UT	7.43	36	RI	17.92	106	UT	2168	35.09	10.43	10.54	347	
NGC 3593	1 F11120+1305	11:14:37.4	+12:49:02	240.43	+63.21		1.52	43	MI	1.96	69	UT	18.47	47	UT	36.44	87	UT	578	5.04	9.08	9.22	607	
NGC 3597	1 F11122-2327	11:14:40.9	-23:43:33	276.02	+34.04		0.67	28	RI	2.18	44	RZ	12.84	36	UT	16.21	126	UT	3485	48.31	10.80	10.97	206	AM1112-232
NGC 3620	2 F11143-7556	11:16:04.1	-76:12:54	297.22	-14.41		1.29	20	MI	4.74	23	MI	45.75	60	UT	67.17	649	UT	1680	19.66	10.59	10.70	297	
NGC 3621	2 F11158-3232	11:18:16.7	-32:48:47	281.21	+26.10		3.53	25	RZ	4.44	48	RZ	29.32	44	RI	77.34	144	RI	727	6.64 <sup>P</sup>	9.61	9.74	577	AM1115-323

TABLE 1—*Continued*

Name		R. A. (J2000)	DEC	$\ell$	$b$	HR	$12\mu m$		$25\mu m$		$60\mu m$		$100\mu m$		$cz$	$D$	$\log(L_{fIR}, L_{iR})$			IG/AGN Names				
Common	IRAS	hh:mm:ss.s	° : ' : "	°	°		Jy	mJy	SMF	Jy	mJy	SMF	Jy	mJy	SMF	Jy	mJy	SMF	km/s	Mpc	$L_{\odot}$	$L_{\odot}$	Rank	
(1)	(2)	(3)	(4)	(5)	(6)	(7)	(8)	(9)	(10)	(11)	(12)	(13)	(14)	(15)	(16)					(17)				
NGC 3627	1F11176+1315	11:20:15.3	+12:59:32.241.96	+64.42			4.82	35	RI	8.55	71	RZ	66.31	59	RI	136.56	118	RI	740	10.04 <sup>P</sup>	10.24	10.38	395	ARP317NED02;VV308a
NGC 3628	1F11176+1351	11:20:17.4	+13:35:19.240.86	+64.78			3.13	48	MI	4.85	63	UT	54.80	77	MI	105.76	240	UT	825	10.04 <sup>P</sup>	10.14	10.25	442	ARP317NED03;VV308b
NGC 3631	1F11182+5326	11:21:01.2	+53:10:18.149.53	+59.03			1.07	23	RI	1.45	32	RI	9.71	40	RI	27.64	128	MI	1158	21.58	10.19	10.30	429	ARP027;VV363
CGCG 011-076	1F11186-0242	11:21:13.3	-02:59:08.263.57	+52.85			0.48	39	RI	0.76	50	UT	5.85	57	MI	9.18	253	UT	7464	106.27	11.20	11.37	94	
NGC 3655	1F11202+1651	11:22:53.5	+16:35:28.235.58	+66.96			0.67	45	MI	1.15	46	RI	8.48	49	MI	19.75	160	UT	1473	26.42	10.23	10.35	407	
NGC 3672	1F11224-0931	11:25:01.6	-09:47:34.270.42	+47.55			1.01	39	RI	0.95	59	RI	9.23	62	RI	25.69	248	MI	1899	27.70	10.37	10.47	366	
IC 2810	1F11231+1456	11:25:47.3	+14:40:23.240.61	+66.50	R		0.14	34	UT	0.62	62	UT	6.20	38	UT	10.39	136	UT	10299	142.89	11.50	11.59	61	
NGC 3675	1F11234+4351	11:26:09.0	+43:35:04.163.66	+66.19			1.43	20	RI	1.67	37	RI	10.48	40	RI	36.56	199	MI	804	12.69 <sup>S</sup>	9.84	9.92	543	
NGC 3683	1F11246+5709	11:27:30.6	+56:52:44.143.82	+56.71			1.16	34	MI	1.48	20	UT	13.87	47	UT	29.30	95	UT	1716	29.06	10.50	10.63	318	
ESO 319-G022	2F11255-4120	11:27:56.1	-41:37:06.286.61	+18.59			0.16	34	UT	0.95	31	UT	7.68	30	UT	9.52	186	UT	4902	72.26	10.93	11.04	185	AM1125-412
NGC 3690/IC 694	1F11257+5850	11:28:32.6	+58:33:40.141.90	+55.41	U		3.97	20	MI	24.51	31	MI	113.05	52	UT	111.42	133	UT	3159	47.74	11.74	11.88	27	MRK171;ARP299;VV118;KPG288
NGC 3717	2F11290-3001	11:31:31.2	-30:18:24.283.13	+29.47			0.85	26	RI	1.32	40	RI	11.92	29	RI	26.04	92	MI	1733	21.39 <sup>S</sup>	10.18	10.29	431	AM1129-300
NGC 3726	1 11306+4718	11:33:19.9	+47:01:49.155.38	+64.88			0.70	27	RI	0.88	22	RI	6.21	25	RI	20.91	117	RI	851	14.53 <sup>S</sup>	9.71	9.78	569	
NGC 3732	NF11316-0934	11:34:13.4	-09:50:40.273.45	+48.56			0.25	28	UT	0.71	43	UT	5.36	26	MI	7.75	144	UT	1692	25.08	9.87	10.01	522	
NGC 3735	1F11330+7048	11:35:57.4	+70:32:08.131.74	+45.28			0.64	31	UT	1.12	18	UT	6.71	43	UT	17.83	90	UT	2696	36.04 <sup>S</sup>	10.45	10.57	339	
NGC 3810	1F11383+1144	11:40:57.8	+11:28:18.252.93	+67.22			1.46	39	RI	1.62	58	RI	13.63	42	RI	35.07	157	MI	1001	15.36 <sup>S</sup>	10.00	10.12	495	
NGC 3877	1F11434+4746	11:46:08.0	+47:29:38.150.72	+65.96			0.85	18	RI	1.10	29	RI	7.72	21	RI	22.42	53	RI	903	15.14 <sup>S</sup>	9.78	9.89	550	
NGC 3882	2 11436-5606	11:46:04.0	-56:23:12.293.93	+5.34			1.51	28	RZ	2.67	26	RZ	19.84	117	RI	37.38	627	UT	1817	20.62	10.32	10.47	367	
NGC 3885	1F11442-2738	11:46:45.1	-27:55:10.285.91	+32.80			0.57	32	RI	1.47	58	UT	11.89	44	UT	16.25	190	UT	1802	22.93	10.13	10.27	437	AM1144-273
NGC 3887	1F11445-1634	11:47:04.0	-16:51:00.281.54	+43.33			0.59	30	RI	0.67	31	RI	5.84	45	RI	16.81	145	MI	1208	16.07	9.71	9.80	565	
NGC 3893	1F11459+4859	11:48:37.7	+48:42:45.148.16	+65.23	S		1.45	27	RI	1.65	31	RI	15.57	54	RI	36.80	63	UT	892	16.35 <sup>S</sup>	10.08	10.20	464	KPG302A
NGC 3938	1F11502+4423	11:52:49.2	+44:07:14.153.88	+69.32			0.90	29	RI	1.23	20	RI	9.18	29	RI	27.50	77	RI	800	14.75	9.85	9.93	542	
ESO 320-G030	2F11506-3851	11:53:12.0	-39:07:54.290.76	+22.36			0.53	21	UT	2.28	28	UT	34.38	71	UT	46.28	225	UT	3232	37.70	11.02	11.10	161	
NGC 3949	1F11510+4808	11:53:42.0	+47:51:31.147.63	+66.41			0.79	23	MI	1.26	24	RI	11.29	34	MI	24.40	133	UT	810	13.61 <sup>S</sup>	9.75	9.87	551	
NGC 3953	1 11511+5236	11:53:48.4	+52:19:44.141.74	+63.02			1.10	18	RZ	1.19	35	RI	7.11	45	RZ	31.12	86	RZ	1016	17.58 <sup>S</sup>	10.05	10.09	503	
NGC 3955	1F11514-2253	11:53:57.5	-23:09:52.286.14	+37.83			1.05	53	RI	1.31	36	RI	8.34	47	UT	17.56	514	UT	1491	19.78	9.94	10.12	493	AM1151-225
NGC 3981	1F11535-1937	11:56:07.1	-19:53:49.285.58	+41.10			0.65	26	RI	0.84	42	RI	7.14	27	RI	20.72	142	MI	1723	23.37	10.13	10.21	456	ARP289;VV008
NGC 3982	1F11538+5524	11:56:27.3	+55:07:36.138.83	+60.27			0.47	20	RZ	0.97	26	RI	7.18	38	MI	16.24	142	UT	1109	21.04	9.95	10.06	511	
NGC 3994/5	1F11551+3233	11:57:41.0	+32:17:10.185.85	+77.25	S		0.50	27	RI	0.90	44	RI	8.53	80	RI	16.88	202	RI	3118	48.22	10.71	10.83	254	ARP313;VV249a/b
NGC 4013	1F11559+4413	11:58:31.5	+43:56:54.151.86	+70.09			0.54	30	RI	0.77	33	RI	7.01	37	RI	24.36	157	MI	834	13.76 <sup>S</sup>	9.73	9.76	574	
NGC 4027	1F11569-1859	11:59:28.8	-19:15:45.286.36	+41.93			0.90	24	RI	1.12	37	MI	12.24	41	RI	27.78	139	MI	1671	22.84	10.26	10.36	404	ARP022NED02;VV066;VIIZw158
NGC 4030	1F11578-0049	12:00:23.8	-01:06:03.277.37	+59.21			1.35	46	RI	2.30	57	RZ	18.49	46	RI	50.92	117	MI	1427	24.50	10.56	10.64	312	
NGC 4038/9	1F11593-1836	12:01:55.1	-18:52:43.286.97	+42.45	*		1.94	44	RI	6.54	31	RI	45.16	63	RI	87.09	195	MI	1563	21.54	10.73	10.84	248	ARP244;VV245;AntennaeGalaxy
NGC 4041	1F11596+6224	12:02:12.8	+62:08:07.132.70	+54.05			1.13	28	RI	1.56	20	MI	14.15	19	MI	31.74	126	UT	1243	22.78	10.31	10.43	382	
NGC 4045	1F12001+0215	12:02:42.3	+01:58:33.275.98	+62.27			0.27	53	RZ	1.02	67	MI	6.75	57	UT	13.69	100	UT	1981	30.89	10.23	10.34	414	
NGC 4051	1F12006+4448	12:03:09.8	+44:31:50.148.88	+70.09			1.35	32	RI	2.20	32	RI	10.53	51	RI	24.93	63	MI	728	13.11	9.72	9.90	547	
NGC 4085	1F12028+5037	12:05:23.3	+50:21:08.140.58	+65.17			0.36	35	RI	0.62	27	UT	5.79	42	MI	14.80	77	UT	752	14.55	9.58	9.66	585	
NGC 4088	1F12030+5049	12:05:35.1	+50:32:24.140.33	+65.01			2.06	26	RI	3.45	32	RI	26.77	33	RI	61.68	137	RI	696	13.37	10.13	10.25	444	ARP018;VV357
NGC 4096	1F12034+4745	12:06:00.1	+47:28:48.143.55	+67.79			0.94	19	RZ	0.89	27	RI	7.46	47	RI	23.19	76	RI	523	9.63 <sup>S</sup>	9.40	9.50	591	
NGC 4100	1F12035+4951	12:06:08.1	+49:35:03.141.11	+65.91			0.77	21	RI	1.03	27	RI	9.35	44	RI	21.94	75	MI	1074	17.73 <sup>S</sup>	9.93	10.04	518	
NGC 4102	1F12038+5259	12:06:23.6	+52:42:36.138.08	+63.07			1.77	16	RI	6.83	23	UT	46.85	57	UT	70.29	106	UT	859	16.89	10.47	10.61	325	
ESO 440-IG058	2F12043-3140	12:06:53.0	-31:57:08.292.02	+29.97	U		0.20	38	UT	0.76	35	UT	7.44	46	UT	12.63	169	UT	6818	100.48	11.27	11.36	96	VV835;AM1204-314
NGC 4123	1F12056+0309	12:08:11.3	+02:52:40.277.98	+63.63			0.70	41	RI	1.33	58	UT	6.47	41	MI	10.73	122	UT	1327	15.29 <sup>S</sup>	9.55	9.76	572	MRK1466;KPG322B
NGC 4151	NZ12080+3940	12:10:34.6	+39:24:09.155.07	+75.07			2.01	46	UT	4.87	29	UT	6.46	73	UT	8.88	132	RZ	995	18.99	9.70	10.20	466	KPG324B
NGC 4157	1F12085+5045	12:11:04.2	+50:29:04.138.47	+65.41			1.72	39	RI	2.12	28	RI	17.71	43	RI	50.67	170	MI	790	13.30 <sup>S</sup>				

TABLE 1—*Continued*

Name		R. A. (J2000) DEC		$l$	$b$	HR	12 $\mu$ m		25 $\mu$ m		60 $\mu$ m		100 $\mu$ m		$cz$	$D$	$\log(L_{\text{FIR}}, L_{\text{IR}})$			IG/AGN Names				
Common	IRAS	hh:mm:ss.s	° : ' : "	°	°	(7)	Jy	mJy	SMF	Jy	mJy	SMF	Jy	mJy	SMF	Jy	mJy	SMF	km/s	Mpc	$L_{\odot}$	$L_{\odot}$	Rank	(17)
(1)	(2)	(3)	(4)	(5)	(6)	(7)	(8)	(9)	(10)	(11)	(12)	(13)	(14)	(15)	(16)	(17)	(18)	(19)	(20)	(21)	(22)	(23)	(24)	(25)
IRAS 12116-5615	2 12116-5615	12:14:21.4	-56:32:32	297.81	+5.96		0.35	26	UT	1.12	25	UT	9.78	103	UT	12.95	505	UT	8125	115.68	11.47	11.59	60	
ESO 380-G001	2 F12121-3513	12:14:44.2	-35:30:31	294.57	+26.77		0.38	23	UT	1.92	37	UT	11.48	46	UT	18.81	79	UT	2688	30.92	10.41	10.54	346	AM1212-351 NED01
NGC 4212	1 12130+1411	12:15:35.4	+13:54:31	268.83	+74.36		0.82	30	RI	1.00	41	RI	6.60	36	RI	16.94	110	UT	-81	15.29 <sup>V</sup>	9.68	9.82	560	
NGC 4214	1 12131+3636	12:15:40.0	+36:19:22	160.26	+78.08		0.58	44	MI	2.46	39	RI	17.57	91	RI	29.08	108	MI	291	3.67	8.74	8.86	618	
NGC 4217	N F12133+4722	12:15:50.3	+47:05:30	139.90	+68.85		1.26	29	RI	1.50	30	RI	11.60	61	RI	41.19	140	MI	1028	17.13 <sup>S</sup>	10.15	10.20	463	
NGC 4219	2 F12138-4302	12:16:27.1	-43:19:26	296.21	+19.09		0.93	31	RI	1.91	30	RI	14.08	49	RI	36.78	229	MI	1985	22.58	10.35	10.44	379	AM1213-430
NGC 4254	1 F12163+1441	12:18:51.0	+14:24:50	270.46	+75.19		3.67	45	RI	4.38	45	RI	37.46	80	RI	91.86	149	RI	2403	15.29 <sup>V</sup>	10.42	10.54	348	
NGC 4273	1 F12173+0537	12:19:56.3	+05:20:34	282.53	+66.96	S	0.77	33	RI	1.65	71	RI	9.38	59	MI	21.76	126	UT	2400	15.29 <sup>V</sup>	9.80	9.93	541	
NGC 4298	1 F12190+1452	12:21:35.7	+14:36:07	272.41	+75.67		0.92	41	RI	1.11	39	RI	7.02	34	RI	25.77	82	MI	1141	15.29 <sup>V</sup>	9.85	9.91	545	KPG332A
NGC 4303	1 F12193+0445	12:21:55.4	+04:28:24	284.38	+66.28		3.28	50	RI	4.90	51	RI	37.27	73	RI	78.74	88	RI	1570	15.29 <sup>V</sup>	10.37	10.51	356	
NGC 4304	2 F12196-3312	12:22:14.6	-33:29:16	295.97	+28.99		0.51	29	RI	0.91	35	UT	6.77	41	RI	11.35	152	UT	2631	30.52	10.17	10.33	417	
NGC 4321	1 F12203+1605	12:22:53.9	+15:49:22	271.12	+76.90		2.52	26	RI	3.10	53	RI	26.00	50	RI	68.37	101	RI	1571	15.20 <sup>P</sup>	10.28	10.39	394	
NGC 4332	1 F12204+6607	12:22:46.3	+65:50:44	127.59	+51.02		0.27	22	UT	0.98	23	MI	7.25	36	UT	13.01	117	UT	2843	43.50	10.53	10.64	313	
NGC 4369	1 F12221+3939	12:24:35.7	+39:23:02	145.75	+76.53		0.28	23	UT	0.69	36	UT	5.75	24	UT	11.28	136	UT	1045	20.21	9.78	9.89	549	MRK0439
IRAS F12224-0624	1 F12224-0624	12:25:02.8	-06:40:44	291.28	+55.59		<0.11	-		0.20	44	UT	5.99	44	UT	8.13	139	UT	7902	112.70	11.23	11.27:	123	
NGC 4383	1 F12229+1644	12:25:26.0	+16:28:04	272.14	+77.76		0.29	29	UT	1.08	55	UT	8.36	25	UT	12.43	118	UT	1710	15.29 <sup>V</sup>	9.64	9.76	573	MRK0769
NGC 4388	1 F12232+1256	12:25:45.9	+12:39:50	279.11	+74.34		1.01	28	UT	3.57	52	UT	10.27	27	UT	17.15	155	UT	2524	15.29 <sup>V</sup>	9.75	10.00	527	
NGC 4402	1 F12235+1323	12:26:07.7	+13:06:47	278.79	+74.79		0.74	43	RI	0.66	45	RI	5.54	36	MI	17.53	123	UT	237	15.29 <sup>V</sup>	9.68	9.78	571	
NGC 4414	1 F12239+3130	12:26:26.9	+31:13:24	174.54	+83.18		2.78	43	RI	3.61	44	RI	29.55	80	RI	70.69	72	UT	720	17.68 <sup>P</sup>	10.43	10.56	340	
NGC 4418	1 F12243-0036	12:26:54.7	-00:52:42	290.05	+61.38		0.99	35	UT	9.67	84	UT	43.89	80	UT	31.94	122	UT	2104	31.90	11.00	11.08	164	KPG337A
NGC 4419	1 F12244+1519	12:26:55.1	+15:02:59	276.42	+76.64		0.67	27	RI	1.88	51	RZ	7.58	31	UT	16.18	151	UT	-261	15.29 <sup>V</sup>	9.68	9.86	553	
NGC 4433	1 F12250-0800	12:27:37.5	-08:16:35	292.84	+54.13		0.63	38	UT	1.52	73	UT	13.35	59	UT	23.83	193	UT	2913	41.68	10.76	10.87	243	
NGC 4490	1 F12281+4155	12:30:34.9	+41:38:47	138.01	+74.87	S	1.82	25	RI	4.92	43	RI	46.92	63	RI	88.61	211	MI	641	10.48	10.11	10.21	459	ARP269 NED02;VV030a;KPG341B
NGC 4501	1 F12294+1441	12:31:57.6	+14:25:20	282.30	+76.51		2.29	27	RI	2.98	73	RI	19.68	93	RI	62.97	145	MI	2284	15.29 <sup>V</sup>	10.24	10.33	418	
NGC 4437	N F12301+0023	12:32:44.5	+00:06:57	292.73	+62.62		0.80	36	RI	1.04	86	RZ	7.87	66	RZ	21.41	139	RI	1121	16.38	9.84	9.94	539	KPG344B
NGC 4526	1 F12315+0758	12:34:02.7	+07:41:57	290.16	+70.14		0.35	38	UT	0.49	59	UT	5.86	37	UT	16.03	96	UT	448	15.29 <sup>V</sup>	9.65	9.71	581	
NGC 4527	1 F12315+0255	12:34:09.9	+02:39:04	292.61	+65.18		2.65	37	RI	3.55	62	RI	31.40	53	RI	65.68	140	MI	1771	15.29 <sup>V</sup>	10.29	10.42	385	
NGC 4532	1 F12317+0644	12:34:18.6	+06:28:11	291.02	+68.94		0.28	34	RI	0.73	65	RZ	9.21	52	MI	15.14	143	UT	2007	15.29 <sup>V</sup>	9.70	9.79	568	
NGC 4535	1 F12317+0828	12:34:19.9	+08:11:52	290.07	+70.64		1.04	33	RI	1.34	42	RI	11.45	47	RI	32.52	138	RI	1957	15.77 <sup>P</sup>	9.98	10.07	510	
NGC 4536	1 F12319+0227	12:34:28.5	+02:11:08	292.96	+64.73		1.55	34	MI	4.04	60	MI	30.26	42	UT	44.51	141	UT	1802	14.92 <sup>P</sup>	10.17	10.32	423	
NGC 4559	1 F12334+2814	12:35:57.0	+27:57:37	198.42	+86.47		0.87	23	RI	1.03	30	RI	10.23	44	RI	25.41	74	RI	816	9.69	9.46	9.56	588	
NGC 4565	1 F12338+2615	12:36:21.0	+25:59:16	230.76	+86.44		1.36	30	RI	1.36	33	RI	7.79	39	RI	34.62	112	MI	1282	9.99 <sup>S</sup>	9.61	9.66	586	
NGC 4568/7	1 F12340+1131	12:36:33.7	+11:14:32	289.80	+73.73	*	1.99	30	RI	2.64	51	RI	20.81	54	RI	56.80	140	MI	2262	15.29 <sup>V</sup>	10.20	10.30	425	VV219;KPG347;SiameseTwins
NGC 4569	1 F12343+1326	12:36:50.8	+13:09:43	288.48	+75.62		1.27	43	RI	2.06	70	RZ	9.80	65	RI	26.56	173	MI	-235	15.29 <sup>V</sup>	9.87	10.02	521	ARP076
NGC 4575	2 F12351-4015	12:37:52.1	-40:32:20	300.15	+22.26		0.46	54	UT	0.85	31	UT	7.74	46	UT	16.31	404	UT	2973	58.21 <sup>G</sup>	10.85	10.96	210	
NGC 4579	1 F12351+1205	12:37:42.6	+11:49:12	290.38	+74.36		1.12	40	RI	0.78	47	RI	5.93	54	RI	21.39	243	MI	1519	15.29 <sup>V</sup>	9.76	9.87	552	
NGC 4605	1 F12378+6152	12:40:00.9	+61:36:28	125.33	+55.47		0.97	18	RZ	1.25	18	RI	14.39	34	RI	30.55	127	UT	117	3.90	8.77	8.87	617	
IC 3639	2 F12381-3628	12:40:51.5	-36:45:13	300.57	+26.07	S	0.72:	33	MIg	2.54:	44	MIg	8.90:	41	RIg	13.79:	180	MIg	3275	34.82	10.39:	10.62:	321	AM1238-3628 NED02
NGC 4631	1 F12396+3249	12:42:07.1	+32:32:33	142.83	+84.22	S	5.16	39	RI	8.97	46	RZ	85.40	62	RZ	160.08	260	RI	630	7.73	10.10	10.22	453	ARP281 NED02;KPG350A
NGC 4647	1 F12410+1151	12:43:32.1	+11:34:59	295.74	+74.34	S	0.99	48	RI	0.76	49	RI	5.77	36	RI	16.59	88	UT	1415	15.29 <sup>V</sup>	9.66	9.81	563	ARP116 NED01;VV206b;KPG353A
NGC 4651	1 F12412+1640	12:43:42.1	+16:23:38	293.06	+79.12		0.47	41	UT	0.66	40	RI	5.60	31	RI	15.56	90	UT	805	15.29 <sup>V</sup>	9.64	9.72	580	ARP189;VV056
NGC 4654	1 F12414+1324	12:43:56.6	+13:07:39	295.43	+75.89		1.01	47	MI	1.73	38	RI	13.39	34	RI	37.77	135	UT	1037	15.29 <sup>V</sup>	10.02	10.10	500	
NGC 4656	1 F12415+3227	12:43:55.0	+32:10:28	140.42	+84.70		0.06	29	MI	0.49	30	RI	6.50	76	RZ	10.70	116	RZ	614	7.38	8.91	8.98	616	KPG350B
NGC 4666	1 F12425-0011	12:45:07.7	-00:27:41	299.53	+62.37		3.34	52	RI	3.89	51	RI	37.11	72	RI	85.95	158	MI	1495	12.82 <sup>S</sup>	10.24	10.36	403	
NGC 4691	1 F12456-0303	12:48:13.5	-03:19:59	301.35	+59.53		0.80	31	MI	3.10	103	RI	14.32	50	UT	22.65								

TABLE 1—*Continued*

Name		R. A. (J2000)	DEC	$l$	$b$	HR	$12\mu m$	$25\mu m$	$60\mu m$	$100\mu m$	$cz$	$D$	$\log(L_{FIR}, L_{IR})$			IG/AGN Names				
Common (1)	IRAS (2)	hh:mm:ss.s (3)	°:':": (4)	° (5)	° (6)	(7)	Jy (8)	mJy SMF (9)	Jy (10)	mJy SMF (11)	km/s (12)	Mpc (13)	$L_{\odot}$ (14)	$L_{\odot}$ (15)	Rank (16)	(17)				
NGC 4808	1 F12532+0434	12:55:48.8	+04:18:18	305.74	+67.15		0.62	44 UT	0.74	49 UT	6.92	41 MI	16.05	119 UT	778	19.72 <sup>S</sup>	9.89	10.01	524	
IC 3908	1 F12540-0717	12:56:41.1	-07:33:46	305.22	+55.29		0.42	49 UT	1.20	69 RI	8.47	40 MI	16.65	137 UT	1296	20.28	9.95	10.07	508	
UGC 08058	1 F12540+5708	12:56:15.0	+56:52:17	121.61	+60.24		1.83	17 UT	8.84	28 UT	30.80	42 UT	29.74	108 UT	12660	171.84	12.31	12.51	1	MRK0231;VHZw490
NGC 4818	1 F12542-0815	12:56:50.0	-08:31:38	305.22	+54.32		0.96	33 MI	4.40	55 MI	20.12	63 UT	26.60	140 UT	1051	9.37 <sup>S</sup>	9.57	9.75	575	MRK9022
NGC 4826	1 F12542+2157	12:56:42.6	+21:41:05	315.65	+84.43		2.36	31 RI	2.86	59 UT	36.70	77 UT	81.65	99 UT	349	3.09	8.98	9.08	612	
ESO 443-G017	2 F12550-2929	12:57:44.3	-29:45:55	304.56	+33.09		0.22	30 UT	0.91	35 UT	5.96	37 UT	8.99	127 UT	3055	35.25	10.22	10.36	405	
NGC 4835	2 F12552-4559	12:58:08.2	-46:15:56	304.14	+16.59		1.28	30 RI	1.89	28 RI	17.69	53 MI	40.22	84 UT	2192	23.96	10.46	10.57	338	AM1255-455
NGC 4845	1 F12554+0150	12:58:01.2	+01:34:32	306.74	+64.40		0.38	32 UT	0.57	54 UT	9.22	44 UT	22.05	155 UT	1224	15.09 <sup>S</sup>	9.79	9.84	555	
NGC 4900	1 F12581+0246	13:00:39.8	+02:30:00	308.45	+65.27		0.49	32 RZ	0.76	69 RI	5.97	41 RI	13.96	104 UT	969	15.36 <sup>S</sup>	9.61	9.73	578	
NGC 4922	1 F12590+2934	13:01:25.9	+29:18:46	78.30	+86.90	U	0.27	35 UT	1.48	30 MI	6.21	40 UT	7.33	93 UT	7071	101.09	11.14	11.32	108	VV609;KPG363A/B
CGCG 043-099	1 F12592+0436	13:01:49.9	+04:20:01	309.60	+67.07		0.30	33 RI	0.47	61 UT	5.25	29 UT	8.06	115 UT	11237	156.31	11.49	11.62	51	VV283
MCG-02-33-098/9	2 F12596-1529	13:02:20.5	-15:46:05	306.78	+47.02	S	0.34	41 UT	1.63	57 MI	7.49	34 UT	9.68	117 UT	4861	72.50	10.93	11.11	158	
ESO 507-G070	2 F13001-2339	13:02:51.3	-23:55:10	306.28	+38.88		0.25	20 RI	0.80	46 UT	13.04	51 UT	15.71	159 UT	6446	96.10	11.42	11.49	79	AM1300-233
NGC 4945	2 F13025-4912 R	13:05:27.6	-49:28:09	305.27	+13.34		27.74	34 RZ	42.34	55 RZ	625.46	133 RZ	1329.70	797 RZ	560	3.92	10.41	10.48	364	
ESO 323-G077	2 F13036-4008	13:06:26.5	-40:24:54	306.02	+22.37		0.68	14 UT	1.24	31 UT	5.73	36 MI	10.73	65 MI	4477	58.21 <sup>G</sup>	10.69	10.91	230	
IRAS 13052-5711	2 13052-5711	13:08:18.4	-57:27:30	305.21	+5.34		0.13	24 UT	0.45	26 UT	8.17	72 UT	14.58:	719 UPc	6364	96.54	11.28:	11.34:	103	
NGC 4984	2 F13063-1515	13:08:58.3	-15:31:07	309.15	+47.14		0.86	29 MI	1.65	54 UT	11.23	47 UT	17.08	118 UT	1252	17.36	9.88	10.05	514	
NGC 5005	1 F13086+3719	13:10:55.7	+37:03:33	101.62	+79.25		1.65	26 RI	2.26	39 RI	22.18	21 RI	63.40	131 MI	950	18.09	10.39	10.46	370	
NGC 5010	N F13097-1531	13:12:25.4	-15:47:45	310.31	+46.77		0.37	37 UT	1.44	65 RI	10.29	55 UT	21.69	114 UT	6400	94.33	11.41	11.50	77	
MCG-03-34-014	2 F13099-1716	13:12:35.1	-17:32:27	310.07	+45.04		0.81	44 RI	1.07	52 RI	7.76	60 UT	17.14	115 UT	2760	36.41	10.46	10.61	323	
NGC 5020	1 F13101+1251	13:12:39.1	+12:36:07	322.85	+74.65		0.36	28 RI	0.72	60 RZ	5.58	50 RI	11.70	86 MI	3360	51.45	10.60	10.72	286	
NGC 5033	1 F13111+3651	13:13:27.2	+36:35:40	98.07	+79.45		1.77	28 RI	2.14	33 RZ	16.20	73 RI	50.23	92 MI	869	13.76 <sup>S</sup>	10.05	10.13	488	
IRAS 13120-5453	2 13120-5453	13:15:06.2	-55:09:24	306.34	+7.56		0.44	27 UT	2.98	21 UT	41.11	66 UT	52.33	200 UT	9222	129.36	12.18	12.26	7	
NGC 5038	2 F13123-1541	13:15:02.5	-15:57:08	311.19	+46.54		0.25	49 UT	1.47	55 MI	9.15	60 UT	13.28	115 UT	2222	29.82	10.25	10.39	393	
IC 0860	1 F13126+2453	13:15:02.2	+24:37:15	8.96	+84.13		<0.14	-	1.34	44 UT	18.61	71 UT	18.66	90 UT	3887	59.11	11.14	11.17:	145	
NGC 5055	1 F13135+4217 R	13:15:49.5	+42:01:39	105.99	+74.29		5.35	26 RZ	6.36	50 RZ	40.00	49 RI	139.82	356 RI	500	7.96 <sup>S</sup>	10.01	10.09	502	
VV 250a	1 F13136+6223	13:15:34.9	+62:07:26	118.04	+54.77	R	0.35	22 UT	1.95	20 UT	11.39	35 UT	12.41	93 UT	9313	127.99	11.61	11.74	40	ARP238NED02;KPG369B
NGC 5054	2 F13143-1622	13:16:59.0	-16:38:04	311.73	+45.80		1.12	42 RI	1.50	66 RI	13.01	60 RI	31.53	145 UT	1737	23.87	10.34	10.46	372	
NGC 5068	N F13161-2046	13:18:52.9	-21:02:25	311.48	+41.38		1.04	38 RI	0.97	62 RI	12.50	57 RI	31.39	311 RI	672	5.61	9.07	9.17	610	
NGC 5073	1 F13166-1434	13:19:18.5	-14:50:30	312.93	+47.49		0.31	31 UT	1.46	59 RI	9.37	50 UT	15.02	170 UT	2744	37.09	10.47	10.60	328	
NGC 5078	2 F13170-2708	13:19:50.0	-27:24:37	310.63	+35.04	S	1.08	30 RI	0.95	45 RI	10.54	44 RI	33.70	202 UT	2168	26.32	10.44	10.50	360	
UGC 08387	1 F13182+3424	13:20:34.9	+34:08:24	82.94	+80.60		0.25	29 UT	1.42	40 UT	17.04	88 UT	24.38	120 UT	7000	99.99	11.59	11.67	46	ARP193;VV821;IZw056
NGC 5104	1 F13188+0036	13:21:24.2	+00:20:27	319.20	+62.26		0.39	34 RI	0.74	91 UT	6.78	49 UT	13.37	103 UT	5578	82.44	11.09	11.20	139	
MCG-03-34-064	2 F13197-1627	13:22:23.5	-16:43:34	313.53	+45.51	S	0.94	40 MI	2.97	45 UT	6.20	40 MI	6.20	143 UT	5152	77.33	10.90	11.24	128	
NGC 5128	2 F13225-4245 R	13:25:27.6	-43:01:12	309.52	+19.42		22.15	39 RZ	28.25	48 RZ	213.29	42 RI	411.89	334 MI	562	4.03	9.94	10.11	498	ARP153;AM1322-424
NGC 5135	2 F13229-2934	13:25:43.0	-29:49:54	311.74	+32.45		0.63	35 UT	2.38	58 UT	16.86	46 UT	30.97	177 UT	4114	52.15	11.06	11.17	143	
NGC 5145	1 F13230+4331	13:25:14.0	+43:16:01	102.13	+72.47		0.41	22 UT	0.64	24 UT	6.29	41 UT	12.27	106 UT	1225	23.33	9.94	10.06	512	
ESO 173-G015	2 13242-5713	13:27:24.4	-57:29:24	307.77	+5.04		1.22:	31 UPn	7.56:	32 UPn	81.44:	97 UPn	100.04:	710 UPn	3006	32.44	11.26:	11.34:	102	
NGC 5194	1 F13277+4727	13:29:53.5	+47:11:42	104.85	+68.56		7.21:	75 RSg	9.56:	77 RSg	97.42:	193 RSg	221.21:	329 RSg	468	8.63	10.31:	10.42:	388	ARP085NED01;VV001a;KPG379A
NGC 5195	1 F13278+4731	13:30:00.0	+47:16:00	104.88	+68.49		0.35:	- RSg	1.02:	- RSg	15.22:	801 RSg	31.33:	368 RSg	450	8.30	9.44:	9.50:	592	ARP085NED02;VV001b;KPG379B
NGC 5188	2 F13286-3432	13:31:27.7	-34:47:36	312.18	+27.36		0.86	27 UT	2.83	38 UT	22.58	74 UT	38.26	150 UT	2425	27.25	10.60	10.72	291	AM1328-343
IC 4280	2 F13301-2356	13:32:52.8	-24:12:23	314.90	+37.70		0.38	39 UT	0.68	52 UT	6.10	69 UT	12.36	472 UT	4930	74.67	10.96	11.08	167	AM1330-235
NGC 5218	1 F13304+6301	13:32:10.6	+62:46:02	115.07	+53.74	S	0.37	20 RI	0.94	24 UT	7.01	22 UT	13.54	95 UT	2880	44.35	10.55	10.67	305	ARP104NED02;VV033b
NGC 5236	2 F13341-2936 R	13:36:58.8	-29:51:46	314.58	+31.98		21.46	52 RZ	43.57	63 RZ	265.84	64 RZ	524.09	302 RZ	522	3.60	9.94	10.10	499	
NGC 5248	1 F13350+0908	13:37:31.8	+08:53:12	335.93	+68.75		1.75	47 RI	3.02	41 RI	20.91	42 RI	53.48	107 MI	1152	13.82 <sup>S</sup>	10.09	10.20	467	
NGC 5247	2 F13353-1737	13:38:03.4	-17:53:04	318.32	+43.59		1.51	21 RI	1.48	43 RI	13.65	61 RI	41.83	122 RI	1362	18.77	10.24	10.32	421	
NGC 5256	1 F13362+4831	13:38:18.2	+48:16:28	102.72	+66.97		0.32	18 UT	1.07	28 MI	7.25	33 UT	10.11	135 UT	8285	115.83	11.34	11.49	80	MRK0266;IZw067;KPG388
NGC 5253	2 F13370-3123	13:39:55.2	-31:38:21	314.86	+30.11		2.50	20 UT	12.07	49 UT	29.84	67 UT	30.08	205 UT	404	3.15 <sup>P</sup>	8.79	9.05	614	AM1337-312NED01
NGC 5257/8	1 F13373+0105	13:39:54.9	+00:50:07	328.81	+61.25	R	0.57	31 UT	1.34	69 UT	10.73	59 UT	19.97	50 UT	6798	98.63	11.43	11.55	71	ARP240;VV055;KPG389
UGC 08696	1 F13428+5608	13:44:41.8	+55:53:14	108.11	+59.68		0.24	17 UT	2.36	21 UT	22.51	42 UT	22.53	70 UT	11324	154.71	12.08	12.14	11	MRK0273;IZw071

TABLE 1—Continued

Name		R.A. (J2000) DEC	$\ell$	$b$	HR	$12\mu\text{m}$		$25\mu\text{m}$		$60\mu\text{m}$		$100\mu\text{m}$		$cz$	$D$	$\log(L_{\text{fir}}, L_{\text{IR}})$			IG/AGN Names	
Common	IRAS	hh:mm:ss.s	° ' "	°	°	Jy	mJy SMF	Jy	mJy SMF	Jy	mJy SMF	Jy	mJy SMF	km/s	Mpc	$L_{\odot}$	$L_{15}$	Rank		
(1)	(2)	(3)	(4)	(5)	(6)	(7)	(8)	(9)	(10)	(11)	(12)	(13)	(14)	(15)	(16)	(17)	(18)	(19)	(20)	
UGC 08739 1	F13470+3530	13:49:15.0	+35:15:17	69.85	+75.23	0.35:	31 UPn	0.42:	38 UPn	5.79:	40 UPn	15.89:	83 UPn	5032	74.18	11.03:	11.08:	165		
ESO 221-IG008 2	F13473-4801	13:50:26.9	-48:16:40	312.97	+13.44	0.30	19 RI	1.12	35 RZ	5.64	73 UT	5.52	359 UT	3190	58.21 <sup>G</sup>	10.61	10.77	272		
ESO 221-IG010 2	F13478-4848	13:50:57.3	-49:03:25	312.86	+12.66	0.74	24 MI	1.82	16 MI	12.92	77 UT	22.00	469 UT	3028	58.21 <sup>G</sup>	11.02	11.17	147		
NGC 5331 N	F13497+0220	13:52:16.6	+02:06:08	335.72	+61.04	*	0.29	27 RI	0.59	51 UT	5.86	43 UT	11.49	106 UT	9909	139.10	11.49	11.59	57	VV253;KPG401
NGC 5371 1	F13535+4042	13:55:39.1	+40:27:34	82.17	+71.20	0.86	30 RZ	0.97	35 RI	5.27	52 RI	18.66	154 RI	2553	41.06	10.57	10.67	304		
NGC 5383 1	F13549+4205	13:57:03.8	+41:50:55	84.79	+70.08	0.35	30 RZ	0.84	23 MI	5.45	51 UT	13.05	110 UT	2230	36.74	10.34	10.45	377	MRK0281	
NGC 5394/5 1	F13564+3741	13:58:35.3	+37:26:51	73.25	+72.50	S	0.59	25 RI	1.40	35 RI	9.38	31 RI	22.02	127 MI	3472	53.40	10.89	11.00	198	ARP084;VV048;KPG404
NGC 5430 1	F13591+5934	14:00:45.0	+59:19:37	107.31	+55.65	0.50	24 UT	1.94	21 MI	10.10	31 UT	20.34	66 UT	2960	45.63	10.74	10.88	240	MRK0799	
NGC 5433 1	F14004+3244	14:02:37.4	+32:30:27	56.45	+73.67	0.27	19 UT	0.85	21 RI	6.31	35 UT	11.67	91 UT	4352	65.30	10.83	10.95	214		
NGC 5427 1	14008-0547	14:03:25.6	-06:01:48	333.28	+52.55	S	1.29	42 RZ	1.48	52 RZ	10.24	50 RZ	25.29	146 RI	2618	38.02	10.65	10.80	261	ARP271NED02;VV021a
NGC 5457 1	14013+5435 R	14:03:09.0	+54:21:24	102.06	+59.77	6.20	- RR	11.78	- RR	88.04	- RR	252.84	- RR	241	6.70 <sup>P</sup>	10.13	10.20	268	ARP026;VV344a	
NGC 5483 N	F14072-4305	14:10:25.0	-43:19:28	317.84	+17.25	0.80	38 RI	0.73	42 RI	6.30	38 RI	17.16	143 MI	1774	20.31	9.93	10.05	515		
ESO 221-G032 2	F14088-4909	14:12:08.9	-49:23:24	316.17	+11.40	0.58	25 RI	0.71	35 UT	6.82	62 MI	13.83	537 UT	2894	58.21 <sup>G</sup>	10.79	10.93	223		
NGC 5506 1	F14106-0258	14:13:14.0	-03:12:24	339.15	+53.81	S	1.29	27 UT	4.17	56 MI	8.42	60 UT	8.87	111 UT	1853	28.07	10.14	10.49	361	MRK1376;KPG419A
CGCG 247-020 1	F14179+4927	14:19:43.5	+49:14:09	91.29	+62.12	0.15	22 UT	0.84	19 UT	6.01	35 UT	8.47	155 UT	7666	107.71	11.20	11.32	109	MRK1490	
IC 4402 2	F14179-4604	14:21:12.6	-46:17:50	318.69	+13.81	0.60	29 RZ	1.19	22 UT	8.86	54 UT	18.19	391 UT	1650	18.90	9.92	10.05	516		
NGC 5600 1	F14214+1451	14:23:49.4	+14:38:21	7.45	+65.14	0.35	29 UT	0.72	32 RI	5.44	46 UT	11.68	89 UT	2311	36.93	10.31	10.43	384	VIIIZw410	
NGC 5595 1	14214-1629	14:24:12.6	-16:43:25	332.78	+40.71	S	0.53	22 MI	0.68	39 UT	9.06	36 RI	18.60	103 MI	2699	36.71	10.51	10.61	324	VV446NED01;VV530
NGC 5597 1	14216-1632	14:24:26.5	-16:45:43	332.81	+40.65	S	0.71	45 RI	1.55	49 UT	8.37	51 UT	16.33	190 MI	2697	36.68	10.46	10.63	315	VV446NED02
NGC 5653-1	F14280+3126	14:30:09.5	+31:12:57	49.60	+68.11	0.64	33 UT	1.37	28 UT	10.57	40 UT	23.03	79 UT	3572	54.88	10.95	11.06	175		
IC 4444 2	F14284-4311	14:31:38.8	-43:25:08	321.57	+15.80	1.40	24 RI	2.33	29 MI	19.13	43 UT	38.07	733 UT	1957	22.47	10.40	10.53	349	AM1428-431	
NGC 5643 2	F14294-4357	14:32:41.1	-44:10:30	321.44	+15.03	1.97	33 RI	4.68	21 RI	23.48	61 RI	48.60	321 MI	1199	13.86	10.08	10.24	449	AM1429-435	
NGC 5665 1	F14299+0818	14:32:24.9	+08:04:50	359.08	+59.44	0.47	22 RI	0.82	35 UT	6.25	20 UT	12.41	101 UT	2222	34.98	10.30	10.44	380	ARP049;VV412	
NGC 5678 1	F14306+5808	14:32:06.2	+57:55:13	100.04	+54.50	0.94	15 RI	1.20	19 RI	9.67	29 RI	25.66	85 UT	1912	32.02	10.50	10.61	322		
NGC 5676 1	F14310+4940	14:32:46.9	+49:27:31	88.68	+60.39	1.13	24 RI	1.70	25 RI	12.04	37 RI	29.91	207 UT	2117	29.63 <sup>S</sup>	10.51	10.63	319		
IRAS F14348-1447 1	F14348-1447	14:37:37.3	-15:00:20	337.59	+40.61	<0.10	-	0.55	62 RI	6.82	40 UT	7.31	151 UT	24723	330.85	12.26	12.30:	5		
NGC 5690 1	F14351+0230	14:37:41.0	+02:17:27	353.15	+54.45	0.75	34 RI	0.99	35 RI	6.94	32 RI	16.84	117 UT	1753	23.84 <sup>S</sup>	10.07	10.21	458		
NGC 5713 1	F14376-0004	14:40:10.9	-00:17:22	351.02	+52.13	1.47	28 RZ	2.84	38 MI	22.10	65 MI	37.28	88 UT	1904	26.74 <sup>S</sup>	10.57	10.72	288	VIIIZw447	
IRAS F14378-3651 2	F14378-3651	14:40:57.8	-37:04:25	326.05	+20.83	<0.10	-	0.67:	38 UPc	6.72:	42 UPc	8.08:	215 UPc	20444	276.04	12.08:	12.15:	10		
NGC 5719 1	F14383-0006	14:40:55.9	-00:19:05	351.22	+51.98	0.52	24 UT	1.09	42 RI	8.61	34 UT	17.96	85 UT	1743	27.14	10.23	10.35	410		
NGC 5728 1	F14396-1702	14:42:24.3	-17:15:16	337.33	+38.10	0.21	37 UT	1.05	39 MI	8.88	49 MI	15.79	144 MI	2788	38.34	10.50	10.60	329		
NGC 5734 2	F14423-2039	14:45:08.5	-20:52:12	335.67	+34.67	S	0.50:	25 UTg	0.74:	63 UTg	7.99:	55 UPg	24.79:	94 RIb	4091	59.28	11.02:	11.06:	178	
ESO 386-G019 2	F14430-3728	14:46:09.9	-37:41:04	326.74	+19.83	0.31	20 UT	0.79	50 UT	5.99	56 UT	10.36	86 RZ	4476	64.00	10.78	10.91	228		
UGCA 394 N	F14446-1714	14:47:24.1	-17:26:49	338.47	+37.30	0.30	32 RI	1.04	55 RZ	5.83	39 RI	10.61	120 MI	2195	30.02	10.11	10.26	440		
NGC 5757 1	F14449-1852	14:47:46.3	-19:04:43	337.47	+35.87	0.77	39 RI	0.94	57 UT	6.57	39 MI	12.56	184 UT	2673	36.29	10.34	10.53	351		
NGC 5775 1	F14514+0344	14:53:58.0	+03:32:32	359.43	+52.42	1.83	25 RI	2.47	28 RI	23.59	46 RI	55.64	97 MI	1642	26.34	10.68	10.78	265	KPG440B	
IC 4518A/B 2	F14544-4255	14:57:43.1	-43:08:01	326.12	+13.98	U	0.36	24 UT	1.53	32 MI	8.07	92 MI	13.65	389 UT	4715	69.94	10.98	11.13	150	VV780;AM1454-425
VV 340a 1	F14547+2449	14:57:00.3	+24:37:01	34.97	+61.72	R	0.36	16 RI	0.41	31 UT	6.95	29 MI	15.16	169 UT	9982	139.36	11.59	11.67	44	ARP302NED02;KPG446B
NGC 5786 2	F14556-4148	14:58:56.9	-42:00:51	326.88	+14.85	0.37	28 UT	0.98	29 RI	5.90	118 RI	15.00	375 UT	2998	35.04	10.35	10.45	373		
NGC 5792 1	F14558-0053	14:58:22.9	-01:05:26	355.35	+48.43	0.97	22 MI	1.00	44 UT	9.08	28 MI	20.32	136 UT	1924	25.36 <sup>S</sup>	10.21	10.36	406		
NGC 5793 1	F14565-1629	14:59:23.5	-16:41:28	341.96	+36.30	S	0.17	31 RZ	0.49	68 UT	6.48	42 UT	9.44	230 UT	3491	50.17	10.56	10.65	311	
UGC 09668 1	F15005+8343	14:56:07.7	+83:31:18	118.96	+32.61	0.29	20 UT	0.89	18 UT	5.24	32 UT	8.49	165 MI	3881	55.64	10.58	10.74	279	MRK0839;KPG451B	
NGC 5866 1	F15051+5557	15:06:30.3	+55:45:49	92.03	+52.49	0.35	22 RI	0.34	10 RI	5.26	27 MI	16.98	60 UT	769	11.63 <sup>S</sup>	9.43	9.45	597		
NGC 5861 1	F15065-1107	15:09:15.4	-11:19:16	348.52	+39.06	0.72	30 RI	1.54	37 RZ	11.41	22 RI	20.53	114 UT	1818	23.84 <sup>S</sup>	10.20	10.34	413		
NGC 5833 2	F15066-7240	15:11:51.0	-72:51:28	312.94	-12.77	0.83	20 RI	0.99	14 RI	7.29	27 MI	22.42	332 RZ	3030	38.65	10.60	10.69	298		
UGCA 402 2	F15106-2029	15:13:30.6	-20:40:29	342.34	+31.11	0.54	20 RI	0.64	53 RI	5.70	32 RI	14.37	416 UT	2272	30.94	10.22	10.34	415		
CGCG 049-057 1	F15107+0724	15:13:12.7	+07:13:30	8.89	+50.96	<0.05	-	0.95	29 MI	21.89	72 UT	31.53	158 UT	3893	59.06	11.23	11.27:	121		
NGC 5900 1	F15132+4223	15:15:05.2	+42:12:35	69.68	+57.17	0.40	17 MI	0.70	14 UT	7.51	26 UT	16.95	189 UT	2511	40.35	10.54	10.63	320		
NGC 5907 1	F15146+5629	15:15:58.9	+56:18:36	91.55	+51.09	1.29	32 RZ	1.44	30 RI	9.14	78 RI	37.43	92 MI	612	12.08 <sup>S</sup>	9.80	9.85	554		
VV 705 1	F15163+4255	15:18:06.7	+42:44:41	70.35	+56.49	U	0.29	19 RI	1.42	16 UT	9.02	21 UT	10.00	91 UT	12336	168.72	11.76	11.89	26	MRK0848;IZw107

TABLE 1—*Continued*

Name		R. A. (J2000) DEC		$l$	$b$	HR	$12\mu\text{m}$		$25\mu\text{m}$		$60\mu\text{m}$		$100\mu\text{m}$		$c z$	$D$	$\log(L_{\text{fIR}}, L_{\text{IR}})$			IG/AGN Names	
Common (1)	IRAS (2)	hh:mm:ss.s (3)	° : ' " (4) (5)				° (6) (7)	Jy (8)	mJy SMF (9)	Jy (10)	mJy SMF (11)	Jy (12)	mJy SMF (13)	Jy (14)			mJy SMF (15)	km/s (16)	Mpc (17)		$L_{\odot}$ (18)
	NGC 5915	1F15188-1254	15:21:33.7	-13:05:34	349.91	+35.74	R	0.46	32 UT	1.36	62 UT	10.71:	62 UPn	16.41:	216 UPn	2291	32.94	10.42:	10.55:	342	
	ESO 099-G004	2 15206-6256	15:24:57.1	-63:07:29	319.30	-5.24		0.29	28 UT	1.46	37 UT	10.30	121 UT	13.65	1272 UT	8779	123.07	11.54	11.67	45	
	NGC 5930	1F15243+4150	15:26:07.4	+41:40:34	67.86	+55.30	R	0.35	27 UT	1.60	19 UT	9.36	35 UT	13.68	109 UT	2672	42.47	10.58	10.72	287	ARPO90NED02;VV823NED02;IZw112NED02
	IRAS F15250+3608	1F15250+3608	15:26:59.9	+35:58:34	57.81	+55.94		0.16	30 RI	1.31	25 UT	7.10	43 UT	5.93	98 UT	16535	223.49	11.92	12.02	18	
	NGC 5936	1F15276+1309	15:30:00.9	+12:59:21	20.06	+50.38		0.48	24 UT	1.47	31 MI	8.73	37 UT	17.66	105 UT	4013	60.81	10.93	11.07	173	
	NGC 5937	1F15281-0239	15:30:46.0	-02:49:45	1.33	+41.31		0.68	31 UT	1.47	46 RI	10.41	26 MI	21.47	210 UT	2807	42.45	10.70	10.83	253	
	NGC 5953	1F15322+1521	15:34:33.0	+15:11:42	23.92	+50.34	*	0.82	27 RI	1.58	30 RI	11.79	45 RI	19.89	154 UT	2008	32.77	10.48	10.63	316	MRK9031;ARPO91NED01;VV244a;KPG468A
	UGC 09913	1F15327+2340	15:34:57.1	+23:30:10	36.63	+53.03		0.61	21 RI	8.00	34 UT	104.09	112 UT	115.29	138 UT	5450	79.90	12.15	12.21	9	ARP220;VV540;KPG470
	NGC 5962	1F15342+1646	15:36:31.4	+16:36:27	26.25	+50.47		0.73	14 RI	1.04	26 MI	8.93	31 MI	21.82	194 UT	1958	32.17	10.44	10.55	341	
	NGC 5990	1F15437+0234	15:46:16.0	+02:24:55	10.02	+41.45		0.60	43 UT	1.60	58 UT	9.59	30 UT	17.14	181 UT	3863	58.42	10.91	11.06	174	
	NGC 6000	2F15467-2914	15:49:49.4	-29:23:11	343.30	+19.17		1.48	25 RI	5.35	41 MI	35.64	137 UT	54.94	650 UT	2173	28.90	10.83	10.97	209	
	NGC 6052	1F16030+2040	16:05:12.3	+20:32:33	35.31	+45.47		0.28	22 UT	0.83	27 UT	6.79	45 UT	10.57	340 UT	4747	70.42	10.89	11.02	194	MRK0297;ARP209;VV086
	NGC 6090	1F16104+5235	16:11:40.8	+52:27:27	81.39	+45.21		0.26	20 UT	1.24	21 MI	6.48	30 UT	9.41	102 UT	8865	122.55	11.35	11.51	76	MRK0496;VV626;IZw135;KPG486
	ESO 137-G014	2 16129-5811	16:17:10.0	-58:18:43	327.30	-5.54		0.29	27 MI	1.00	26 UT	6.16	139 UT	8.12:	1682 UPn	2764	34.99	10.21:	10.37:	401	
	IC 4595	2F16154-7001	16:20:44.4	-70:08:35	319.03	-14.13		0.70	16 RI	0.67	19 UT	7.05	26 RI	18.64	193 UT	3419	45.75	10.68	10.78	267	
	IRAS F16164-0746	2F16164-0746	16:19:10.3	-07:53:57	5.73	+28.74		0.17:	30 USf	0.59:	35 UPn	10.29	50 UT	13.22	480 UT	8140	115.46	11.48	11.55:	69	
	CGCG 052-037	1F16284+0411	16:30:56.2	+04:04:58	19.27	+32.90		0.25	30 UT	0.81	31 UT	7.00	22 UT	11.23	133 UT	7342	104.72	11.26	11.38	91	
	ESO 452-G005	2 16285-2759	16:31:40.2	-28:06:11	351.00	+13.58		1.03	47 RI	1.18	53 RI	6.44	856 UT	---	UUC	4175	61.25	10.88	10.90	231	
	NGC 6181	1F16301+1955	16:32:21.7	+19:49:29	37.17	+39.21		0.63	27 MI	1.41	34 RI	8.94	33 MI	20.83	339 UT	2382	30.70 <sup>S</sup>	10.39	10.51	357	
	NGC 6156-2	2 16304-6030	16:34:51.9	-60:37:08	327.19	-8.76		1.23	17 RI	2.71	24 MI	17.17	49 MI	32.00	878 UT	3300	43.96	10.92	11.07	169	
	ESO 069-IG006	2F16330-6820	16:38:11.4	-68:26:07	321.40	-14.15		0.25	17 UT	0.71	19 UT	7.08	48 UT	12.68	276 UT	13926	188.61	11.82	11.92	224	AM1633-682
	NGC 6217	1F16350+7817	16:32:39.1	+78:11:50	111.32	+33.36		0.74	14 RI	2.03	16 RI	11.35	15 MI	20.62	79 UT	1353	23.49	10.19	10.34	411	ARP185
	IRAS F16399-0937	2F16399-0937	16:42:39.2	-09:43:11	7.89	+22.98		0.27:	28 UPn	1.13:	41 UPn	8.42:	68 UPn	14.72:	1179 UPc	8098	114.61	11.44:	11.56:	68	
	ESO 453-G005	2F16443-2915	16:47:29.8	-29:21:17	352.31	+10.13		<0.11	-	0.61	32 RI	9.56:	94 UPn	12.17:	1154 UTb	6335	91.55	11.24:	11.29:	116	
	NGC 6215	2 16467-5854	16:51:06.7	-58:59:38	329.78	-9.27		1.94	24 RI	3.53	32 RI	29.97	104 RI	47.55	642 UT	1560	19.04	10.39	10.54	344	
	NGC 6221	2 16484-5908	16:52:46.1	-59:13:00	329.74	-9.57		3.11	26 RI	7.48	28 RI	49.07	61 RI	86.06	188 MI	1482	18.02	10.58	10.73	284	AM1648-590
	NGC 6240	2F16504+0228	16:52:58.6	+02:24:03	20.73	+27.29		0.59	25 UT	3.55	20 UT	22.94	54 UT	26.49	174 UT	7298	103.86	11.73	11.85	30	VV617
	IRAS F16516-0948	2F16516-0948	16:54:24.2	-09:53:22	9.50	+20.50		0.27	20 UT	0.49	34 UT	5.32:	139 UPn	11.65:	668 UPn	6755	96.87	11.15:	11.24:	129	
	NGC 6286	1F16577+5900	16:58:30.8	+58:56:19	88.01	+37.43	S	0.47	15 RI	0.62	17 RI	9.24	43 MI	23.11	48 MI	5637	79.78	11.26	11.32	107	ARP293NED02
	NGC 6300	2F17123-6245	17:17:00.3	-62:49:13	328.49	-14.05		1.71	21 RI	3.25	26 RI	16.72	31 RI	42.45	145 MI	1110	13.11	9.94	10.09	505	VV734
	IRAS F17132+5313	1F17132+5313	17:14:20.5	+53:10:34	80.61	+35.75		0.24	21 RI	0.65	24 UT	6.07	34 UT	7.90	105 UT	15212	204.26	11.77	11.89	25	
	IRAS F17138-1017	2F17138-1017	17:16:36.3	-10:20:40	12.24	+15.67		0.63	28 UT	2.12	38 UT	15.18	58 UT	19.02	339 UT	5197	75.84	11.27	11.42	86	
	IRAS F17207-0014	2F17207-0014	17:23:21.4	-00:17:00	22.22	+19.36		0.20	25 UT	1.61	29 UT	32.13	57 UT	36.08:	555 UPc	12852	175.68	12.35:	12.39:	2	
	ESO 138-G027	2F17222-5953	17:26:43.7	-59:55:56	331.65	-13.51		0.33	29 UT	1.35	30 UT	9.53	58 UT	11.05	628 UT	6215	88.80	11.21	11.34	104	AM1722-595
	IC 4662	2F17422-6437	17:47:06.9	-64:38:17	328.55	-17.84		0.27	36 RI	1.27	29 MI	8.82	35 MI	11.38	82 UT	307	1.69	7.72	7.85	628	
	CGCG 083-025	2F17468+1320	17:49:06.6	+13:19:56	38.18	+19.74		<0.15	-	0.50	29 RI	7.10	78 UT	9.81	292 UT	4881	70.98	10.90	10.95	213	
	NGC 6503	1F17499+7009	17:49:27.9	+70:08:35	100.57	+30.64		1.08	8 RI	1.06	16 RI	10.08	16 RI	29.29	69 MI	-18	3.75	8.69	8.78	621	
	UGC 11041	2F17530+3447	17:54:51.7	+34:46:35	60.52	+26.02		0.51	17 RI	0.69	17 UT	5.84	20 UT	12.78	85 UT	4843	69.92	10.91	11.04	186	
	CGCG 141-034	2F17548+2401	17:56:55.2	+24:01:03	49.50	+22.16		0.18	18 UT	0.56	24 UT	6.24	37 UT	10.55	241 MI	5944	84.56	11.04	11.13	152	
	IRAS 17578-0400	2 17578-0400	18:00:32.0	-04:00:55	23.45	+9.42		0.22:	36 USf	1.14	40 UT	27.69	201 UT	33.10	1696 UT	3968	58.62	11.31	11.35:	98	
	IRAS 18090+0130	2 18090+0130	18:11:37.3	+01:31:40	29.73	+9.55		0.30	31 UT	0.81	31 UT	7.73:	80 UPn	15.64:	480 UPn	8662	120.21	11.49:	11.58:	64	
	IC 4687/6	2F18093-5744	18:13:38.6	-57:43:36	336.54	-17.91	R	1.01:	24 RIb	3.55:	20 RIb	20.20:	34 RIb	27.54:	95 MIb	5188	74.12	11.39:	11.55:	70	AM1809-574
	NGC 6574	2F18095+1458	18:11:51.0	+14:58:53	42.15	+15.41		0.91	31 UT	1.73	40 UT	14.57	167 UT	26.03	777 UT	2286	35.94	10.66	10.80	262	
	ESO 140-G012	2F18097-6006	18:14:17.4	-60:05:30	334.27	-18.88		0.41	30 UT	1.02	31 UT	5.69	42 UT	9.51	462 UT	3159	43.60	10.41	10.58	333	AM1809-600
	NGC 6621	2F18131+6820	18:12:55.2	+68:21:47	98.47	+28.60	R	0.31	17 UT	0.97	12 UT	6.78	22 UT	12.01	87 UT	6234	86.42	11.10	11.23	132	ARPO81NED01;VV247a;VII Zw778;KPG534A
	CGCG 142-034	2F18145+2205	18:16:39.6	+22:06:44	49.43	+17.23	R	0.30	28 UT	0.55	21 UT	6.25	64 UT	11.94	309 UT	5599	79.74	11.01	11.11	157	
	NGC 6643	2F18212+7432	18:19:47.4	+74:34:09	105.54	+28.17		1.26	19 RI	1.42	23 RI	12.02	28 RI	31.63	84 UT	1485	21.85 <sup>S</sup>	10.26	10.37	396	
	IRAS F18293-3413	2F18293-3413	18:32:40.2	-34:11:26	0.15	-11.30		1.14	33 UT	3.98	43 UT	35.71	79 UT	53.38	388 UT	5449	77.76	11.69	11.81	33	
	NGC 6670A/B	2F18329+5950	18:33:35.6	+59:53:20	89.31	+25.42	R	0.36	25 UT	1.05	17 UT	8.98	37 UT	14.20	183 UT	8684	118.38	11.48	11.60	53	VII Zw812
	IC 4734	2F18341-5732	18:38:26.5	-57:29:24	338.00	-20.94		0.38	26 UT	1.33	37 UT	14.04	55 UT	25.31	178 UT	4813	68.57	11.22	11.30	114	





TABLE 1—*Continued*

Name		R. A. (J2000) DEC		$\ell$	$b$	HR	$12\mu\text{m}$			$25\mu\text{m}$			$60\mu\text{m}$			$100\mu\text{m}$			$cz$	$D$	$\log(L_{\text{IR}}, L_{\text{IR}})$			IG/AGN Names	
Common (1)	IRAS (2)	hh:mm:ss.s (3)	°:':" (4)	° (5)	° (6)	(7)	Jy	mJy	SMF	Jy	mJy	SMF	Jy	mJy	SMF	Jy	mJy	SMF	km/s (12)	Mpc (13)	$L_{\odot}$ (14)	$L_{\odot}$ (15)	Rank (16)	(17)	
	NGC 7465	1 F22594+1542	23:01:58.4	+15:58:11	88.06	-39.38	S	0.26	42	UT	0.67	39	RI	5.47	42	RI	8.14:	237	RIb	1968	27.44	9.96:	10.10:	501	MRK0313
	NGC 7469	1 F23007+0836	23:03:15.5	+08:52:25	83.10	-45.47	S	1.59	39	RI	5.96	32	UT	27.33	40	UT	35.16	599	UT	4922	65.23	11.40	11.59	59	ARP298NED01;MRK1514;KPG575A
	NGC 7479	1 F23024+1203	23:04:57.7	+12:19:29	86.28	-42.84		1.37	28	RI	3.86	71	MI	14.93	49	RI	26.73	247	MI	2364	32.36	10.58	10.79	263	
	CGCG 453-062	1 F23024+1916	23:04:55.2	+19:33:01	91.16	-36.66		0.19	38	UT	0.54	38	UT	7.19	47	UT	11.73:	163	UPn	7524	98.96	11.23:	11.31:	110	
	NGC 7496	2 F23069-4341	23:09:46.1	-43:25:43	347.84	-63.80		0.58	34	RI	1.93	34	MI	10.14	39	MI	16.57	67	MI	1649	22.34	10.07	10.23	451	VV771
	IRAS 23085+6723	2 23085+6723	23:10:32.0	+67:39:40	113.55	+6.65		0.44	23	UT	1.94	22	UT	7.64:	38	UPn	8.26:	857	UPn	1478	23.26	9.94:	10.13:	490	
	NGC 7541	1 F23121+0415	23:14:43.3	+04:32:00	82.84	-50.65	S	1.52	54	RI	2.09	46	RI	20.08	55	MI	41.87	104	UT	2663	30.09 <sup>S</sup>	10.69	10.81	258	KPG578B
	ESO 148-IG002	2 F23128-5919	23:15:46.6	-59:03:14	323.73	-54.04		0.35	24	RI	1.64	26	UT	10.94	37	UT	10.68	100	UT	13403	177.75	11.89	12.00	19	AM2312-591
	NGC 7552	2 F23133-4251	23:16:09.5	-42:35:09	348.15	-65.23	S	3.76	82	RI	11.92	30	UT	77.37	92	UT	102.92	188	UT	1585	21.44	10.88	11.03	189	VV440;GrusQuartetNED01
	IC 5298	1 F23135+2517	23:16:01.7	+25:33:33	97.30	-32.52		0.34	24	RI	1.95	53	MI	9.06	51	UT	11.99	97	UT	8241	108.19	11.37	11.54	73	
	NGC 7582	2 F23156-4238	23:18:22.2	-42:22:19	348.08	-65.69	S	2.30	33	RI	7.39	22	MI	52.20	114	MI	82.86	109	MI	1575	21.29	10.73	10.87	244	GrusQuartetNED02
	NGC 7591	1 F23157+0618	23:18:15.7	+06:35:06	85.76	-49.44		0.28	36	UT	1.27	62	RI	7.87	51	MI	14.87	321	UT	4961	65.49	10.94	11.05	180	
	NGC 7592	1 F23157-0441	23:18:22.2	-04:24:56	74.49	-58.24	U	0.26	31	UT	0.97	56	UT	8.05	49	UT	10.58	137	UT	7242	95.13	11.21	11.33	106	VV731
	NGC 7593	2 F23161-4230	23:18:55.5	-42:14:17	348.23	-65.85	S	0.69	38	RI	0.89	26	UT	7.69	42	MI	20.79	98	MI	1596	21.58	10.06	10.16	482	GrusQuartetNED03
	NGC 7599	2 F23165-4231	23:19:20.6	-42:15:25	348.09	-65.91	S	0.74	27	RI	0.77	26	MI	6.39	48	MI	18.31:	88	UPn	1654	22.38	10.04:	10.14:	486	GrusQuartetNED04
	NGC 7625	1 F23179+1657	23:20:30.0	+17:13:34	93.91	-40.47		0.61	32	UT	1.04	36	UT	8.64	32	UT	18.51	146	UT	1611	22.73	10.08	10.20	462	ARP212;VV280;IIIZw102
	ESO 077-IG014	2 F23180-6929	23:21:05.0	-69:12:49	314.22	-45.88	U	0.20	16	RI	0.45	22	UT	5.70	19	UT	9.90	104	UT	12460	166.27	11.61	11.70	42	AM2317-692
	NGC 7674	1 F23254+0830	23:27:56.9	+08:46:46	90.63	-48.79		0.68	37	UT	1.92	34	UT	5.36	42	UT	8.33	141	UT	8688	113.64	11.22	11.50	78	ARP182NED01;VV343a;MRK0533;HCG096A
	NGC 7678	1 F23259+2208	23:28:27.0	+22:25:09	98.88	-36.55		0.63	25	RI	1.16	29	RZ	6.98	70	MI	14.84	115	UT	3482	46.49	10.61	10.77	271	ARP028;VV359
	NGC 7679	1 23262+0314	23:28:47.0	+03:30:46	86.68	-53.44		0.50	38	UT	1.12	69	UT	7.40	42	UT	10.71	100	UT	5143	67.70	10.88	11.05	182	ARP216NED01;VV329a;MRK0534
	NGC 7714	1 F23336+0152	23:36:14.2	+02:09:17	88.22	-55.56	S	0.47	36	UT	2.88	59	UT	11.16	62	UT	12.26	125	UT	2858	38.16	10.53	10.72	290	ARP284NED01;VV051a;MRK0538;KPG587A
	IRAS F23365+3604	2 F23365+3604	23:39:01.7	+36:21:14	107.00	-24.27		<0.09	-		0.94	25	MI	7.44	46	UT	9.01	216	UT	19330	251.84	12.04	12.13:	12	
	MCG -01-60-022	N F23394-0353	23:42:02.2	-03:36:48	84.74	-61.23	S	0.41	29	RI	1.06	66	RI	5.39	34	MI	8.26	119	UT	6966	91.19	11.02	11.21	137	VV034a;ARP295B
	IRAS 23436+5257	2 23436+5257	23:46:05.8	+53:14:00	113.13	-8.39		0.17	29	UT	0.74	22	UT	5.66	44	MI	9.01:	185	UPn	10233	134.78	11.40:	11.51:	75	
	NGC 7752/3	N F23444+2911	23:47:01.3	+29:28:11	106.51	-31.34	R	0.59	42	RI	0.83	53	RI	5.79	59	RI	11.58	555	UT	5118	67.46	10.84	11.01	197	ARP086;VV005;KPG591
	NGC 7771	1 F23488+1949	23:51:24.7	+20:06:39	104.26	-40.57	S	0.99	36	RI	2.17	36	RI	19.67	135	UT	40.12	839	UT	4336	57.11	11.23	11.34	105	MRK9006;KPG592B
	MRK 0331	1 F23488+2018	23:51:26.1	+20:35:08	104.46	-40.12	U	0.52	35	UT	2.54	26	MI	18.00	46	UT	22.70	194	UT	5371	70.46	11.28	11.41	87	KPG593B
	NGC 7793	2 F23552-3252	23:57:48.5	-32:35:28	4.52	-77.17		1.32	38	RI	1.67	48	RI	18.14	48	RI	54.07	89	RI	230	3.10 <sup>S</sup>	8.79	8.84	619	AM2355-325
	UGC 12914/5	1 F23591+2312	00:01:40.7	+23:29:37	108.42	-37.97	R	0.46	40	RI	0.83	43	RI	6.41	37	MI	14.11	178	UT	4534	59.62	10.81	10.93	221	VV254;IIIZw125;KPG603;TAFFYGALAXY

NOTE.—See the text for explanations of the column contents, flags, and codes.

### 3.1. Annotated Images from the Digitized Sky Survey

Figure 1 presents images extracted from the Digitized Sky Survey (DSS1)<sup>10</sup> for all objects in the RBGS. They are intended to quickly visualize the optical morphology in context with the angular and metric size of each object. Horizontal bars on the bottom of each plot show the angular scale labeled in arcminutes, and vertical bars on the lower right side of each plot show the metric scale labeled in kiloparsecs. Metric sizes are derived using the source distance estimates listed in Table 1. The ellipses represent 3-sigma uncertainties in the *IRAS* positions from the FSC and PSC. Note that for the LMC and SMC, no ellipse is shown because there is no point source from the FSC or PSC corresponding to the “center” of these large, diffuse galaxies. In general there is very good agreement between the *IRAS* catalog source position and the coordinates of the optical galaxy. A notable exception is the position of *IRAS* 10574-6603 taken from the PSC, which has a large offset from the optical galaxy ESO 093-G003. The fact that this offset is in the direction of the major axis of the *IRAS* positional uncertainty ellipse ( $PA = 150^\circ$ ), and that SCANPI shows a peak in the *IRAS* emission that is coincident with the position of the optical galaxy, confirms this cross-identification. In some cases the *IRAS* source position is located between components of optical pairs or groups of galaxies. This is a clear indication that more than one galaxy contributes significantly to the *IRAS* emission. Such objects (e.g., AM 0702-601, ESO 297-G011/12, IC 563/4, NGC 7465) are a subset of the pairs and groups investigated using HIRES processing of the *IRAS* data (Surace, Sanders & Mazzarella 2003), which are flagged by “(H)” following the object names in Figure 1.

---

<sup>10</sup>The Digitized Sky Survey was produced at the Space Telescope Science Institute under U.S. Government grant NAG W-2166. The images of these surveys are based on photographic data obtained using the Oschin Schmidt Telescope on Palomar Mountain and the UK Schmidt Telescope. The plates were processed into the present compressed digital form with the permission of these institutions.

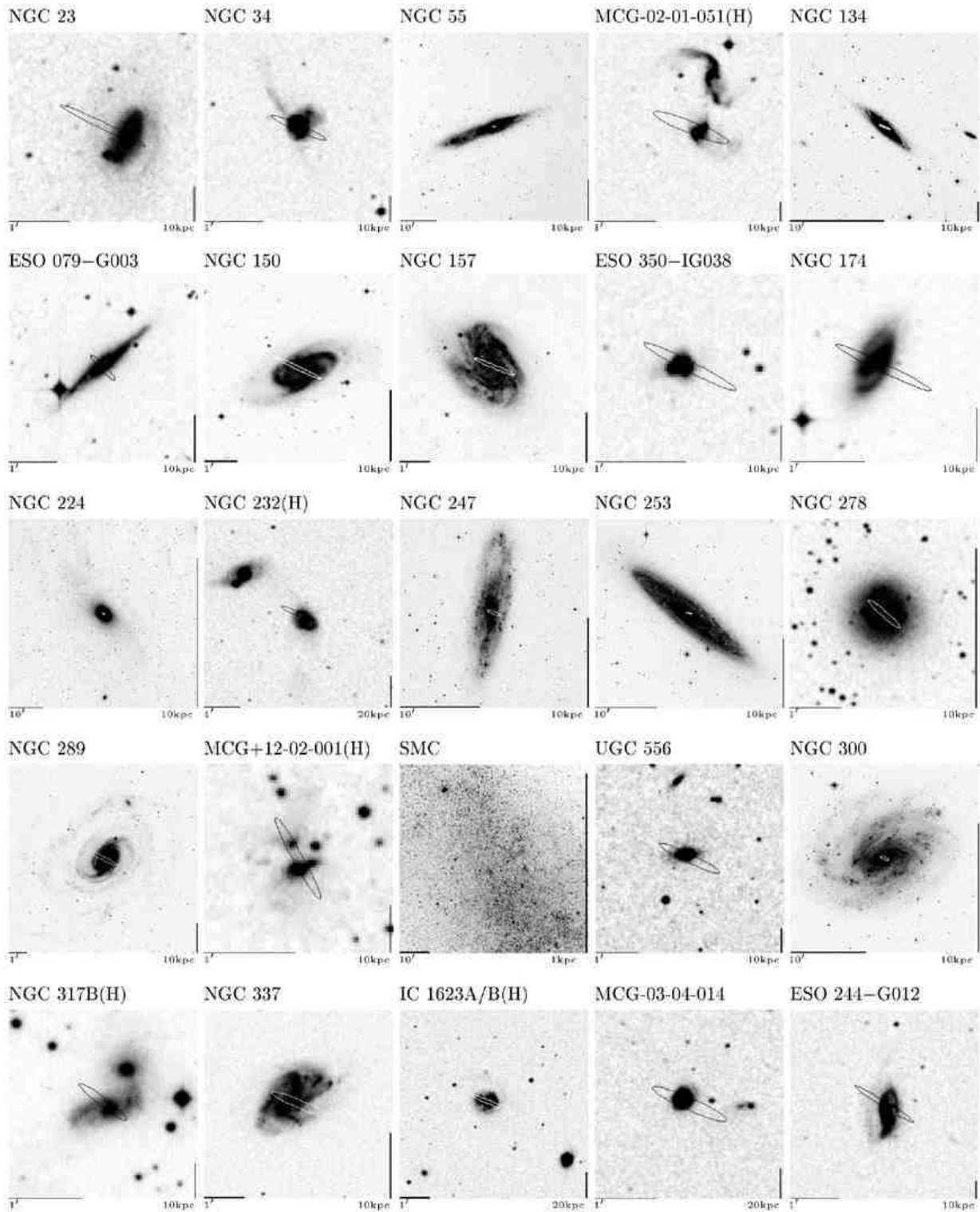


Fig. 1.— DSS1 images of each RBGS object. Horizontal bars on the bottom of each plot show the angular scale labeled in arcminutes, and vertical bars on the lower right side of each plot show the metric scale labeled in kiloparsecs. The ellipses represent 3-sigma uncertainties in the IRAS positions. (Note: For the LMC and SMC, no ellipse is shown because there is no FSC or PSC source corresponding to the “center” of these large, diffuse galaxies.) Pairs and groups for which improved 2-D spatial resolution has been attempted using HIRES processing of the IRAS data (Surace, Sanders & Mazzarella 2003) are indicated by “(H)” following the object name. **NOTE: Due to astro-ph size limits, only 1 of 26 pages in Figure 1 is included here, and it is degraded by bit-mapping. A complete, full resolution version of this figure will be published in the *Astronomical Journal* and is also available at [http://nedwww.ipac.caltech.edu/level5/March03/IRAS\\_RBGS/Figures/Fig1p\\*.ps.gz](http://nedwww.ipac.caltech.edu/level5/March03/IRAS_RBGS/Figures/Fig1p*.ps.gz).**



### 3.2. Revisions from the Original BGS<sub>1</sub> and BGS<sub>2</sub>

Table 2 is a list of objects from the BGS<sub>1</sub>+BGS<sub>2</sub> that have been omitted from the RBGS because their revised 60  $\mu$ m flux density is less than or equal to 5.24 Jy. The table caption explains why some of these objects were listed with  $S_\nu(60\mu m) \leq 5.24$  Jy in BGS<sub>1</sub>.

Table 3 is a list of objects from the BGS<sub>1</sub>+BGS<sub>2</sub> which have revised cross-identifications in various catalogs. These corrected, revised cross-identifications were determined by visualizing the *IRAS* uncertainty ellipses superimposed on the DSS images (Figure 1), and by using current information available in NED.

Table 4 is a summary of the 39 objects which are new members of the RBGS. These objects were missed during compilation of the BGS<sub>1</sub>+BGS<sub>2</sub> for a variety of reasons. Their presence in the RBGS is the result of comprehensive searches utilizing NED in conjunction with queries of the *IRAS* catalogs, followed by examination of the *IRAS* scan data using SCANPI.

TABLE 2  
BGS<sub>1</sub> + BGS<sub>2</sub> OBJECTS OMITTED DUE TO REVISED  $S_\nu(60\mu m) \leq 5.24$  JY

Name	Revised $S_\nu(60\mu m)$ Jy	Status
NGC 0578	$4.64 \pm 0.04$	BGS <sub>1</sub> had $S_\nu(60\mu m) = 4.64$ Jy <sup>a</sup>
NGC 1012	$5.19 \pm 0.04$	BGS <sub>2</sub> had $S_\nu(60\mu m) = 5.37$ Jy
NGC 1141/2	$5.06 \pm 0.02$	BGS <sub>1</sub> had $S_\nu(60\mu m) = 5.06$ Jy <sup>a</sup>
UGC 2789	$5.23 \pm 0.03$	BGS <sub>2</sub> had $S_\nu(60\mu m) = 5.24$ Jy
ESO 484-G036	$5.10 \pm 0.04$	BGS <sub>1</sub> had $S_\nu(60\mu m) = 5.44$ Jy; named IR 0433-25 in BGS <sub>1</sub>
VII Zw 019	$5.05 \pm 0.03$	BGS <sub>2</sub> had $S_\nu(60\mu m) = 5.35$ Jy
IRAS F00555+7614	$5.14 \pm 0.05$	BGS <sub>2</sub> had $S_\nu(60\mu m) = 5.32$ Jy; named IR 00555+7614 in BGS <sub>2</sub>
IRAS F06035-7102	$5.18 \pm 0.03$	BGS <sub>2</sub> had $S_\nu(60\mu m) = 5.34$ Jy; named IR 06035-7102 in BGS <sub>2</sub>
NGC 2820	$4.34 \pm 0.03$	BGS <sub>1</sub> had $S_\nu(60\mu m) = 4.23$ Jy <sup>a</sup>
NGC 2990	$5.20 \pm 0.03$	BGS <sub>1</sub> had $S_\nu(60\mu m) = 5.49$ Jy
NGC 3353	$5.17 \pm 0.05$	BGS <sub>1</sub> had $S_\nu(60\mu m) = 5.54$ Jy
ESO 174-G005	$5.23 \pm 0.13$	BGS <sub>2</sub> had $S_\nu(60\mu m) = 5.29$ Jy
NGC 4395	$4.69 \pm 0.06$	BGS <sub>1</sub> had $S_\nu(60\mu m) = 4.21$ Jy <sup>a</sup>
NGC 4438	$3.87 \pm 0.03$	BGS <sub>1</sub> had $S_\nu(60\mu m) = 3.86$ Jy <sup>a</sup>
NGC 4594	$4.28 \pm 0.03$	BGS <sub>1</sub> had $S_\nu(60\mu m) = 3.98$ Jy <sup>a</sup>
NGC 4618	$5.13 \pm 0.03$	BGS <sub>1</sub> had $S_\nu(60\mu m) = 4.92$ Jy <sup>a</sup>
MCG +08-23-097	$4.91 \pm 0.04$	BGS <sub>1</sub> had $S_\nu(60\mu m) = 4.79$ Jy <sup>a</sup>
ESO 383-G027	$5.16 \pm 0.05$	BGS <sub>2</sub> had $S_\nu(60\mu m) = 5.31$ Jy
UGC 09668	$5.24 \pm 0.03$	BGS <sub>1</sub> had $S_\nu(60\mu m) = 5.70$ Jy
IRAS F15335-0513	$5.16 \pm 0.03$	BGS <sub>1</sub> had $S_\nu(60\mu m) = 5.25$ Jy; named IR 1533-05 in BGS <sub>1</sub>
IRAS 18587-1653	$5.20 \pm 0.12$	BGS <sub>2</sub> had $S_\nu(60\mu m) = 5.51$ Jy
AM 1925-724	$5.16 \pm 0.03$	BGS <sub>2</sub> had $S_\nu(60\mu m) = 5.30$ Jy
IRAS 19279+3534	$5.22 \pm 0.09$	BGS <sub>2</sub> had $S_\nu(60\mu m) = 5.43$ Jy
IRAS 20100-4156	$5.19 \pm 0.04$	BGS <sub>2</sub> had $S_\nu(60\mu m) = 5.44$ Jy
IC 4946	$5.24 \pm 0.03$	BGS <sub>2</sub> had $S_\nu(60\mu m) = 5.31$ Jy; named A2020-44 in BGS <sub>2</sub>
NGC 6015	$4.40 \pm 0.03$	BGS <sub>1</sub> had $S_\nu(60\mu m) = 4.42$ Jy <sup>a</sup>
NGC 6070	$5.10 \pm 0.03$	BGS <sub>1</sub> had $S_\nu(60\mu m) = 5.07$ Jy <sup>a</sup>
NGC 7673	$4.98 \pm 0.05$	BGS <sub>1</sub> had $S_\nu(60\mu m) = 4.98$ Jy <sup>a</sup>

<sup>a</sup>These objects were listed in Table 1(b) of BGS<sub>1</sub> (Soifer et al. 1989) as having  $S_\nu(60\mu m) < 5.24$  Jy. However, they were also included in the main BGS<sub>1</sub> catalog listing [Table 1(a)], because of their presence in an earlier compilation (Soifer et al. 1987). Since some readers may have been confused regarding the status of these objects, these sources are listed here again and omitted in Table 1 of this work to clarify their status.

TABLE 3  
CATALOG CROSS-IDENTIFICATION CHANGES

Name	Status
MCG -02-01-051/2 (Arp 256)	IRAS emission identified with MCG -02-01-051 in BGS <sub>1</sub> <sup>a</sup>
SMC	Named A0051-73 in BGS <sub>2</sub> (not recognized by NED)
NGC 0317B	IRAS emission identified with pair NGC 317A/B in BGS <sub>2</sub> <sup>b</sup>
CGCG 436-030	Named MCG +02-04-035 in BGS <sub>1</sub> (same object)
NGC 0716	Named UGC 1351 in BGS <sub>1</sub> (same object)
ESO 297-G011/12	IRAS emission identified with largest galaxy in the pair (NGC 633 = ESO 297-G011) in BGS <sub>2</sub> <sup>c</sup>
IC 0214	Named UGC 1720 in BGS <sub>1</sub> (same object)
IRAS F03217+4023	Named IRAS 03217+4022 in BGS <sub>2</sub> (same object)
CGCG 465-012	Named Zw 465.012 in BGS <sub>2</sub> (same object)
ESO 550-IG02	Named MCG -03-12-002 in BGS <sub>1</sub> (same object)
ESO 485-G003	Named MCG -04-12-003 in BGS <sub>1</sub> (same object)
ESO 491-G020/021	Named ESO 491-G020 in BGS <sub>2</sub> (same object)
CGCG 011-076	Named MCG +00-29-023 in BGS <sub>2</sub> (same object)
NGC 4175	Mistakenly named NGC 4174 (12h12m26.9s, +29d08m58s J2000) in BGS <sub>1</sub>
NGC 2798	IRAS emission identified with NGC 2799 (SE companion) in BGS <sub>1</sub>
MCG +08-18-013	IRAS emission identified with MCG +08-18-012 (SW companion) in BGS <sub>1</sub>
IC 2810	Named UGC 6436 in BGS <sub>1</sub> (same object)
NGC 3994/5	IRAS emission identified with NGC 3994 in BGS <sub>1</sub> <sup>d</sup>
NGC 4568/7	IRAS emission identified with NGC 4568 (SE component of pair) in BGS <sub>1</sub>
NGC 4793	Mistakenly named NGC 4783 (12h54m36.6s, -12d33m28s J2000) in BGS <sub>1</sub>
CGCG 043-099	Named MCG +01-33-036 in BGS <sub>1</sub> (same object)
MCG -02-33-098/9	Named MCG -02-33-098 in BGS <sub>2</sub> ; IRAS emission dominated by MCG -02-33-098
MCG -03-34-014	Named A1309-17 in BGS <sub>2</sub> (not recognized by NED)
VV 250a	IRAS emission identified with UGC 8335 = VV 250 in BGS <sub>1</sub> <sup>e</sup>
MCG -03-34-064	IRAS emission identified with MCG -03-34-063 in BGS <sub>2</sub>
NGC 5257/8	IRAS emission identified with NGC 5257 in BGS <sub>1</sub> <sup>f</sup>
CGCG 247-020	Named Zw 247.020 in BGS <sub>1</sub> (same object)
NGC 5665	Mistakenly named NGC 5663 (14h33m56.3s, -16d34m52s J2000) in BGS <sub>1</sub>
VV 340a	IRAS emission identified with UGC 9618 = VV 340 in BGS <sub>1</sub> <sup>g</sup>
CGCG 049-057	Named Zw 049.057 in BGS <sub>1</sub> (same object)
VV 705	Named I Zw 107 in BGS <sub>1</sub> (same object)
NGC 5930	IRAS emission identified with NGC 5929 in BGS <sub>1</sub> <sup>h</sup>
CGCG 052-037	Mistakenly named MCG +01-42-088 in BGS <sub>1</sub> (no such object in NED)
NGC 6286	IRAS emission identified with NGC 6285/6 in BGS <sub>1</sub>
CGCG 083-025	Named Zw 083.025 in BGS <sub>2</sub> (same object)
CGCG 141-034	Named Zw 141.034 in BGS <sub>2</sub> (same object)
NGC 6621	IRAS emission identified with NGC 6621/22 in BGS <sub>2</sub>
CGCG 142-034	Named Zw 142.034 in BGS <sub>2</sub> (same object)
IC 4946	Named A2020-44 in BGS <sub>2</sub> ((not recognized by NED)
CGCG 448-020	Named Zw 448.020 in BGS <sub>2</sub> (same object)
ESO 602-G025	Named MCG -03-57-017 in BGS <sub>1</sub> (same object)
CGCG 453-062	Named Zw 453.062 in BGS <sub>1</sub> (same object)
IC 5298	Named Zw 475.056 in BGS <sub>1</sub> (same object)

<sup>a</sup>IRAS centroid is on the SE component of the pair, but both galaxies are within the IRAS beam (Fig. 1); see also Surace, Sanders & Mazzarella 2003.

<sup>b</sup>IRAS centroid is clearly on the SE component of NGC 317; see Fig. 1.

<sup>c</sup>IRAS centroid is clearly between the NW (NGC 633 = ESO 297-G011) and SE (ESO 297-G012) pair components; see Fig. 1.

<sup>d</sup>IRAS centroid is clearly between SW (NGC 3994) and NE (NGC 3995) pair components; see Fig. 1.

<sup>e</sup>IRAS centroid is clearly dominated by VV 250a = MCG +10-19-057; see Fig. 1.

<sup>f</sup>IRAS centroid is clearly between NGC 5257/8; see Figure 1.

<sup>g</sup>IRAS centroid is clearly dominated by VV 340a = MCG +04-35-019; see Fig. 1.

<sup>h</sup>NGC 5929 is the SW companion of the dominant IRAS source NGC 5930; see Fig. 1.

TABLE 4  
 ADDITIONS TO THE RBGS

Name	Revised $S_\nu(60\mu\text{m})$ Jy	Status
NGC 0289	5.47	Found in IRAS PSC/FSC and confirmed with SCANPI
NGC 0300	15.30	Large optical galaxy (Rice et al. 1993) <sup>a</sup>
NGC 0925	7.82	Large optical galaxy (Rice et al. 1988) <sup>a</sup>
IC 0356	6.77	Found in IRAS PSC/FSC and confirmed with SCANPI
NGC 1532	9.63	Found in IRAS PSC/FSC and confirmed with SCANPI
CGCG 468-002	9.66	Orion region with high Galactic foreground confusion (see Fig. 5)
NGC 1819	6.85	Orion region with high Galactic foreground confusion (see Fig. 5)
IRAS F05170+0535	14.4	Orion region with high Galactic foreground confusion (see Fig. 5)
IRAS F05405+0035	7.03	Orion region with high Galactic foreground confusion (see Fig. 5)
UGCA 116	6.57	Orion region with high Galactic foreground confusion (see Fig. 5)
IRAS F06076-2139	6.43	Orion region with high Galactic foreground confusion (see Fig. 5)
IC 2163	17.55	Orion region with high Galactic foreground confusion (see Fig. 5)
UGCA 127	17.61	Orion region with high Galactic foreground confusion (see Fig. 5)
UGCA 128	5.38	Orion region with high Galactic foreground confusion (see Fig. 5)
NGC 2221	6.41	Found in IRAS PSC/FSC and confirmed with SCANPI
ESO 557-G002	7.42	Orion region with high Galactic foreground confusion (see Fig. 5)
AM 0702-601	6.70	Found in IRAS PSC/FSC and confirmed with SCANPI
UGCA 150	6.03	Found in IRAS PSC/FSC and confirmed with SCANPI
NGC 2992	7.51	Each component of NGC 2992/3 has $S_\nu(60\mu\text{m}) > 5.24$ Jy
IC 2522	6.47	Found in IRAS PSC/FSC and confirmed with SCANPI
NGC 3125	5.33	Found in IRAS PSC/FSC and confirmed with SCANPI
NGC 3732	5.36	Found in IRAS PSC/FSC and confirmed with SCANPI
NGC 4151	6.46	Found in IRAS FSC Rejects (IRAS Z12080+3940) and confirmed with SCANPI
NGC 4217	11.60	Found in IRAS PSC/FSC and confirmed with SCANPI
NGC 4437	7.87	Large optical galaxy (Rice et al. 1988) <sup>a</sup>
NGC 5010	10.29	Found in IRAS PSC/FSC and confirmed with SCANPI
NGC 5068	12.50	Found in IRAS PSC/FSC and confirmed with SCANPI
NGC 5331	5.86	In Soifer et al. (1987) sample but dropped in BGS <sub>1</sub>
NGC 5483	6.30	Found in IRAS PSC/FSC and confirmed with SCANPI
UGCA 394	5.83	Found in IRAS PSC/FSC and confirmed with SCANPI
IRAS 16399-0937	8.42	Found in IRAS PSC/FSC and confirmed with SCANPI
NGC 6744	18.92	Large optical galaxy (Rice et al. 1988) <sup>a</sup>
NGC 6786/UGC 11415	7.58	Found in IRAS PSC/FSC and confirmed with SCANPI
NGC 6822	47.63	Large optical galaxy (Rice et al. 1988) <sup>a</sup>
IRAS 19542+1110	6.18	Found in IRAS PSC/FSC and confirmed with SCANPI
NGC 7331	45.00	Large optical galaxy (Rice et al. 1988) <sup>a</sup>
NGC 7418	6.67	Found in IRAS PSC/FSC and confirmed with SCANPI
MCG -01-60-022	5.39	Found in IRAS PSC/FSC and confirmed with SCANPI
NGC 7752/3	5.79	Found in IRAS PSC/FSC and confirmed with SCANPI

<sup>a</sup>SCANPI  $S_\nu(60\mu\text{m})$  profile zero-crossing size is comparable to optical size of the galaxy, and SCANPI  $S_\nu(12\mu\text{m})$  and  $S_\nu(25\mu\text{m})$  values are larger than or comparable to those of Rice et al. (1988) and Rice (1993), so SCANPI zero-crossing values are adopted in RBGS for this object.



## 4. Discussion

The main purpose for compiling the RBGS was to produce a more accurate and complete list of *IRAS* bright galaxies, one that both incorporates the improved final calibration of the *IRAS* Level 1 Archive and one that makes use of the best available SCANPI tools to more accurately compute total *IRAS* flux densities in all four *IRAS* wavebands. Just as important was the desire to provide a more accurate assessment of the various sources of uncertainty (e.g. source confusion, cirrus contamination, etc.) in the final list of tabulated flux densities. This was not always clear in the earlier published versions of the BGS<sub>1</sub>+BGS<sub>2</sub>. The reader can use the flags in the RBGS tables to decide when it may be desirable to use the SCANPI tool available through the Infrared Science Archive (IRSA) at IPAC<sup>11</sup> for a direct visual inspection of the scan profiles. Also, rather than leave it to the reader to compute infrared luminosities for each source, we have attempted to compile the most recent and accurate redshifts from the literature. We then list the adopted source distances which have been used to compute total far-infrared (using *IRAS* bands 3 and 4) and infrared (all 4 *IRAS* bands) luminosities according to standardized prescriptions that are now widely adopted in the literature (e.g., Sanders & Mirabel 1996).

We begin the discussion of the RBGS data by first providing a detailed comparison of how the “new” *IRAS* flux densities compare with the “old” previously published values. This is followed by a discussion of the survey sky coverage and distribution of sources on the sky, plus a discussion of the completeness of the survey in all four *IRAS* bands. Various properties of the RBGS are then discussed, ending with the presentation of the new infrared luminosity function for *IRAS* bright galaxies selected at 60  $\mu\text{m}$ .

### 4.1. Comparison Between Revised and Previous Flux Density Measurements

Figure 2 shows the ratio of the new RBGS total flux density measurements to the previously published BGS<sub>1</sub>+BGS<sub>2</sub> measurements versus the new total flux density measurements in each *IRAS* band. In general the largest differences occur at

the low end of the range of measured flux densities in all four *IRAS* bands, with the 12  $\mu\text{m}$  and 25  $\mu\text{m}$  bands showing the most dramatic changes, up to a factor of  $\pm 2$  in the few most extreme cases. Much of these differences can be accounted for simply by more mature data processing, which had the greatest effect near the survey lower limits in each of the *IRAS* bands. At 60  $\mu\text{m}$  and 100  $\mu\text{m}$ , where the measured fluxes were often substantially above the *IRAS* FSC survey limits, the maximum change is typically a more modest factor of  $\pm 30\%$ . At flux densities more than a factor of 2 above the *IRAS* FSC limits the “new” and “old” values differ by typically  $< 15\%$ . There is a noticeable tendency for the revised flux density measurements to be systematically higher, on average  $\sim 5\%$ , among objects brighter than about 35 Jy at 60  $\mu\text{m}$ , and across the entire range of observed flux densities at 100  $\mu\text{m}$ . This is due to a better understanding of the fact that for many of the extended sources with high signal-to-noise ratios, some of the flux extends beyond the previously adopted  $f_\nu(t)$  aperture size, and is better measured by using  $f_\nu(z)$ . In addition, the original processing used for BGS<sub>1</sub>+BGS<sub>2</sub> based the choice of whether to use  $f_\nu(t)$  instead of  $f_\nu(\text{template})$  only on the coadded scan profile widths (a comparison of FWHM and the width at 25% peak to nominal values observed for pure point sources). However, many galaxies have profile widths which are not significantly broader than what is expected for a point source, yet there is extended emission in a faint “pedestal” that can be reliably measured as a statistically significant excess of the  $f_\nu(t)$  aperture value over the  $f_\nu(\text{template})$  point source fitted value; see the Appendix (Fig. 16) for further details.

<sup>11</sup>See <http://irsa.ipac.caltech.edu/>.

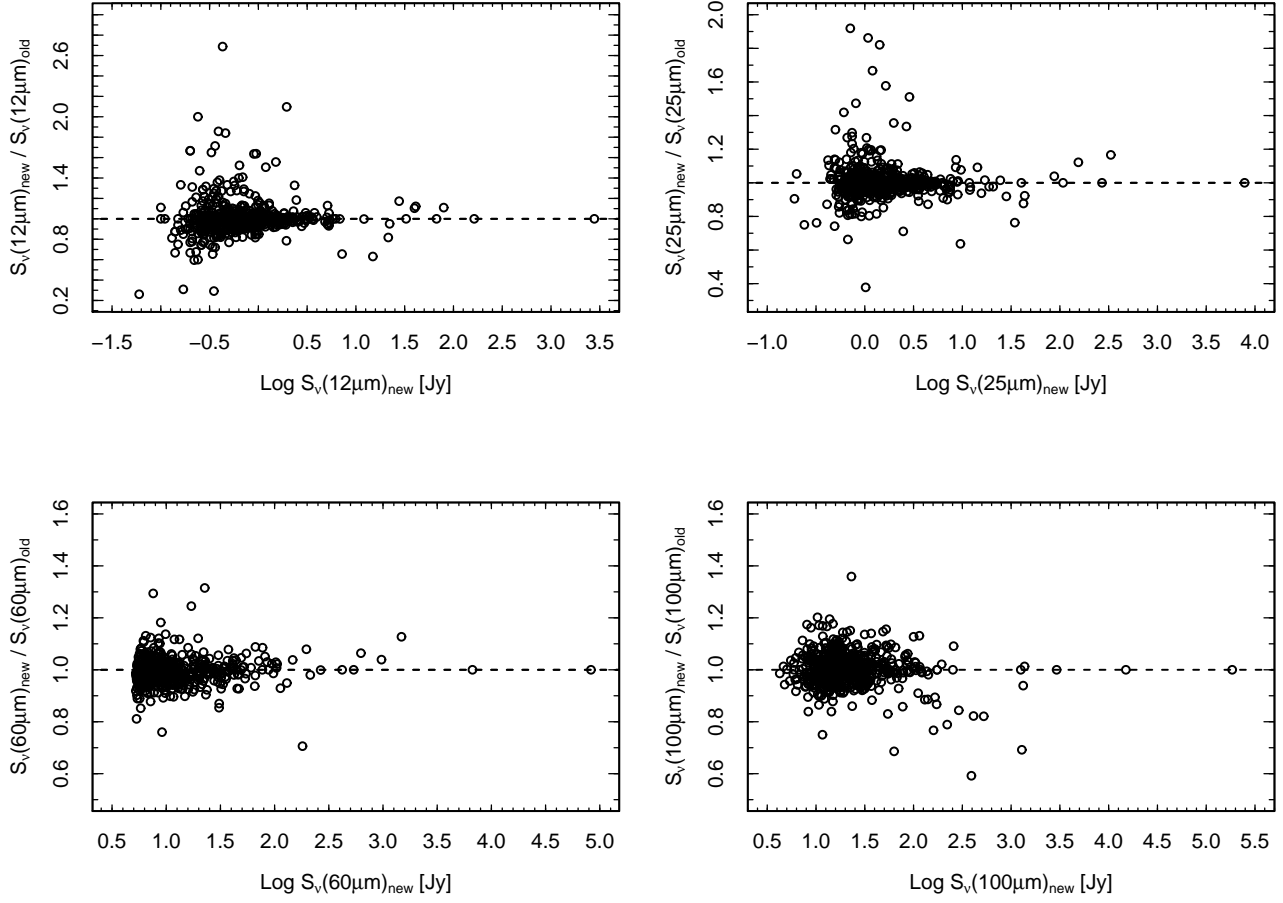


Fig. 2.— The ratio of new total flux density measurements to original estimates versus the base 10 log of the new total flux density at  $12\ \mu\text{m}$ ,  $25\ \mu\text{m}$ ,  $60\ \mu\text{m}$  and  $100\ \mu\text{m}$ .

All sources with extreme  $S_\nu(\text{new})/S_\nu(\text{old})$  flux ratios in Figure 2 were examined in detail, and they are explained by various improvements in the revised processing. Some objects with  $S_\nu(\text{new})/S_\nu(\text{old}) < 0.8$  are cases where the RBGS flux densities have been estimated by using SCLEAN (see Appendix) or peak values to minimize confusion from companion galaxies in pairs, nearby stars, or cirrus, where in BGS<sub>1</sub>+BGS<sub>2</sub> the  $f_\nu(t)$  method was used and therefore the flux densities quoted there were contaminated (over estimated). Examples are NGC 5194 and NGC 5195, where SCLEAN was used in RBGS to separate the components of this galaxy pair (M 51) at 12  $\mu\text{m}$  and 25  $\mu\text{m}$ . Another example is IRAS F16516-0948 at 100  $\mu\text{m}$  ( $S_\nu(\text{new})/S_\nu(\text{old}) = 0.75$ ), where cirrus confusion has been minimized by using the peak flux estimate in RBGS, and  $f_\nu(t)$  was contaminated (resulting in an over estimated flux density) in BGS<sub>2</sub>. Most objects with  $S_\nu(\text{new})/S_\nu(\text{old}) > 1.2$  are cases where the RBGS flux selection algorithm resulted in the choice of  $f_\nu(t)$  or  $f_\nu(z)$  over  $f_\nu(\text{template})$ , where in BGS<sub>1</sub>+BGS<sub>2</sub> a lower flux density estimate was made for reasons explained in the previous paragraph (also see the Appendix). Examples are NGC 3147 at 12  $\mu\text{m}$  ( $S_\nu(\text{new})/S_\nu(\text{old}) = 2.10$ ) and MCG+07-23-019 at 25  $\mu\text{m}$  ( $S_\nu(\text{new})/S_\nu(\text{old}) = 1.92$ ). Other extreme ratios are due simply to differences between the  $f_\nu(t)$  results obtained using the final (PASS3) *IRAS* archive calibration versus the earlier versions utilized in BGS<sub>1</sub>+BGS<sub>2</sub>; an example is NGC 4565 at 60  $\mu\text{m}$  ( $S_\nu(\text{new})/S_\nu(\text{old}) = 0.79$ ). Most of the remaining outliers in Figure 2 are explained by the use of the SCANPI  $f_\nu(z)$  measurement for all objects smaller than 25 arcminutes in size, where in BGS<sub>1</sub>+BGS<sub>2</sub> flux measurements from Rice et al. (1983; 1988) were always used when available. Examples are NGC 134 at 60  $\mu\text{m}$  ( $S_\nu(\text{new})/S_\nu(\text{old}) = 1.32$ ) and NGC 4631 at 100  $\mu\text{m}$  ( $S_\nu(\text{new})/S_\nu(\text{old}) = 0.77$ ). As discussed in Section 2, comparison of the Rice et al. measurements with SCANPI  $f_\nu(z)$  measurements for galaxies with optical sizes less than 25 arcminutes showed relatively uniform scatter in the residuals, indicating that the use of SCANPI  $f_\nu(z)$ , when significantly larger than  $f_\nu(t)$ , is the best choice for these objects to insure uniformity and consistency in the calibration with the rest of the RBGS

objects.

Figure 3 shows the ratio of total flux density to the peak flux density in the coadded scans at 12  $\mu\text{m}$ , 25  $\mu\text{m}$ , 60  $\mu\text{m}$  and 100  $\mu\text{m}$ . The  $f_\nu(\text{peak})$  value is used here rather than  $f_\nu(\text{template})$  because the latter measurement does not exist for objects in which the point source template (PSF) fit failed, while for pure point sources  $f_\nu(\text{total}) \approx f_\nu(\text{template})$  and thus the ratio  $S_\nu(\text{total})/S_\nu(\text{peak})$  is very close to unity. This figure illustrates the degree to which point-source fitted measurements in the *IRAS* PSC and *IRAS* FSC underestimate the total flux densities for objects in the RBGS. There are likely numerous errors in the literature concerning the infrared flux densities and infrared colors of galaxies, due to the fact that some users of *IRAS* data have not fully appreciated the fact that most bright infrared galaxies in the local universe, as represented here in the RBGS, are marginally extended or resolved by *IRAS*.

A summary of the percentages of sources that were found to be extended in each of the *IRAS* bands is given in Table 5. The most notable result is that at 60  $\mu\text{m}$  and 100  $\mu\text{m}$ , where S/N is highest and distinctions can be reliably made, there are significantly more resolved or marginally resolved objects than previously thought: 48% in the RBGS versus 45% as previously reported in the BGS<sub>1</sub>+BGS<sub>2</sub> at 60  $\mu\text{m}$ , and 30% in the RBGS versus 23% as previously reported in the BGS<sub>1</sub>+BGS<sub>2</sub> at 100  $\mu\text{m}$ . This is due to a more careful definition of resolved or marginally extended objects as those having significantly more flux between the baseline zero-crossings,  $f_\nu(z)$ , than within the nominal detector size,  $f_\nu(t)$ , in combination with a comparison of W25 and W50 measurements to point-source values. We should emphasize that the BGS<sub>1</sub>+BGS<sub>2</sub> used only W25 and W50 to determine whether sources are resolved, and always chose  $f_\nu(t)$  to estimate the flux for the R and M (U+) objects. The revised processing has resulted in significantly fewer objects with underestimated total fluxes in the RBGS compared to BGS<sub>1</sub>+BGS<sub>2</sub>.

TABLE 5  
IRAS SOURCE DETECTION TYPES<sup>†</sup>

Detection Type	12 $\mu m$	25 $\mu m$	60 $\mu m$	100 $\mu m$
RBGS Resolved <sup>a</sup> - R	338 (54%)	266 (42%)	219 (35%)	81 (13%)
BGS <sub>1</sub> +BGS <sub>2</sub> Resolved - R	349 (56%)	321 (52%)	195 (32%)	72 (12%)
RBGS Marginally Resolved <sup>a</sup> - M	43 (7%)	77 (12%)	82 (13%)	105 (17%)
BGS <sub>1</sub> +BGS <sub>2</sub> Marginally Resolved - U+	84 (14%)	112 (18%)	80 (13%)	71 (11%)
RBGS Unresolved <sup>a</sup> - U	229 (36%)	286 (46%)	328 (52%)	443 (70%)
BGS <sub>1</sub> +BGS <sub>2</sub> Unresolved - U	179 (29%)	185 (30%)	343 (55%)	471 (76%)
RBGS Upper Limits	19 (3%)	0	0	0
RBGS Uncertain fluxes <sup>b</sup>	34 (5%)	37 (6%)	40 (6%)	59 (9%)

<sup>†</sup>The number and approximate percentages of objects in each category are listed. The RBGS contains 629 objects and BGS<sub>1</sub>+BGS<sub>2</sub> contains 618 objects.

<sup>a</sup>IRAS scan profile size information as identified with the size code (S) following each flux density and uncertainty listed in Table 1. See the description of columns (8) – (11) in Table 1, and Figure 14 (Appendix) for examples of coadded scan profiles that illustrate size codes “R”, “M”, and “U”.

<sup>b</sup>Various types of measurement uncertainties as encoded in the flag (F) following some flux density and uncertainty values listed in Table 1. See the description of columns (8) – (11) in Table 1, and Figure 16 (Appendix) for examples of scan profiles that illustrate the uncertainty flags “g”, “b”, “c”, and “n”.

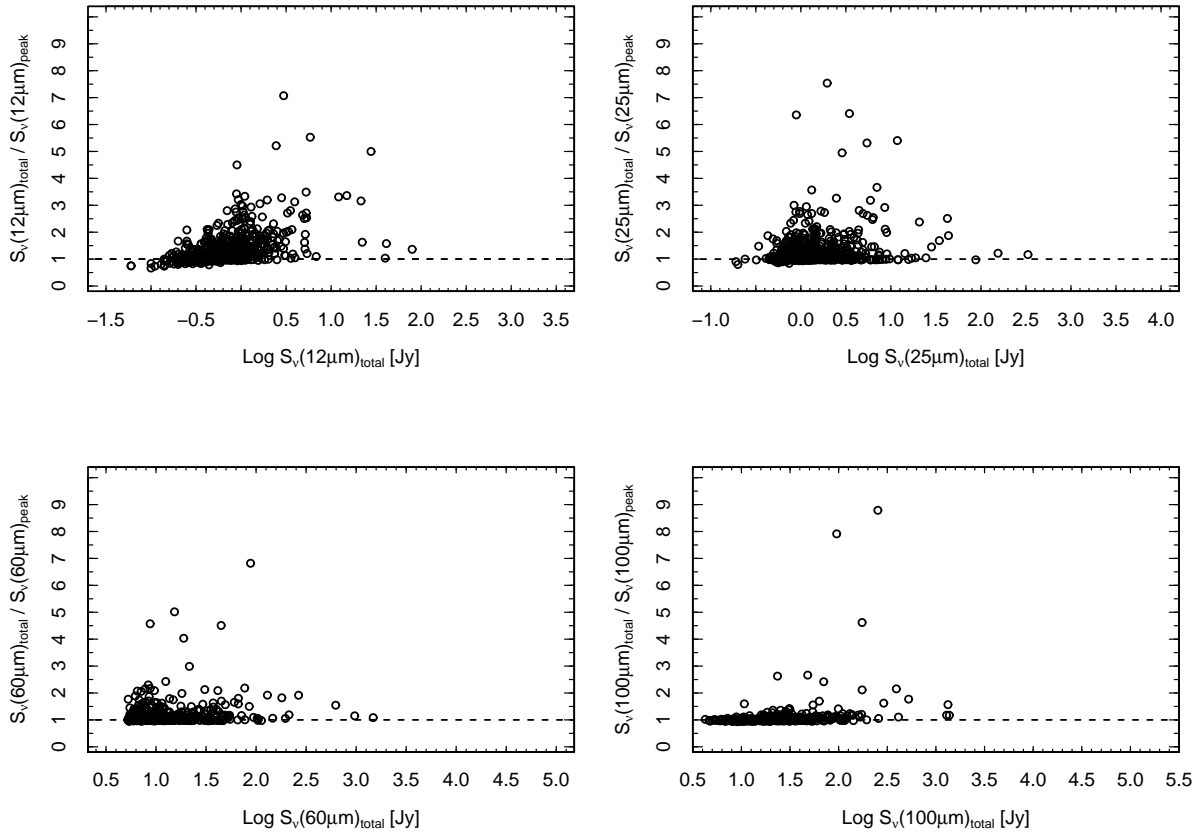


Fig. 3.— Ratio of the best estimate of the total flux density to the peak value in the coadded scan vs the base 10 log of the new total flux density at  $12\mu\text{m}$ ,  $25\mu\text{m}$ ,  $60\mu\text{m}$  and  $100\mu\text{m}$ . Only a few objects with very large ratios are outside the plot region; the selected range in the ratio was chosen to show details for the largest number of points.

## 4.2. *IRAS* Flux Densities – Completeness

With the exception of 19 sources which were not detected at  $12\ \mu\text{m}$ , the objects in the RBGS were detected in all four *IRAS* bands. Therefore, despite the fact that the RBGS was selected only on the basis of  $60\ \mu\text{m}$  flux, the flux distributions and infrared colors involving all four of the *IRAS* bands (see Table 1) are a fair representation of the true distributions of the *IRAS* properties of galaxies selected at  $60\ \mu\text{m}$ .

The distribution of fluxes in Table 1 can be compared with the distribution  $N(S_\nu) \propto S_\nu^{-1.5}$  expected for a complete sample of objects in a non-evolving Euclidean universe that should be a reasonable approximation for the relatively small redshift range covered by the objects in the RBGS. Figure 4 shows the integral and differential  $\log N - \log S_\nu$  plots for each *IRAS* band. The apparent turn over in the faintest bin of the differential source counts suggests a possible incompleteness near the  $60\ \mu\text{m}$  sample flux limit. However, this interpretation is based on the assumption that the volume shell containing the bulk of these objects is as uniformly filled with galaxies as the shells containing the brighter galaxies; studies of large-scale structure indicate that such uniformity is not actually present. In addition, the error bars plotted in Figure 4 are merely statistical uncertainties,  $\sqrt{N}$ ; they do not account for other possible errors. The relatively constant slope of the number of sources versus flux density at  $60\ \mu\text{m}$  down to the selection limit, with a power law fit of  $-1.48 \pm 0.13$  in the integral counts, shows that at  $60\ \mu\text{m}$  the RBGS is reasonably complete to the selection limit of  $5.24\ \text{Jy}$ .

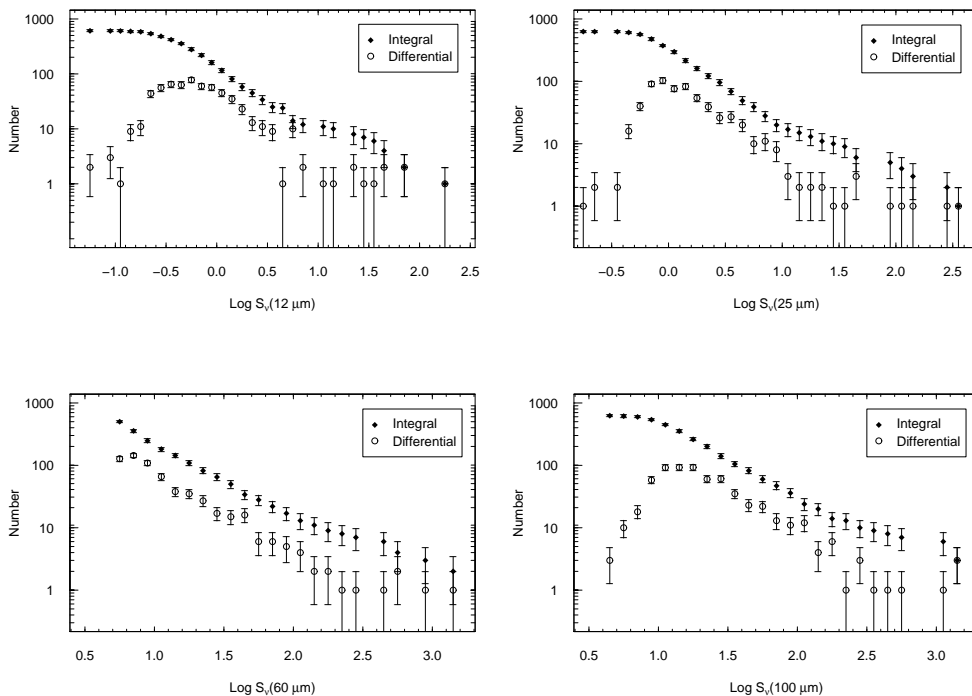


Fig. 4.— Integral and differential number counts vs. flux density ( $\log N - \log S$ ) for objects in the RBGS. Nineteen objects with upper limits are not included in the  $12\ \mu\text{m}$  plot. The bins have width  $d(\log S) = 0.1$ , and the thin vertical bars represent statistical uncertainties (i.e.,  $\sqrt{N}$ ).

At  $12\ \mu\text{m}$ ,  $25\ \mu\text{m}$ , and  $100\ \mu\text{m}$ , there is a portion of the  $\log N$ - $\log S_\nu$  plot that follows the  $-1.5$  power-law relation, suggesting that the RBGS sample contains a complete flux-density-limited sample at those wavelengths to the turnover point in the plots (i.e. near  $\log S_\nu = -0.1, 0.0,$  and  $1.1$  at  $12\ \mu\text{m}$ ,  $25\ \mu\text{m}$ , and  $100\ \mu\text{m}$  respectively). The turnover point represents the flux-density value beyond which a significant population of sources is being lost as a result of the  $60\ \mu\text{m}$  selection criterion. At  $100\ \mu\text{m}$  the turnover is at a value  $S_\nu \sim 16\ \text{Jy}$ , nearly 10 times the completeness limit of the PSC at  $100\ \mu\text{m}$  (*IRAS Explanatory Supplement* 1988), and is consistent with the rare occurrence of “extremely cold” galaxies with  $S_{100}/S_{60} > 3.5$ . At  $25\ \mu\text{m}$  the turnover point at  $0.8\ \text{Jy}$  is only a factor of  $\sim 2.2$  above the PSC completeness limit at  $25\ \mu\text{m}$ , and the turnover reflects a true loss of “warm” *IRAS* galaxies with  $S_{25}/S_{60} > 0.15$  from the RBGS. Similarly at  $12\ \mu\text{m}$  where the turnover at  $\sim 0.75\ \text{Jy}$  is again approximately twice the PSC completeness limit at  $12\ \mu\text{m}$ , there is a true loss of objects with  $S_{12}/S_{60} > 0.1$  from the RBGS.

### 4.3. Sky Coverage

The final RBGS covered all of the sky surveyed by *IRAS* except for a thin strip within  $|b| < 5^\circ$  degrees of the Galactic Plane. Figure 5 displays a Hammer-Aitoff projection in Galactic coordinates of all source positions in the RBGS. Also indicated in Figure 5 are three small regions suffering heavy contamination from nearby Galactic molecular clouds (Orion:  $5^{\text{h}}0^{\text{m}} < \text{R.A.} < 6^{\text{h}}40^{\text{m}}, -20^\circ < b < -10^\circ$ ; Ophiuchus:  $16^{\text{h}}15^{\text{m}} < \text{R.A.} < 16^{\text{h}}30^{\text{m}}, -26^\circ < \delta < -20^\circ$ ) and an area of confusion near the Large Magallenic Cloud (LMC:  $5^{\text{h}}01^{\text{m}} < \text{R.A.} < 6^{\text{h}}11^{\text{m}}, -72^\circ 45' < \delta < -66^\circ 45'$ ). These three regions were excluded from the BGS<sub>2</sub> (see Figure 1 of Sanders et al. 1995). However, with the more thorough data processing carried out for the RBGS, and the fact that the aerial density of sources in these regions is not significantly different from regions of high Galactic latitude, we now believe that most if not all *IRAS* bright galaxies within these regions have been identified. Sources that lie within these regions are included in Table 1 along with a flag (an asterisk following the *IRAS* source name in Column 2) indicating that they are located in a region of high Galactic

foreground confusion.

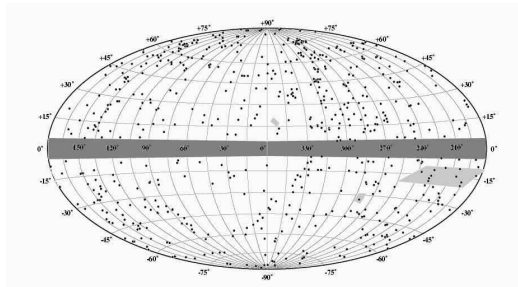


Fig. 5.— Aitoff projection in Galactic coordinates of all sources in the RBGS. The dark shaded region represents the Galactic plane region excluded from the survey ( $|b| < 5^\circ$ ). The three small lightly shaded regions denote areas with extensive contamination from nearby Galactic molecular clouds and the LMC (see text for detailed boundaries). The total survey area is  $37,658\ \text{deg}^2$ , or  $91.3\%$  of the sky. **NOTE: This figure is degraded by bit-mapping to meet the astro-ph size limit. Full resolution version available at [http://nedwww.ipac.caltech.edu/level5/March03/IRAS\\_RBGS/Figures/hammer.ps.gz](http://nedwww.ipac.caltech.edu/level5/March03/IRAS_RBGS/Figures/hammer.ps.gz).**

In the BGS<sub>2</sub>, Sanders et al. (1995) explored the effect that decreasing Galactic latitude might have on our ability to detect all of the real  $60\ \mu\text{m}$  bright galaxies present. On the basis of the fact that there was no statistically significant decrease in the density of sources detected versus  $|b|$ , it was concluded that the BGS<sub>2</sub> was essentially complete down to the limit of  $\pm 5^\circ$ . We have re-examined this issue using the new RBGS data. Figure 6 shows the surface density of RBGS sources versus Galactic latitude. Although the three bins (bin width  $\Delta b = 5^\circ$ ) with the lowest surface density of sources all lie at  $b < 40^\circ$ , there is again no observed systematic decrease in source density with Galactic latitude, and the three lowest points are not that extreme. However, we do not rule out the possibility that a few sources have been missed at lower Galactic latitude, and in particular, that the systematic low values at  $b = -35^\circ$  to  $-5^\circ$  may reflect this fact. What is most noticeable in the data of Figure 6 is the large excess surface density of sources in the northern hemisphere compared to the south. This reflects the effect of the Local Supercluster (e.g., Tully 1982).

#### 4.3.1. Clustering

In the original discussion of the properties of *IRAS* bright galaxies (i.e. the 324 galaxies in the original BGS<sub>1</sub> – Soifer et al. 1987) significant

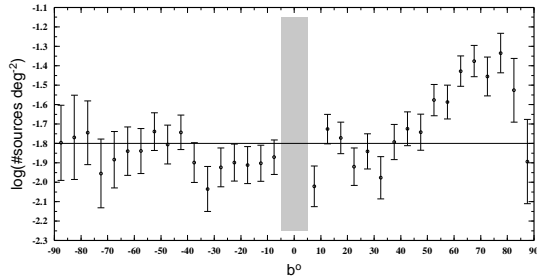


Fig. 6.— Surface density of RBGS objects versus Galactic latitude ( $b$ ). The shaded region denotes the omitted survey region of  $\pm 5^\circ$  around the Galactic plane. The line indicates the median value of  $\log_{10}(\# \text{ source}/\text{deg}^2) = -1.80$ , or 0.016 sources per square degree for the whole sample. This plot illustrates the well-known excess of *IRAS* galaxies in the northern compared to the southern Galactic hemisphere, due primarily to the Virgo cluster centered near  $b = +74^\circ$  as well as the local supercluster .

attention was given to the effect of the nearby Virgo cluster, which was found to be reflected in the BGS<sub>1</sub> sample as an “over density” of sources due to  $\sim 30$  galaxies within a  $\sim 20^\circ$  radius around M87 (taken to be the center of the Virgo cluster). These “Virgo galaxies” were shown to be gas-rich spirals with relatively modest luminosity, i.e.  $\log(L_{\text{ir}}/L_\odot) \sim 9.8 - 10.4$ . While nearly all of these galaxies remain in the RBGS, the overall effect of Virgo on the full RBGS sample is less. This is partly due to the  $\sim 2\times$  increase in the total number of galaxies in the RBGS, but is also due to the realization that Virgo is simply one (albeit the largest) of several galaxy concentrations within the Local Supercluster (e.g. Tully 1982; Tully & Shaya 1984). We have chosen not to formally separate out the properties of Virgo galaxies from the overall properties of the RBGS, but instead will simply point out the effect of Virgo on the distribution of RBGS galaxy properties where appropriate.

In the Aitoff all-sky plot shown in Figure 5, one of the most obvious features is the asymmetry in the relative number of *IRAS* bright galaxies found in the north (370) versus the south (259). Tully (1982) has previously shown that this asymmetry is also found for optically selected galaxies, and that it can be accounted for by a relatively small number of “concentrations” within the Local Supercluster, which lies almost entirely at high Galactic latitude. The cumulative af-

fect of the Local Supercluster produces the prominent broad peak in the surface density distribution of *IRAS* bright galaxies versus Galactic latitude ( $b \sim +50^\circ$  to  $+85^\circ$ ) in Figure 6.

#### 4.4. *IRAS* Colors

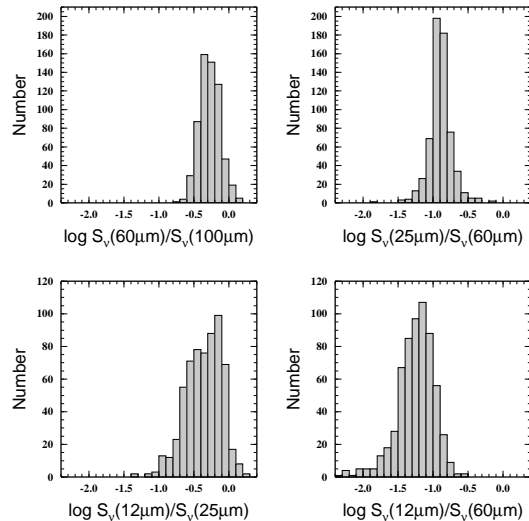


Fig. 7.— Distributions of total *IRAS* flux density ratios: (a)  $S_\nu(12\mu\text{m})/S_\nu(25\mu\text{m})$ , (b)  $S_\nu(12\mu\text{m})/S_\nu(60\mu\text{m})$ , (c)  $S_\nu(25\mu\text{m})/S_\nu(60\mu\text{m})$ , and (d)  $S_\nu(60\mu\text{m})/S_\nu(100\mu\text{m})$ .

A full discussion of the *IRAS* colors for this sample is beyond the scope of this paper. However, it is worth pointing out here that the primary statistical trends reported previously in BGS<sub>1</sub> (Soifer et al. 1989) have not changed substantially when using the more accurate RBGS fluxes. We discuss the *IRAS* colors of the RBGS objects briefly below.

Figure 7 shows the distributions of the RBGS *IRAS* flux density ratios observed in individual sources. The largest range is found for the ratios  $12\mu\text{m}/25\mu\text{m}$  and  $12\mu\text{m}/60\mu\text{m}$  ( $\sim 1.5$  dex), while the ratios  $60\mu\text{m}/100\mu\text{m}$  and  $25\mu\text{m}/60\mu\text{m}$  cover a narrower range ( $\sim 0.8$  dex).

All of the galaxies in the RBGS exhibit SEDs whose infrared emission increases between  $25\mu\text{m}$  and  $60\mu\text{m}$  with the bulk of the sample having  $S_{60}/S_{25}$  in the range  $\sim 5 - 15$ . This simply reflects the dominance of thermal emission from relatively “cool” dust (i.e.  $T_{\text{dust}} \sim 25 - 70\text{K}$ ) in the infrared SEDs of the  $60\mu\text{m}$  selected *IRAS* bright galaxies. This range of dust temperature is also con-



sistent with the range of observed  $S_{100}/S_{60}$  ratios ( $\sim 4 - 0.5$ ). Several authors have now shown that this latter ratio is correlated with infrared bolometric luminosity, with the most luminous *IRAS* sources having the largest values of  $S_{60}/S_{100}$  (see Sanders & Mirabel 1996 for references).

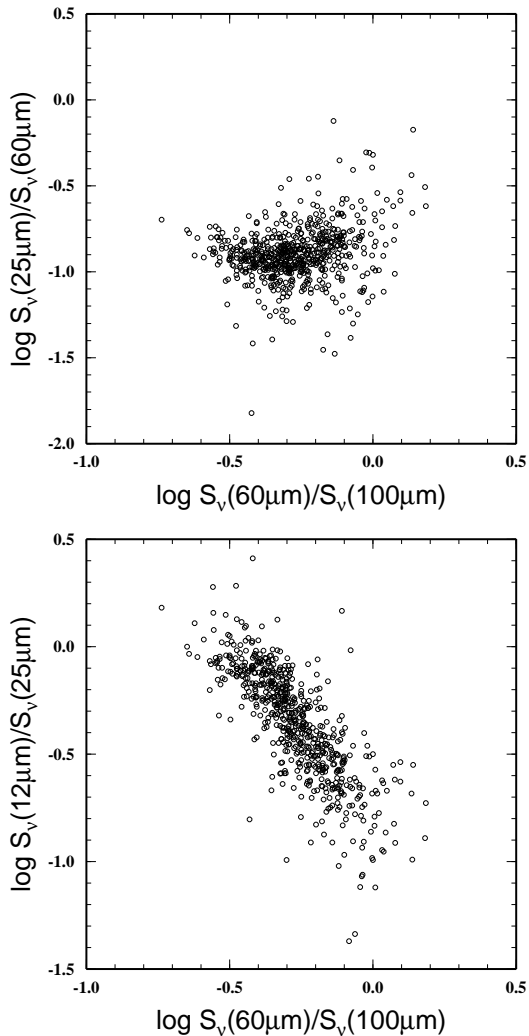


Fig. 8.— *IRAS* flux density ratio correlations using the revised total flux estimates in Table 1.

Not all of the observed *IRAS* flux ratios can be simply understood in terms of a single dust temperature component. For example, the relatively flat distribution found for  $S_{25}/S_{60}$  versus  $S_{60}/S_{100}$  (Figure 8, top panel) likely reflects the combined effects of more than one prominent dust temperature component. Although most galaxies have

a dominant “cool” dust component as discussed above, a significant fraction also show a secondary “warm” dust component that typically peaks near  $25\mu\text{m}$  and that appears to be associated with the presence of Seyfert/AGN activity (e.g. Miley et al. 1984; deGrijp et al. 1985).

One of the more surprising results concerning the *IRAS* colors of galaxies in the RBGS is seen in the inverse correlation between the  $60\mu\text{m}/100\mu\text{m}$  ratio and the  $12\mu\text{m}/25\mu\text{m}$  ratio (Figure 8, bottom panel). Soifer & Neugebauer (1991) previously showed that this ratio was also strongly correlated with galaxy infrared luminosity (see their Figs. 5 and 6). One plausible “simple” interpretation that has been proposed is that the component of “hot” ( $T \sim 100 - 200\text{K}$ ) dust found in the SEDs of most “normal” spiral disks decreases due to the increasing destruction rate of small grains as the intensity of the nuclear radiation field increases with increasing total galaxy infrared luminosity.

#### 4.5. Luminosity Function

An appropriate quantity for comparing the RBGS galaxies with other classes of extragalactic objects selected at other wavelengths is the infrared luminosity,  $L_{\text{ir}}(8 - 1000\mu\text{m})$ , computed using all four *IRAS* bands (Soifer et al. 1987; Sanders & Mirabel 1996). Soifer et al. (1987) first used the “infrared bolometric luminosity” to compare *IRAS* BGS galaxies with the total bolometric luminosity for several optically selected galaxy samples (Seyferts, starbursts, QSOs, etc). Here we reconstruct the infrared bolometric luminosity function using the new *IRAS* measurements listed in Table 1 for the RBGS galaxies. All of the RBGS objects have measured redshifts, and all have measured flux densities in all four *IRAS* bands (except for a very small percentage of objects with upper limits at  $12\mu\text{m}$ ). The space density of the galaxies,  $\rho$ , is the number of objects per cubic megaparsec per unit absolute magnitude interval. The units of  $\rho$  are  $\text{Mpc}^{-3} M_{\text{ir}}^{-1}$ , where  $M_{\text{ir}}$  signifies infrared absolute magnitude bins computed using logarithmic intervals in which each luminosity bin boundary is a factor of  $10^{0.4}$  larger than the previous one<sup>12</sup>.

<sup>12</sup>This effectively converts intervals of infrared luminosity ( $L_{\text{ir}}/L_{\odot}$ ) to equivalent intervals of absolute magnitude ( $M_{\text{ir}}$ ); an alternate way to express the units of  $\rho$  is  $\text{Mpc}^{-3} [0.4 * \log_{10}(L_{\text{ir}}/L_{\odot})]^{-1}$ .

Figure 9 plots the distribution of heliocentric radial velocities ( $c * z$ ) for the complete RBGS using the redshifts tabulated in Table 1 taken from the references given in Table 7. The sharp peak in the 1000-2000  $\text{km s}^{-1}$  redshift bin is largely due to the Virgo cluster. Otherwise, the redshift distribution for the RBGS shows a relatively smooth high redshift tail out to a cut-off near  $cz \sim 26,000 \text{ km s}^{-1}$ .

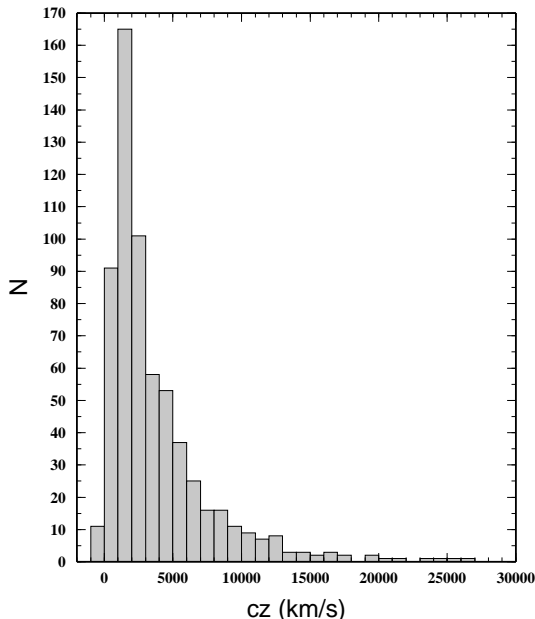


Fig. 9.— Distribution of heliocentric radial velocities ( $c * z$ ) for the RBGS.

Distances for the RBGS galaxies have been computed using the new cosmic attractor flow model outlined in Appendix A of Mould et al. (2000), assuming  $H_0 = 75 \text{ km s}^{-1} \text{ Mpc}^{-1}$  and adopting a flat cosmology,  $\Omega_M = 0.3$  and  $\Omega_\Lambda = 0.7$ . Figure 10 plots the distribution of distances (Mpc) as tabulated in Table 1. Again, the effect of the Virgo cluster can be seen as affecting the strength of the peak in the 10-20 Mpc bin (assuming our adopted distance to Virgo of 15.3 Mpc).

The resulting distribution of infrared luminosities is shown in Figure 11. The prescription and references used for computing  $L_{\text{ir}}$  are given in the column notes to Table 1. Except for a modest excess of objects at  $L_{\text{ir}} \sim 10^{10} L_\odot$  (largely due to

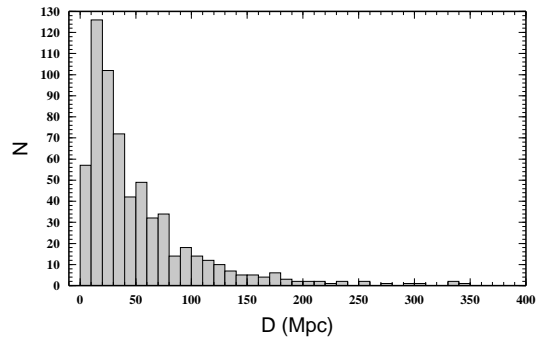


Fig. 10.— Distribution of estimated distances (Mpc) for sources in the RBGS.

Virgo) the distribution shows a relatively broad peak over the luminosity range  $\log(L_{\text{ir}}/L_\odot) \sim 9.8 - 11.4$  (half-power). The median observed luminosity,  $\log(L_{\text{ir}}/L_\odot) \sim 10.65$ , is somewhat larger than the total bolometric luminosity of the Milky Way, and the maximum observed luminosity in the sample,  $\log(L_{\text{ir}}/L_\odot) = 12.51$  (Mrk 231), is nearly 100 times larger than the median.

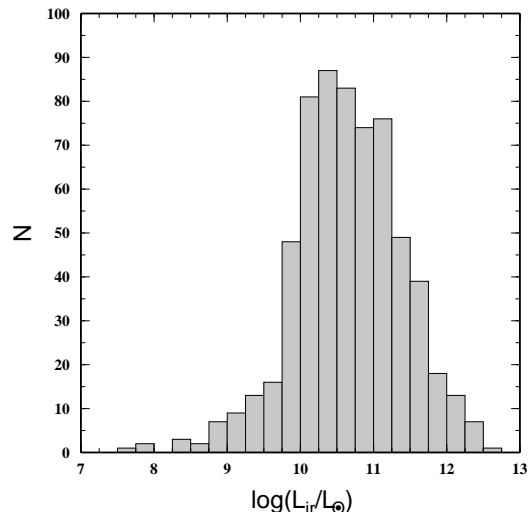


Fig. 11.— Distribution of the base ten logarithm of the total infrared luminosity in Solar units.

The luminosities plotted in Figure 11 were used to compute the infrared bolometric luminosity function for the RBGS (Figure 12), using the  $1/V_{\text{max}}$  method (Schmidt 1968). The computed values are listed in Table 6. The “double power-law” shape of the luminosity function for *IRAS*

bright galaxies is similar to that derived earlier for the BGS<sub>1</sub> (e.g. Soifer et al. 1987), except for improved statistics at both low and high infrared luminosities, plus the decreased influence of the Virgo cluster in the all-sky sample as compared to its effect in the smaller BGS<sub>1</sub> survey. The best fit power-laws,  $\phi(L) \propto L^\alpha$ , give  $\alpha = -0.6 (\pm 0.1)$  and  $\alpha = -2.2 (\pm 0.1)$  below and above  $L_{\text{ir}} \sim 10^{10.5} L_\odot$  respectively.

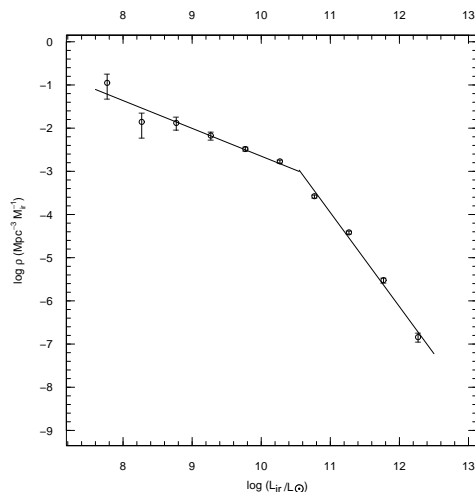


Fig. 12.— The infrared luminosity function for the RBGS, computed using the  $1/V_{\text{max}}$  method. The space densities and uncertainties plotted are those listed in Table 6; the points represent the center of each luminosity bin, and each bin has a uniform width of 0.5 in units of  $\log(L_{\text{ir}}/L_\odot)$ . The solid lines are linear least-square fits to the data points below and above the “characteristic” infrared luminosity  $L_{\text{ir}}^* \sim 10^{10.5} L_\odot$ , respectively. The corresponding power laws,  $\phi(L) \propto L^\alpha$ , have  $\alpha = -0.6 (\pm 0.1)$  and  $\alpha = -2.2 (\pm 0.1)$ .

## 5. Summary

This paper presents the complete list of objects in the *IRAS* Revised Bright Galaxy Sample, a sample of extragalactic objects selected at  $60\mu\text{m}$  from the *IRAS* all-sky survey. The observed slope of  $-1.49 \pm 0.10$  in the  $\log N$ – $\log S_\nu$  relation at  $60\mu\text{m}$  confirms that the RBGS is statisti-

cally complete down to the limit of  $S_{60} = 5.24\text{Jy}$ . The properties of the RBGS objects were computed using the final release of the *IRAS* Level 1 Archive and thus the RBGS replaces the earlier BGS samples which were determined using older versions of the *IRAS* data products. The RBGS contains 39 objects which were not present in the BGS<sub>1</sub>+BGS<sub>2</sub>, and 28 objects from the BGS<sub>1</sub>+BGS<sub>2</sub> have been dropped from the RBGS because their revised  $60\mu\text{m}$  flux densities are not greater than  $5.24\text{Jy}$ . Improved methods were used to measure the total *IRAS* flux densities of individual sources, resulting in typical changes of 5-25% when compared to previous values reported for the BGS<sub>1</sub>+BGS<sub>2</sub>, with changes of up to a factor of 2 for the faintest sources at  $12\mu\text{m}$  and  $25\mu\text{m}$ . Better procedures for resolving position uncertainties and resolving cross-identifications with other galaxy catalogs resulted in name changes for  $\sim 7\%$  of the previous BGS<sub>1</sub>+BGS<sub>2</sub> compilations. This work presents the most accurate estimates to date of the total *IRAS* flux densities and derived infrared luminosities of galaxies in the local Universe. Basic properties of the RBGS galaxies are summarized below.

1. The RBGS sample contains a total of 629 galaxies with  $S_{60} > 5.24\text{Jy}$  in an area of  $37,657.5$  square degrees (91.3% of the sky) covering the entire sky surveyed by *IRAS* down to Galactic latitude  $|b| = 5^\circ$ ;
2. Extended flux ( $> 0.77'$ ) at  $12\mu\text{m}$ , ( $> 0.78'$ ) at  $25\mu\text{m}$ , ( $> 1.44'$ ) at  $60\mu\text{m}$ , and ( $> 2.94'$ ) at  $100\mu\text{m}$  is detected in 61%, 54%, 48%, and 30% of the galaxies respectively.
3. The mean and median redshift for the entire RBGS sample is  $z = 0.0126$  ( $cz = 3777\text{km s}^{-1}$ ) and  $z = 0.0082$  ( $cz = 2458\text{km s}^{-1}$ ), respectively. The object with the highest redshift is IRAS 07251 – 0248 ( $z = 0.0876$ ), and the object with the largest computed infrared luminosity in this local sample is Mrk 231 ( $L_{\text{ir}} = 3.2 \times 10^{12} L_\odot$ ).
4. The bolometric infrared luminosity function,  $\phi(L_{\text{ir}})$ , for infrared bright galaxies in the Local Universe remains best fit by a double power law,  $\phi(L) \propto L^\alpha$ , with  $\alpha = -0.6 \pm 0.1$ , and  $\alpha = -2.2 \pm 0.1$  below and above  $L_{\text{ir}} \sim 10^{10.5} L_\odot$ , respectively.

TABLE 6  
INFRARED LUMINOSITY FUNCTION

$L_{\text{ir}}$	$N$	$V/V_{\text{max}}$	$\rho$ ( $\text{Mpc}^{-3} \text{M}_{\text{ir}}^{-1}$ )
7.75	3	$0.16 \pm 0.03$	$11.2 \pm 6.5 \times 10^{-2}$
8.25	3	$0.28 \pm 0.05$	$14.0 \pm 8.1 \times 10^{-3}$
8.75	9	$0.39 \pm 0.04$	$13.2 \pm 4.3 \times 10^{-3}$
9.25	24	$0.37 \pm 0.02$	$6.7 \pm 1.3 \times 10^{-3}$
9.75	69	$0.56 \pm 0.02$	$32.9 \pm 4.0 \times 10^{-4}$
10.25	168	$0.44 \pm 0.01$	$17.0 \pm 1.3 \times 10^{-4}$
10.75	157	$0.45 \pm 0.01$	$26.5 \pm 2.1 \times 10^{-5}$
11.25	122	$0.53 \pm 0.02$	$38.6 \pm 3.5 \times 10^{-6}$
11.75	56	$0.50 \pm 0.02$	$30.1 \pm 4.0 \times 10^{-7}$
12.25	18	$0.44 \pm 0.03$	$14.5 \pm 3.4 \times 10^{-8}$

We thank George Helou for helpful discussions, and the anonymous referee for comments that improved the presentation of this material. This research made extensive use of the NASA/IPAC Extragalactic Database (NED), which is operated by the Jet Propulsion Laboratory, California Institute of Technology, under contract with the National Aeronautics and Space Administration. Queries of the *IRAS* catalogs and scan coadd processing using SCANPI were supported by the NASA/IPAC Infrared Science Archive (IRSA), which is operated by the Jet Propulsion Laboratory, California Institute of Technology, under contract with the National Aeronautics and Space Administration. DBS acknowledges support from a Senior Award from the Alexander von Humboldt-Foundation and from the Max-Planck-Institut für extraterrestrische Physik as well as support from NASA grant NAG 90-1217. JMM, DCK, and JS were supported by the Jet Propulsion Laboratory, California Institute of Technology, under contract with NASA. DCK is grateful for financial support from KOSEF grant No. R14-2002-058-01000-0 and from the BK21 project of the Korean Government. JS and BTS are supported by the SIRTf Science Center at the California Institute of Technology; SIRTf is carried out at JPL, under contract with NASA.

## APPENDIX

### Data Reduction and Detailed SCANPI Measurements

Many sources in the RBGS are near enough such that they appear resolved or marginally extended in one or more of the *IRAS* detector bands, while others are unresolved. Therefore, an objective and consistent procedure had to be developed to select the best estimate of the total flux density for each object in each of the four *IRAS* bands. Table 7 lists the *IRAS* SCANPI measurements for all sources in the RBGS; these data were used along with the coadded scan plots to determine the “best” flux density estimates as listed in Table 1. These measurements are from the SCANPI median (1002) method of *IRAS* scan coaddition (Helou et al. 1988). Table 7 includes the coaddition results from all four SCANPI methods (“zc”, “tot”, “template”, “peak”) for each source in the RBGS. Our automated processing methods selected the final flux densities listed in Table 1 based on the relative values from these four coadd methods, plus the use of important additional information concerning source extent, and possible confusion due to blended sources, companions, Galactic cirrus, or excessive noise. Examples of how these choices were made are illustrated in Figures 14-16, and more thoroughly discussed in the captions to these figures.

The column entries in Table 7 are as follows:

- (1) *Name* – The Common name as listed in Table 1.
- (2) *Redshift Reference* – 19 digit reference code from NED for the redshift listed in Table 1.
- (3) *N/O* – Ratio of the new *IRAS* flux density estimate to the old flux density estimate published previously in BGS<sub>1</sub> or BGS<sub>2</sub> at 12  $\mu\text{m}$ ; objects new to the RBGS have missing values (“—”) in this and following columns.
- (4) *zc* – flux density from SCANPI’s zero-crossing measurement,  $f_\nu(z)$  (Jy) at 12  $\mu\text{m}$ .
- (5) *tot* – flux density from SCANPI’s in-band total measurement,  $f_\nu(t)$  (Jy) at 12  $\mu\text{m}$ .
- (6) *temp* – flux density from SCANPI’s template amplitude measurement, tmpamp (Jy) at 12  $\mu\text{m}$ .
- (7) *peak* – flux density from SCANPI’s peak measurement, peak (Jy) at 12  $\mu\text{m}$ .
- (8) *W25* – scan profile full width (arcminutes) measured at 25% of the peak signal at 12  $\mu\text{m}$ .
- (9) *W50* – scan profile full width (arcminutes) measured at 50% of the peak signal at 12  $\mu\text{m}$ .
- (10–16) – Same measurements as in columns (3) – (9), but at 25  $\mu\text{m}$ .
- (17–23) – Same measurements as in columns (3) – (9), but at 60  $\mu\text{m}$ .
- (24–30) – Same measurements as in columns (3) – (9), but at 100  $\mu\text{m}$ .

TABLE 7  
REVISED BRIGHT GALAXY SAMPLE — IRAS ADDSCAN/SCANPI FLUX DENSITIES AND SIZES

Name	Redshift	Reference	12 $\mu$ m							25 $\mu$ m							60 $\mu$ m							100 $\mu$ m							
			N/O	zc Jy	tot Jy	temp Jy	peak Jy	W25 <sub>r</sub>	W50 <sub>r</sub>	N/O	zc Jy	tot Jy	temp Jy	peak Jy	W25 <sub>r</sub>	W50 <sub>r</sub>	N/O	zc Jy	tot Jy	temp Jy	peak Jy	W25 <sub>r</sub>	W50 <sub>r</sub>	N/O	zc Jy	tot Jy	temp Jy	peak Jy	W25 <sub>r</sub>	W50 <sub>r</sub>	
(1)	(2)	(3)	(4)	(5)	(6)	(7)	(8)	(9)	(10)	(11)	(12)	(13)	(14)	(15)	(16)	(17)	(18)	(19)	(20)	(21)	(22)	(23)	(24)	(25)	(26)	(27)	(28)	(29)	(30)		
	NGC 0023	1991ApJ...	.370...	1.12	0.68	0.66	0.45	0.48	1.20	0.89	1.04	1.28	1.29	1.07	1.17	1.08	0.75	1.03	9.41	9.34	9.03	9.26	2.00	1.45	1.05	15.82	15.79	15.66	15.86	3.88	3.00
	NGC 0034	1991RC3.9C...	.00004	0.97	0.40	0.37	0.35	0.41	0.88	0.68	1.00	2.51	2.42	2.39	2.47	1.03	0.76	1.06	16.84	16.72	17.05	17.20	1.89	1.38	0.99	17.61	17.12	16.86	17.50	3.79	2.88
	NGC 0055	1991RC3.9C...	.00004	1.00	1.48	1.38	0.00	0.64	2.61	1.52	1.00	5.26	4.50	0.00	2.53	2.21	1.43	1.00	60.57	52.19	0.00	35.25	3.34	2.18	1.00	107.67	100.77	77.24	82.31	5.09	3.56
MCG-02-01-051/2	1993AJ...	.105.1637H	1.22	0.32	0.28	0.23	0.27	1.78	0.75	1.02	1.19	1.16	1.20	1.23	1.07	0.79	1.02	7.52	7.48	7.04	7.05	2.10	1.48	1.02	9.67	9.68	9.66	9.99	3.87	2.91	
	NGC 0134	1991RC3.9C...	.00004	1.33	2.45	2.35	1.49	1.63	1.62	1.13	0.97	2.59	2.59	1.79	1.83	1.63	1.14	1.31	22.83	22.65	20.01	19.97	2.22	1.59	0.96	59.77	58.87	55.54	56.43	4.05	3.04
ESO 079-0003	1996ApJ...	.107...97M	1.00	0.43	0.42	0.30	0.31	1.48	1.13	0.99	0.88	0.88	0.70	0.71	1.45	0.97	0.97	7.07	7.05	6.52	6.51	2.16	1.56	1.00	17.88	17.52	17.41	17.56	3.90	2.98	
	NGC 0150	1991RC3.9C...	.00004	0.90	0.65	0.66	0.49	0.51	1.28	0.96	1.01	1.72	1.66	1.53	1.58	1.16	0.83	1.00	9.68	9.66	8.97	9.03	2.09	1.51	1.02	17.55	17.56	17.72	18.29	3.81	2.89
	NGC 0157	1995ApJ...	.98...219Y	1.03	1.60	1.61	0.77	0.86	1.99	1.85	1.04	2.20	2.17	0.93	1.08	2.18	1.74	1.02	17.98	17.93	13.80	13.79	2.62	1.88	0.98	42.66	42.43	38.89	39.81	4.21	3.08
ESO 350-IG038	1981A&S...	.46...57W	1.27	0.54	0.52	0.43	0.45	1.01	0.80	0.99	2.35	2.31	2.51	2.49	1.04	0.78	0.99	6.68	6.68	6.88	7.05	1.89	1.36	1.00	5.10	5.01	5.04	5.13	3.75	2.92	
	NGC 0174	1998A&S...	.130...333T	1.05	0.94	0.94	0.41	0.41	0.94	0.72	0.99	1.45	1.37	1.27	1.34	1.02	0.75	1.05	11.29	11.26	11.36	11.42	1.89	1.41	1.04	19.83	19.64	19.77	20.30	3.79	2.92
	NGC 0224	2001ApJ...	.553...47F	1.00	10.89	7.58	1.41	2.64	-0.10	2.30	1.00	6.90	4.39	0.92	1.61	-0.10	2.20	1.00	47.19	34.10	9.61	15.26	-0.10	3.44	1.00	114.50	89.76	26.63	43.02	-0.10	-0.10
	NGC 0232	1996AJ...	.111...696K	1.00	0.47	0.43	0.36	0.43	0.95	0.66	1.05	1.30	1.28	1.02	1.06	1.41	0.91	1.00	10.54	10.51	10.05	10.10	2.00	1.45	1.02	16.97	16.97	17.14	17.55	3.83	2.91
	NGC 0247	1991RC3.9C...	.00004	---	0.18	0.22	0.14	0.19	1.29	0.63	---	0.89	0.32	0.00	0.14	-0.10	1.71	1.10	8.73	4.89	0.80	1.91	-0.10	-0.10	0.86	23.50	16.78	6.51	8.95	-0.10	5.77
	NGC 0253	1995ApJ...	.98...219Y	1.12	41.04	37.87	22.38	26.03	1.49	0.90	1.12	184.67	145.05	121.57	126.94	1.15	0.83	1.04	999.50	967.81	820.10	840.55	2.20	1.58	0.69	1328.28	1288.15	1091.46	1097.46	4.44	3.36
	NGC 0278	1995ApJ...	.98...219Y	0.99	1.66	1.65	1.28	1.37	1.30	0.91	1.02	2.65	2.65	2.13	2.23	1.33	0.93	1.00	25.13	25.03	23.58	23.75	2.07	1.49	1.01	45.97	45.90	44.46	45.38	3.95	3.00
	NGC 0289	1997AJ...	.113.1591W	---	0.46	0.45	0.24	0.29	1.91	1.05	---	0.64	0.60	0.54	0.51	1.49	1.09	---	5.51	5.47	4.59	4.56	2.31	1.68	---	16.99	16.90	15.86	16.19	4.03	3.07
MCG+12-02-001	1992ApJ...	.83...29S	1.00	0.71	0.77	0.78	0.82	0.94	1.07	0.92	3.48	3.47	3.51	3.58	1.07	0.78	0.96	21.84	21.83	21.92	22.84	1.88	1.37	1.00	27.78	27.72	29.11	29.83	3.73	2.90	
	SMC 1999ApJ...	.522...280S	---	---	---	---	---	---	---	---	---	---	---	---	---	---	---	---	---	---	---	---	---	---	---	---	---	---	---	---	---
	UGC 00556	1988ApJ...	.335...104M	1.03	0.28	0.26	0.34	0.34	0.90	0.67	1.02	0.39	0.40	0.45	0.42	1.05	0.80	1.04	5.58	5.58	5.57	5.61	1.94	1.45	1.09	11.07	10.98	10.84	11.19	3.68	2.83
	NGC 0300	2001ApJ...	.553...47F	---	0.90	0.62	0.05	0.20	-0.10	-0.10	---	1.96	0.95	0.00	0.26	-0.10	3.15	---	15.30	9.19	0.00	3.05	-0.10	-0.20	---	48.04	38.58	12.15	18.03	-0.10	-0.20
	NGC 0317B	1991RC3.9C...	.00004	1.00	0.17	0.16	0.20	0.23	0.73	0.58	0.98	1.07	1.05	1.03	1.05	1.07	0.81	0.99	9.31	9.28	9.16	9.17	1.95	1.43	1.02	13.69	13.48	13.60	13.74	3.79	2.92
	NGC 0337	1995ApJ...	.98...219Y	0.60	0.36	0.40	0.24	0.29	1.28	0.93	1.01	0.74	0.76	0.60	0.61	1.33	0.94	0.97	9.12	9.07	7.86	7.95	2.27	1.60	1.05	20.35	20.11	18.30	18.64	4.17	3.16
	IC 1623A/B	1991ApJ...	.370...158S	1.05	1.10	1.03	0.70	0.77	1.13	0.85	1.06	3.89	3.79	3.65	3.85	1.05	0.76	1.03	23.70	23.59	22.93	23.16	1.95	1.46	1.04	31.71	31.69	31.55	31.23	3.81	2.93
MCG-03-04-014	1995ApJ...	.98...129K	0.72	0.38	0.36	0.34	0.34	1.26	1.01	1.02	0.88	0.90	0.90	0.92	1.06	0.78	1.07	7.01	7.02	7.25	7.05	1.92	1.45	1.01	10.63	10.61	10.33	10.32	3.95	3.00	
ESO 244-0012	1991ApJ...	.98...955A	1.22	0.64	0.59	0.21	0.39	0.86	0.56	1.08	1.95	1.95	1.79	1.85	1.07	0.79	0.96	9.22	9.22	9.27	9.42	1.90	1.39	0.96	11.85	11.83	11.76	12.20	3.79	2.91	
	NGC 0470	1991RC3.9C...	.00004	1.02	0.47	0.46	0.42	0.43	1.10	0.85	0.80	1.33	1.28	1.11	1.13	1.31	0.88	1.02	7.37	7.37	7.22	7.21	2.03	1.48	1.02	12.74	12.70	12.20	12.54	4.01	2.95
CGCG 436-030	1988ApJ...	.335...104M	0.78	0.27	0.29	0.21	0.24	0.10	0.78	1.09	1.38	1.35	1.54	1.52	1.01	0.76	1.00	10.54	10.54	10.71	10.83	1.91	1.42	1.01	9.26	9.22	9.67	9.62	3.78	2.93	
	UGC 00903	1993AJ...	.105.1271G	1.03	0.44	0.42	0.37	0.39	1.08	0.81	1.08	0.58	0.64	0.56	0.65	0.93	0.67	0.98	7.87	7.88	7.78	7.63	1.96	1.47	1.06	14.64	14.58	15.45	15.05	3.71	2.89
	NGC 0520	1995ApJ...	.98...219Y	0.99	0.86	0.90	0.70	0.74	1.12	0.85	1.06	3.21	3.22	2.85	2.96	1.10	0.81	1.00	32.09	31.96	31.52	31.51	1.97	1.45	1.02	47.43	47.30	47.37	47.30	3.83	2.96
	NGC 0598	2001ApJ...	.553...47F	1.00	7.02	3.90	0.57	1.11	-0.10	2.29	1.00	10.46	4.19	1.11	1.77	-0.20	1.45	1.00	86.06	39.74	9.95	17.84	-0.10	4.08	1.00	249.65	146.40	27.57	67.29	-0.10	-0.10
	NGC 0613	1991RC3.9C...	.00004	0.97	2.33	2.25	0.89	1.24	2.72	1.05	1.01	4.40	4.32	2.27	2.83	2.09	0.92	1.00	27.79	27.68	19.44	20.27	2.75	1.80	1.04	59.54	59.21	51.81	53.00	4.41	3.21
ESO 353-0020	1991RC3.9C...	.00004	1.19	0.38	0.37	0.25	0.32	1.02	0.69	1.00	0.64	0.60	0.71	0.71	1.10	0.76	0.88	7.24	7.19	7.17	7.12	1.93	1.43	0.98	15.63	15.65	15.54	15.96	3.78	2.90	
	NGC 0625	1991RC3.9C...	.00004	0.77	0.23	0.26	0.20	0.25	1.23	0.62	1.01	1.36	1.30	0.93	1.02	1.30	0.86	0.98	5.85	5.86	5.73	5.86	1.97	1.42	0.96	8.77	8.76	8.63	8.64	3.89	2.98
	NGC 0628	1995ApJ...	.98...219Y	1.18	2.45	1.83	0.00	0.47	-0.20	-0.20	1.51	2.87	2.10	0.00	0.58	-0.20	-0.20	1.03	21.54	17.89	3.57	7.21	-0.20	-0.20	0.83	56.65	54.45	33.23	35.04	6.52	4.63
ESO 297-G011/012	1997ApJ...	.111...181D	1.28	0.42	0.37	0.00	0.27	0.98	0.72	0.99	1.59	1.55	0.52	0.79	2.14	0.92	0.99	7.81	7.77	5.45	5.38	2.83	2.23	0.98	13.03	12.90	11.90	11.95	4.29		



For some objects, values of  $temp$  are 0.00 or values of  $W25$  and  $W50$  are negative in Table 7. These are indications that the point source template amplitude fit failed, which occurred for some very extended objects best measured using the  $f_\nu(z)$  flux estimator; see the example of NGC 1532 at  $25\mu\text{m}$  as plotted in panel (a) of Figure 15.

Perhaps of most immediate interest to those familiar with the previous  $BGS_1+BGS_2$  data are the  $N/O$  values given in columns (3), (10), (17) and (24) of Table 7. Part of the differences in the “new” versus “old” flux densities is simply that due to the improved “Pass 3” calibration adopted for the final release of the *IRAS* Level 1 Archive. However, a significant effect is that due to the improved methods of estimating the total flux, in particular the use of  $f_\nu(z)$  when this flux measurement was significantly larger than the other coadd methods due to extended emission not captured by  $f_\nu(t)$ . In addition, as mentioned in Section 4.1, many galaxies have profile widths which are not significantly broader than what is expected for a point source, yet there is extended emission in a faint “pedestal” that can be easily seen in the profiles, and reliably measured as a statistically significant excess of the  $f_\nu(t)$  aperture value over the  $f_\nu(template)$  point source fitted value. Figure 13 shows the distribution of the ratio  $f_\nu(t)/f_\nu(template)$  at  $60\mu\text{m}$ ; also plotted are Gaussian fits intended to model the distribution expected solely from noise in the relative  $f_\nu(t)$  and  $f_\nu(template)$  measurements for unresolved objects, data for a sample of comparably bright stars, and  $60\mu\text{m}$  profiles for representative RBGS objects. This information was used as follows to establish the threshold for when  $f_\nu(t)$  could be selected as a reliable, confident indicator of extended emission in excess of the value measured by the point source template fit.

A sample of candidate stars was selected from the *IRAS* Point Source Catalog (PSC) using the joint criteria of  $f_\nu(60\mu\text{m}) > 5.24 Jy$ , a high point source fit correlation coefficient (99%), and positional association with objects in one or more star catalogs. The resulting candidate list (195 objects) was further filtered by cross-identification of each *IRAS* source with known stars using information available in SIMBAD. Some are planetary nebulae or unknown object types and were therefore omitted for this purpose of identifying a large sample of pure  $60\mu\text{m}$  point sources. The remaining sample of confirmed stars were then processed with SCANPI using the same procedure as the RBGS objects. The distribution of the measured ratios of  $f_\nu(t)/f_\nu(template)$  for 121 confirmed bright stars with high quality  $60\mu\text{m}$  *IRAS* scans (e.g., not confused by cirrus, excessive noise, or companions) is plotted in the same bins as the RBGS objects in Figure 13 (asterisks). The presence of stars with ratios greater than  $\sim 1.05$  was unexpected, and this complicated the goal of building a comparison sample of pure *IRAS*  $60\mu\text{m}$  point sources; close inspection of the data showed that each of these objects have  $60\mu\text{m}$  scan profiles similar to the RBGS galaxy profiles plotted in Figure 13, with faint “pedestals” of faint emission under a dominating point source. Larger ratios correspond to higher or more extended pedestals well above the background noise in the scans. These are clear candidates for stars embedded in extended circumstellar dust disks, shells or nebulae; some objects have published data that support this interpretation, including spectral classifications such as carbon stars, emission-line stars, and stars with known OH/IR envelopes. These objects are not considered further in this paper, but their presence required omitting stars outside the range 0.95 - 1.05 to form a Gaussian fit representative of unresolved stars measured by SCANPI. This fitted distribution of stars (dotted line, with a mean of  $1.000 \pm 0.004$ ) was then scaled to match the peak of the Gaussian fit to the RBGS objects (solid line), and plotted as a dashed line in Figure 13.



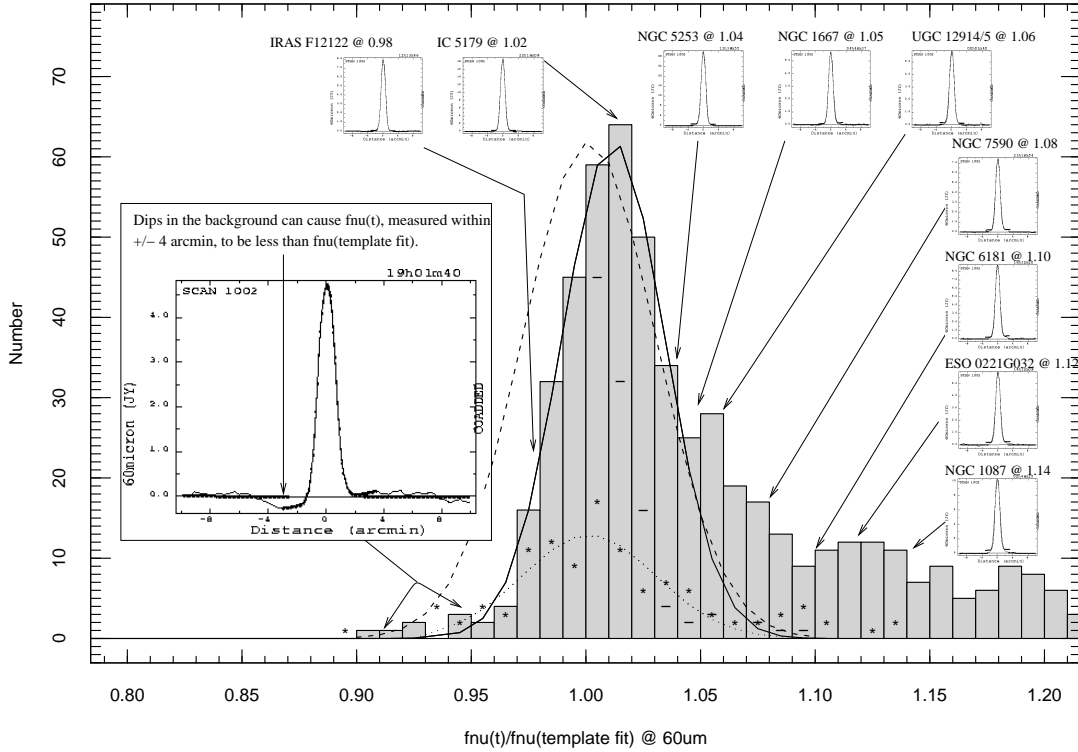


Fig. 13.— Histogram illustrating the distribution of the ratio  $f_\nu(t)/f_\nu(\text{template})$  at  $60\ \mu\text{m}$ . The entire range of this parameter is not shown in order to highlight details of the distribution for objects that have a ratio near unity. The solid line is a Gaussian fit to the upper envelop of the galaxy distribution, constructed by rejecting objects outside the range 0.95 – 1.05 from the fit. The asterisks show counts in the same bins for a sample of 121 stars selected from the *IRAS* Point Source Catalog (PSC) with  $f_\nu(60\ \mu\text{m}) > 5.24\ \text{Jy}$  and positional associations with objects in various star catalogs; cross-identification of these *IRAS* sources with stars was confirmed using SIMBAD. The dotted line is a Gaussian fit to the distribution for the stars, again omitting objects outside the range 0.95 - 1.05 from the fit. The dashed line is a Gaussian distribution with the same mean and standard deviation as the fit to the star distribution (dotted line), but scaled to the peak of the galaxy distribution (solid line). Horizontal line segments have been drawn in the bins with  $f_\nu(t)/f_\nu(\text{template})$  values between 1.0 and 1.10; these represent a “reflection” of the bins with  $f_\nu(t)/f_\nu(\text{template})$  values between 0.90 and 1.00 for the RBGs objects, indicating the expected counts if differences between  $f_\nu(t)$  and  $f_\nu(\text{template})$  were due only to noise and not real excess, extended emission detected in the  $f_\nu(t)$  measurement. The small plots inset around the top and right sides of the figure illustrate representative coadded  $60\ \mu\text{m}$  scan profiles from SCANPI; the object name and corresponding value of  $f_\nu(t)/f_\nu(\text{template})$  at  $60\ \mu\text{m}$  is listed above each plot. The larger inset plot on the left illustrates how dips in the background noise cause  $f_\nu(t)$  to be less than the template fit (point spread function) value for some objects; in such cases,  $f_\nu(\text{template})$  was chosen over  $f_\nu(t)$ . This diagram was used to establish the threshold requirement of  $f_\nu(t)/f_\nu(\text{template}) > 1.05$  for selecting  $f_\nu(t)$  as a confident measurement of at least marginally extended emission in excess of the value measured by the point source template fit.

Another approach to predicting the expected distribution for unresolved galaxies with  $f_\nu(t)/f_\nu(template) > 1.0$  is based on the assumption that small differences between the two measurements (whether negative or positive) are due solely to noise in the coadded scans and uncertainties in the *IRAS* point source template fits. That is, if all galaxies with  $f_\nu(t)/f_\nu(template)$  between 1.00 and 1.10 were unresolved by *IRAS* at  $60\ \mu\text{m}$ , we would expect the observed RBGS histogram bins over this range to match a reflection of the distribution over the range 0.90 - 1.00, where differences between  $f_\nu(t)$  and  $f_\nu(template)$  are clearly not physical and therefore due solely to noise. These expected counts are shown as horizontal line segments drawn within the bins with  $f_\nu(t)/f_\nu(template)$  values between 1.0 and 1.10. Using this noise symmetry argument to predict the  $f_\nu(t)/f_\nu(template)$  ratios expected for truly unresolved objects over the range 1.0 - 1.1, there is a clear excess of galaxies with ratios as small as 1.04 - 1.05 that likely have real (but weak) extended components; roughly 50% of the RBGS objects in these bins are in this category. However, since we cannot distinguish, using visual inspection of the coadded scan profiles, between galaxies that have true extended emission and those which have  $f_\nu(t) > f_\nu(template)$  due only to noise among these objects, we cannot reliably use a threshold ratio smaller than 1.05 to classify specific objects as marginally extended. Although the bins with  $f_\nu(t)/f_\nu(template)$  in the range 1.05 - 1.10 have counts that suggest some of these objects may be explained by the Gaussian fits described above for unresolved objects, visual inspection of the SCANPI profiles shows that every object in this range (and of course larger values) have clear, obvious extended emission as shown in the example profiles inset in Figure 13. Finally, the reality of extended emission for RBGS objects with ratios  $f_\nu(t)/f_\nu(template) > 1.05$  is visualized in Figure 13 through the progressive increase in the height or spatial extent of the pedestals corresponding to an increase in the flux ratio, all clearly defined well above the background noise in the coadded scans.

The threshold ratio of  $f_\nu(t)/f_\nu(template) > 1.05$  (5% excess flux over the point source template fit) was therefore used for defining marginally extended objects (M). Visual examination of the coadded scan profiles widths in conjunction with the flux ratio distribution in Figure 13 lead to selection of a threshold of  $f_\nu(t)/f_\nu(template) > 1.20$  (20% flux excess over the point source template fit) to flag a source as fully resolved (R), even if there is no additional excess flux measured by the  $f_\nu(z)$  method and therefore the  $f_\nu(t)$  value is selected. The final algorithm chosen for selecting the best SCANPI method for estimating the total flux density and for assigning *IRAS* source size codes in each *IRAS* band is as follows:

1. If the condition  $[f_\nu(t) \geq 1.05 * f_\nu(template) \text{ AND } f_\nu(t) \geq f_\nu(template) + 3 * sigma]$  is true OR the condition  $[W50 \geq W50_{psf} \text{ OR } W25 \geq W25_{psf}]$  is true,  $f_\nu(t)$  is selected and the source is classified as marginally extended (M). The  $sigma$  above and in other conditions that follow is the standard deviation of the coadded data measured by SCANPI in the background noise outside the signal range; these values are tabulated in columns (8) - (11) of Table 1 in units of mJy.  $W50_{psf}$  and  $W25_{psf}$  are the thresholds used to establish when a galaxy profile's width at 50% peak (FWHM) or 25% peak are significantly larger than observed among unresolved point sources. The  $W50_{psf}$  and  $W25_{psf}$  thresholds adopted, rather conservatively, are the computed mean plus 3 times the rms dispersion observed in each *IRAS* band for a large sample of point sources:  $1.04'$  and  $1.40'$  at  $12\ \mu\text{m}$ ,  $1.00'$  and  $1.38'$  at  $25\ \mu\text{m}$ ,  $1.52'$  and  $2.06'$  at  $60\ \mu\text{m}$ , and  $3.22'$  and  $4.32'$  at  $100\ \mu\text{m}$ . For reference, the nominal FWHM of the *IRAS* detectors is  $0.77'$  ( $12\ \mu\text{m}$ ),  $0.78'$  ( $25\ \mu\text{m}$ ),  $1.44'$  ( $60\ \mu\text{m}$ ), and  $2.94'$  ( $100\ \mu\text{m}$ ).
2. If the condition  $[f_\nu(t) \geq 1.20 * f_\nu(template) \text{ AND } f_\nu(t) \geq f_\nu(template) + 3 * sigma]$  is true OR the condition  $[W50 \geq W50_{psf} \text{ AND } W25 \geq W25_{psf}]$  is true,  $f_\nu(t)$  is selected and the object is classified as resolved (R).
3. If the condition  $[f_\nu(z) \geq f_\nu(t) + 3 * sigma]$  is true, AND the condition  $[f_\nu(z) \geq f_\nu(peak)]$  is true, AND the condition  $[f_\nu(z) \geq 1.05 * f_\nu(t)]$  is true,  $f_\nu(z)$  is selected and the source is classified as resolved (R).
4. If none of the above conditions are satisfied, the  $f_\nu(template)$  method is selected and the source is classified as unresolved (U).

5. For coadded scans that display confusion from nearby sources, blends of close pairs, excessive noise, cirrus contamination, etc., based on visual inspection made for all of the data, selections resulting from the algorithm above were overridden using flags specified in the input data. For example, the peak flux value is a better estimate (flagged with method code “P” in Table 1) when the  $f_\nu(t)$  value is tainted by a bad point source template fit due to a nearby confusing source or cirrus (e.g., IRAS 02572 + 7002 at  $60\ \mu\text{m}$ ; see Fig. 15.). Another example is when the SCLEAN algorithm was used in an attempt to de-blend components of a pair (e.g., NGC 5194/95 = M 51; see Fig. 15.).

Figures 14 – 16 display coadded *IRAS* scan profiles that illustrate the meaning of the source size codes (S), SCANPI flux density methods (M), and uncertainty flags (F) as listed for each source in Table 1.

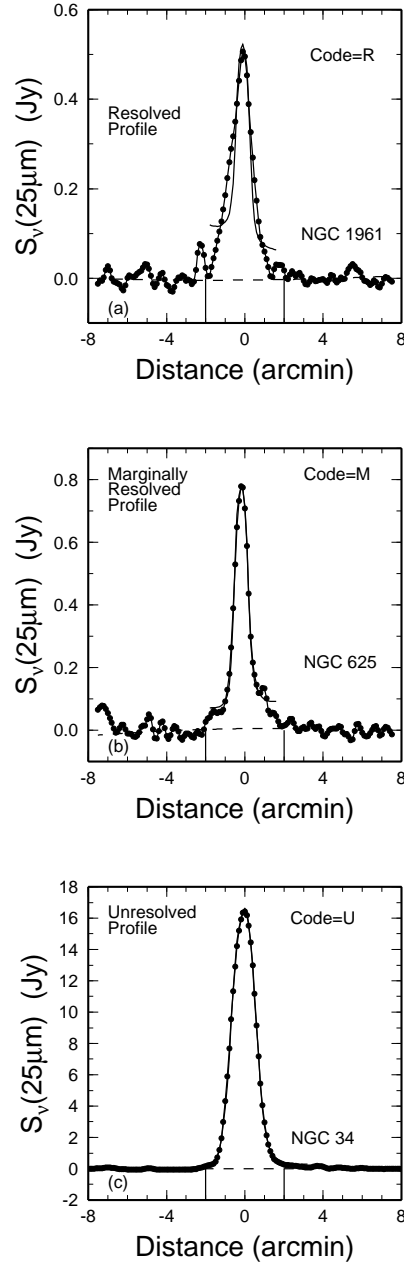


Fig. 14.— Coadded *IRAS* scan profiles that illustrate source size codes listed in columns (8) – (11) of Table 1 (the “S” in “SMF”). Panel (a) R - resolved source NGC1961. Panel (b) M - marginally resolved source (called “U+” in BGS<sub>1</sub>+BGS<sub>2</sub>) NGC625. Panel (c) U - unresolved source NGC34. In this figure, as well as in Figs. 15 and 16, the solid points are the median coadded *IRAS* scan data (SCANPI coadd method 1002), the dashed lines are the baseline fits to the background noise, and the solid lines are the point source template fits (point-spread function). The vertical bars below the fitted baseline show the integration range used for the total flux density estimation,  $f_\nu(t)$ , which is measured within a defined region; the default SCANPI ranges for  $f_\nu(t)$  were used, which are  $\pm 2, \pm 2, \pm 2.5$  and  $\pm 4$  arcminutes at  $12 \mu\text{m}$ ,  $25 \mu\text{m}$ ,  $60 \mu\text{m}$  and  $100 \mu\text{m}$ .

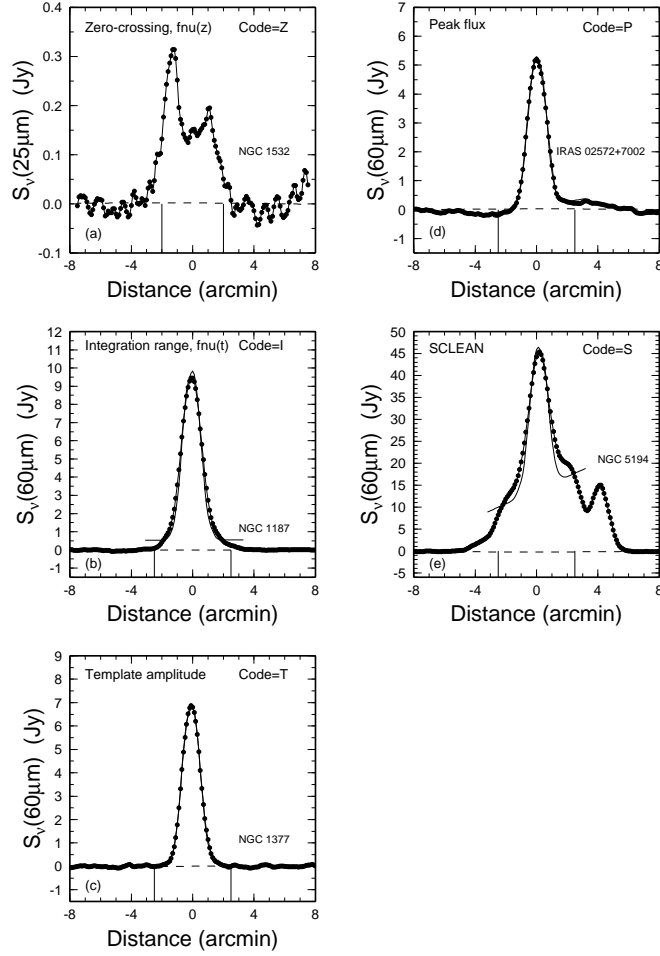


Fig. 15.— Coadded *IRAS* scan profiles that illustrate flux density estimator methods listed as codes in columns (8) – (11) of Table 1 (the “M” in “SMF”). Panel (a): Z - total flux density estimated from integration of the averaged scan between the zero crossings; called “ $f_\nu(z)$ ” in SCANPI output. Panel (b): I - total flux density estimated from integration of the coadded scan between fixed points defining an integration range; called “ $f_\nu(t)$ ” in SCANPI output. Note the slightly raised point source template fit, which is another indicator of small, but statistically significant excess emission compared to the case of a pure point source. The default SCANPI ranges for  $f_\nu(t)$  were used, which are  $\pm 2, \pm 2, \pm 2.5$  and  $\pm 4$  arcminutes at  $12 \mu\text{m}$ ,  $25 \mu\text{m}$ ,  $60 \mu\text{m}$  and  $100 \mu\text{m}$ . Panel (c): T - flux density estimated from the best-fitting point source template; called ‘template amplitude’ in the SCANPI output. This is the method most often selected by the software for unresolved sources with no confusion. Note that the point source template fit is not raised with respect to the baseline fit of the background emission; this is a visual confirmation of the result found by the automated method selection— within the statistical noise,  $f_\nu(t)$  is not larger than the template fit. Panel (d): P - the maximum flux density measured within the signal range; called “peak” in SCANPI output. This method was used when emission from a nearby source or cirrus confused the template fit and contaminated the  $f_\nu(t)$  and  $f_\nu(z)$  methods. Panel (e): S - result of SCLEAN point source subtraction (see Appendix); this method was used to estimate the flux density of components of some pairs, for comparison with generally more reliable HIRES results (Surace, Sanders & Mazzarella 2003). The first four codes are referred to as “peak”, “temp”, “tot” and “zc”, respectively, in the header of Table 7. Another value of the measurement method code listed in Table 1 is “R”; this indicates that the total flux estimate from Rice (1993) or Rice et al. (1988) was used because the SCANPI 1-D scan coaddition method does not work well for objects larger than  $\sim 25$  arcminutes. See text for details.

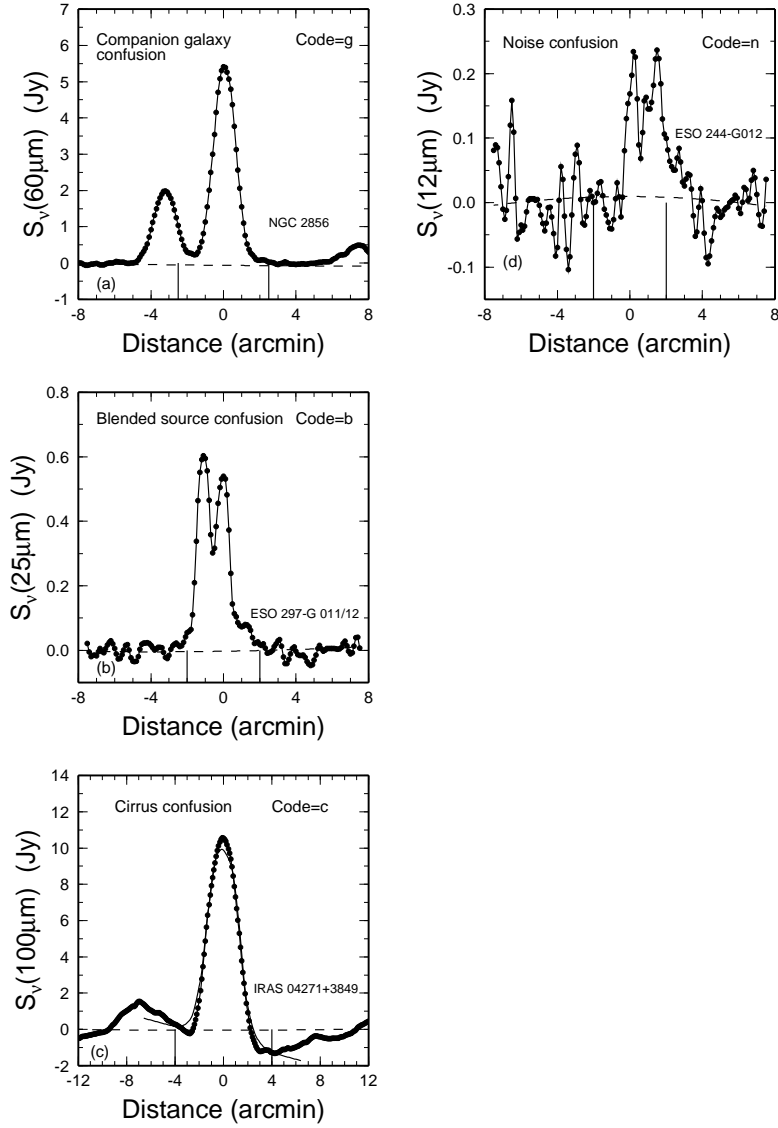


Fig. 16.— Coadded *IRAS* scan profiles that illustrate uncertainty codes listed in columns (8) – (11) of Table 1 (the “F” in “SMF”). These codes identify the origin of large uncertainty flagged generally by a colon (“:”) following the associated flux density measurement in Table 1. Panel (a): g - a nearby **companion galaxy** influenced the choice of flux estimator. Panel (b): b - emission from two or more galaxies is **blended**; the components are unresolved by *IRAS* at the indicated wavelength. Panel (c): c - prominent Galactic **cirrus** taints the measurement. Panel (d): n - excessive **noise** or source confusion prevented a reliable flux density estimate.

The flux estimates chosen by the final processing are indicated by the “Method” codes following the flux densities quoted in Table 1: Z = “zero crossing” (“zc” in Table 7); I = “in-band total” (“tot” in Table 7); T = “template fit” (“temp” in Table 7); P = “peak value” (“peak” in Table 7); S = “deconvolution with SCLEAN”<sup>13</sup>; R = from Rice et al. (1988). For objects with “R” listed as the Method code in Table 1 (objects larger than  $\sim 25$  arcminutes) the SCANPI measurements were not used; they are included in Table 7 just for reference.

Table 5 (Section 4.1) lists the distribution among the size codes (U,M,R) for the sources at each wavelength, and reflects primarily the changing angular resolution of the *IRAS* detectors as a function of wavelength, although the increased sensitivity of the *IRAS* detectors at  $60\ \mu\text{m}$  partially compensates for the larger size of the  $60\ \mu\text{m}$  detectors compared to the smaller angular resolution of the detectors at  $12\ \mu\text{m}$  and  $25\ \mu\text{m}$ . The number of resolved or marginally resolved objects (i.e. size codes “M” or “R” respectively in Table 1) is 61% at  $12\ \mu\text{m}$ , 54% at  $25\ \mu\text{m}$ , 48% at  $60\ \mu\text{m}$ , and drops to 30% at  $100\ \mu\text{m}$ , as listed in Table 5.

---

<sup>13</sup>SCLEAN is a simple routine that fits an *IRAS* point-source template at an input position and subtracts (“cleans”) the fit from the 1-D coadded profile. This allows the user to estimate the flux remaining in a source which is not accounted for by point source component(s). SCLEAN was used to estimate the flux densities for components of pairs and a number of confused objects, as indicated in Table 1.

## REFERENCES

- Aaronson, M., et al 1982a, ApJ, 258, 64.
- Aaronson, M., et al 1982b, ApJS, 50, 241.
- Aaronson, M., & Mould, J. 1983, ApJ, 265, 1.
- Aaronson, M., Mould, J., & Huchra, J. 1980, ApJ, 237, 655
- Aumann, H. H., Fowler, J. W., & Melnyk, M. 1990, AJ, 99, 1674
- Cataloged Galaxies and Quasars Detected in the *IRAS* Survey 1985, prepared by C. J. Lonsdale, G. Helou, J. C. Good, & W. L. Rice (JPL D1932).
- da Costa, L. N., Pellegrini, P. S., Davis, M., Meiksin, A., Sargent, W. L. W., & Tonry, J. L. 1991, ApJS, 75, 935.
- Dale, D. A., Helou, G., Contursi, A., Silbermann, N. A., & Kilhatkar, S. 2001, ApJ, 549, 215.
- de Carvalho, R. R., Ribeiro, A. L. B., Capelato, H. V., & Zepf, S. E. 1997, ApJS, 110, 1.
- de Grijp, M. H. K., Miley, G. K., Lub, J., & de Jong, T. 1985, Nature, 314, 240.
- de Vaucouleurs, G., de Vaucouleurs, A., Corwin, JR., H. G., Buta, R. J., Paturel, G., & Fouque, P. 1991, Third Reference Catalogue of Bright Galaxies, Austin: University of Texas Press.
- de Vaucouleurs, G., de Vaucouleurs, A., & Corwin, J. R. 1976, Second Reference Catalogue of Bright Galaxies, Austin: University of Texas Press.
- Dey, A., Strauss, M. A., & Huchra, J. 1990, AJ, 99, 463.
- Fajardo-Acosta, S. B., Stencel, R. E. & Backman, D. E. 1997, ApJ, 487, 151.
- Ferrarese, L. et al. 2000, ApJS, 128, 431.
- Freedman, W. L. et al. 2001, ApJ, 553, 47.
- Giovanelli, R. & Haynes, M. P. 1993, AJ, 105, 1271.
- Giovanelli, R., Haynes, M. P., Herter, T., Vogt, N. P., Wegner, G., Salzer, J. J., da Costa, L. N., & Freudling, W. 1997, AJ, 113, 22.
- Giovanelli, R., Avera, E., & Karachentsev, I. D. 1997, AJ, 114, 122.
- Gudehus, D. H. 1976, ApJ, 208, 267.
- Haynes, M. P., Giovanelli, R., Herter, T., Vogt, N. P., Freudling, W., Maia, M. A. G., Salzer, J. J., & Wegner, G. 1997, AJ, 113, 1197.
- Haynes, M. P., van Zee, L., Hogg, D. E., Roberts, M. S., & Maddalena, R. J. 1998, AJ, 115, 62.
- Helou, G., Kahn, I. R., Malek, L., & Boehmer, L. 1988, ApJS, 68, 151.
- Huchra, J., Davis, M., Latham, D., & Tonry, J. 1983, ApJS, 52, 89.
- Huchra, J., Latham, D. W., da Costa, L. N., Pellegrini, P. S., & Willmer, C. N. A. 1993, AJ, 105, 1637.
- Huchra, J., P. et al. 1992, CfA Redshift Catalog (ZCAT).
- Huchra, J. P., Geller, M. J., & Corwin, H. G. 1995, ApJS, 99, 391.
- Huchra, J. P., Vogeley, M. S., & Geller, M. J. 1999, ApJS, 121, 287.
- IRAS* Catalogs and Atlases – Explanatory Supplement 1985 (NASA RP-1190).
- IRAS* Catalogs and Atlases: Small Scale Structure Catalog 1988, eds. G. Helou & D. Walker (Washington, DC: GPO) (SSS).
- IRAS* Catalogs and Atlases: Point Source Catalog 1988, (Washington, DC: GPO) (PSC Version 2).
- IRAS* Faint Source Survey, Explanatory Supplement version 2, 1992, eds. M. Moshir, G. Kopman, T. Conrow (Pasadena: IPAC).
- Keel, W. C. 1996, AJ, 111, 696.
- Keel, W. C. 1996, ApJS, 106, 27.
- Kim, D.-C., Sanders, D. B., Veilleux, S., Mazarella, J. M., & Soifer, B. T. 1995, ApJS, 98, 129.
- Kirshner, R. P. 1977, ApJ, 212, 319.



- Kirshner, R. P., Oemler, A., & Schechter, P. L. 1978, *AJ*, 83, 1549.
- Lauberts, A. & Valentijn, E. A. 1989, "The Surface Photometry Catalogue of the ESO-Uppsala Galaxies," (Garching: European Southern Observatory).
- Lebofsky, M. J. & Rieke, G. H. 1979, *ApJ*, 229, 111.
- Lu, N. Y., Dow, M. W., Houck, J. R., Salpeter, E. E., & Lewis, B. M. 1990, *ApJ*, 357, 388.
- Lu, N. Y., Hoffman, G. L., Groff, T., Roos, T., & Lamphier, C. 1993, *ApJS*, 88, 383.
- Mathewson, D. S., Ford, V. L., & Buchhorn, M. 1992, *ApJS*, 81, 413.
- Madore, B. F., & Freedman, W. L. 1998, in "Stellar Astrophysics for the Local Group: VIII Canary Islands Winter School of Astrophysics." Edited by A. Aparicio, A. Herrero, & F. Sanchez. Cambridge; New York: Cambridge University Press, p.263
- Mathewson, D. S. & Ford, V. L. 1996, *ApJS*, 107, 97.
- Miley, G., Neugebauer, G., Soifer, B. T., Clegg, P. E., Harris, S., Rowan-Robinson, M., & Young, E. 1984, *ApJ*, 278, L79
- Mirabel, I. F. & Sanders, D. B. 1988, *ApJ*, 335, 104.
- Moshir, M., Kopan, G., Conrow, T., McCallon, H., Hacking, P., Gregorich, D., Rohrbach, G., Melnyk, M., Rice, W., Fullmer, L., White, J., & Chester, T. 1992, Explanatory Supplement to the *IRAS* Faint Source Survey, Version 2, JPL D-10015 8/92 (Pasadena: JPL)
- Mould, J. R. et al. 1991, *ApJ*, 383, 467
- Mould, J. R. et al. 2000, *ApJ*, 529, 786
- Murphy, T. W., Soifer, B. T., Matthews, K., Armus, L., & Kiger, J. R. 2001, *AJ*, 121, 97.
- Neugebauer, G., et al. 1984, *ApJ*, 278, L1.
- Nordgren, T. E., Chengalur, J. N., Salpeter, E. E., & Terzian, Y. 1997, *AJ*, 114, 77.
- Nordgren, T. E., Chengalur, J. N., Salpeter, E. E., & Terzian, Y. 1997, *AJ*, 114, 913.
- Palumbo, G. G. C., Tanzella-Nitti, G., & Vetolani, G. 1983, "Catalogue of Radial Velocities of Galaxies," New York, Gordon and Breach Science Publishers, 592 pp.
- Pantoja, C. A., Altschuler, D. R., Giovanardi, C., & Giovanelli, R. 1997, *AJ*, 113, 905.
- Perault, M. 1987, Structure et Evolution des Nuages Moleculaires, PhD thesis, Univ. Paris
- Ribeiro, A. L. B., de Carvalho, R. R., Coziol, R., Capelato, H. V., & Zepf, S. E. 1996, *ApJ*, 463, L5.
- Rice, W. 1993, *AJ*, 105, 67.
- Rice, W. L., Lonsdale, C. J., Soifer, B. T., Neugebauer, G., Kopan, E. L., Lloyd, L. A., deJong, T., & Habing, H. 1988, *ApJS*, 68, 91.
- Rubin, V. C., Kenney, J. D. P., & Young, J. S. 1997, *AJ*, 113, 1250.
- Sandage, A., Bell, R. A., & Tripicco, M. J. 1999, *ApJ*, 522, 250.
- Sandage, A., & Tammann, G. A. 1981, A Revised Shapley-Ames Catalog of Bright Galaxies (Carnegie Institute, Washington, DC) (RSA).
- Sanders, D. B., & Mirabel, I. F. 1996, *ARA& A*, 34, 749.
- Sanders, D. B., Egami, E., Lipari, S., Mirabel, I. F., & Soifer, B. T. 1995, *AJ*, 110, 1995 (BGS<sub>2</sub>).
- Sanders, D. B., Scoville, N. Z., & Soifer, B. T. 1991, *ApJ*, 370, 158.
- Schmidt, M. 1968, *ApJ*, 151, 393
- Schneider, S. E., Thuan, T. X., Magri, C., & Wadiak, J. E. 1990, *ApJS*, 72, 245.
- Schneider, S. E., Thuan, T. X., Mangum, J. G., & Miller, J. 1992, *ApJS*, 81, 5.
- Shier, L. M. & Fischer, J. 1998, *ApJ*, 497, 163.
- Shostak, G. S. 1975, *ApJ*, 198, 527.

- Soifer, B. T., Boehmer, L., Neugebauer, G., & Sanders, D. B. 1989, *AJ*, 98, 766 (BGS<sub>1</sub>).
- Soifer, B. T., Sanders, D. B., Madore, B. F., Neugebauer, G., Danielson, G. E., Elias, J. H., Lonsdale, C. J., & Rice, W. L. 1987, *ApJ*, 320, 238.
- Soifer, B. T., Sanders, D. B., Neugebauer, G., Danielson, G. E., Lonsdale, C. J., Madore, B. F., & Persson, S. E. 1986, *ApJ*, 303, L41.
- Solomon, P. M., Downes, D., Radford, S. J. E., & Barrett, J. W. 1997, *ApJ*, 478, 144.
- Storchi-Bergmann, T., Rodriguez-Ardila, A., Schmitt, H. R., Wilson, A. S., & Baldwin, J. A. 1996, *ApJ*, 472, 83.
- Strauss, M. A., Huchra, J. P., Davis, M., Yahil, A., Fisher, K. B., & Tonry, J. 1992, *ApJS*, 83, 29.
- Surace, J. A., Sanders, D. B., & Mazzarella, J. M. 2003, *ApJS*, submitted.
- Tift, W. G. & Cocke, W. J. 1988, *ApJS*, 67, 1.
- Tinney, C. G., Scoville, N. Z., Sanders, D. B., & Soifer, B. T. 1990, *ApJ*, 362, 473.
- Tully, R. B. 1982, *ApJ*, 257, 389.
- Tully, R. B., & Shaya, E. 1984, *ApJ*, 281, 31.
- Walsh, W., Staveley-Smith, L., & Oosterloo, T. 1997, *AJ*, 113, 1591.
- Young, J. S. et al. 1995, *ApJS*, 98, 219.
- Zwicky, F., et al (1961-68), *Catalog of Galaxies and Clusters of Galaxies*, (California Institute of Technology, Pasadena).
- Zwicky, F., & Zwicky, M. A. 1971, *Catalog of Selected Galaxies and Post-Eruptive Galaxies*, (Zurich: Offsetdruck L. Speich).